INFLUENCE OF GRAIN SIZE ON FATIGUE CRACK GROWTH IN FCC AND HCP METALS

by

Larry W. Sarver
and
R. Rodger Seeley

Submitted in Partial Fulfillment of the Requirements

for the Degree of

Master of Science in Engineering

in the

Metallurgical Engineering Program

_____

Adviser Date

_____

Dean of the Graduate School Date

YOUNGSTOWN STATE UNIVERSITY

March, 1974

ABSTRACT

INFLUENCE OF GRAIN SIZE ON FATIGUE CRACK GROWTH IN FCC AND HCP METALS

Larry W. Sarver
and
R. Rodger Seeley

Master of Science in Engineering

Youngstown State University, 1973

The influence of grain size on fatigue crack growth was studied for several single-phase materials representing the face-centered-cubic (FCC) and hexagonal-close-packed (HCP) crystal systems. These materials furthermore represented various levels of stacking fault energy (SFE). The materials employed in this work are pure aluminum (high SFE) and an austenitic stainless steel (low SFE) from the FCC crystal system, and commercially pure titanium (low SFE) and a titanium-8% aluminum binary alloy (low SFE) from the HCP system. Mechanical property tests were conducted at room temperature to determine monotonic tensile properties and fatigue crack growth properties. A metallographic survey and grain size determination was made for each material. Transmission electron microscopy work was carried out to characterize the plastically deformed substructure of each material. Examination of fatigue fracture surfaces by scanning electron microscopy and of replicas of fatigue fracture surfaces by transmission electron microscopy characterized the features of fatigue fracture and microplastic behavior of each material.

The tensile properties were analyzed with respect to grain size. The fatigue crack growth properties were also analyzed with respect to grain size but within the framework of a constant state of stress at the tip of the fatigue crack. This analysis technique is suggested by the observations of other researchers concerning the effects of material yield strength and test specimen thickness on fatigue crack growth and also by the macroscopic behavior of test specimens during fatigue testing. The fatigue crack growth properties were correlated with the deformed substructures and the fracture surface features of the materials studied.

The results of this work indicate grain size has an appreciable influence on fatigue crack growth for constant states of stress in materials of low stacking fault energy. Materials of high stacking fault energy exhibit little or no grain size influence on crack growth. The sensitivity of grain size influence in low SFE materials is related to the state of stress, i.e., higher states of stress result in greater sensitivity. There is little or no stress state sensitivity for the high SFE materials. The grain size dependency of fatigue crack growth and the stress state sensitivity is related to the stacking fault energy and subsequent deformation substructure morphology of the materials.

ACKNOWLEDGEMENTS

The authors wish to thank the Babcock and Wilcox Company, Alliance Research Center for permission to use various pieces of research equipment during the experimental phase of this work.

The authors also wish to express their thanks to Dr. Shaffiq Ahmed, Professor, Department of Chemical Engineering and Material Science, Youngstown State University, for his guidance and assistance in the study.

TABLE OF CONTENTS

TABLE OF CONTENTS (cont'd)

TABLE OF CONTENTS (cont'd)

LIST OF FIGURES

LIST OF FIGURES (cont'd)

LIST OF FIGURES (cont'd)

LIST OF FIGURES (cont'd)

LIST OF FIGURES (cont'd)

LIST OF FIGURES (cont'd)

LIST OF TABLES

CHAPTER I

INTRODUCTION

The effect of grain size on deformation and mechanical properties of polycrystalline metals has been studied by many investigators. For many metals, tensile yield strength and ultimate strength have been examined as a function of grain size. The general effect of increasing grain size has been found to be to decrease the strength level of most metals studied. These findings have led to the familiar Hall-Petch relationship[1]* of strength and grain size.

Fatigue properties have also been studied as a function of grain size, but most of the earlier work on 70/30 brass[2], copper, 70/30 brass, and aluminum[3], copper, 70/30 brass, and several Cu-Al alloys[4], and pure aluminum[5] has been based on the number of loading cycles to failure of the specimen. Such failure lives were on the order of 10^4 to 10^8 cycles. Most correlations with grain size were made for endurance strength at 10^6 or greater cycles. These works indicated grain size dependence of long life fatigue for brass and Cu-Al, but not for copper or aluminum. There is some discrepancy regarding the effects of grain size. Thompson and Backofen found no grain size effect whereas Hoeppner does report a grain size effect in fatigue of aluminum.

---

*Numbers in parentheses refer to referenced works.

The fatigue life of a polycrystalline metal consists of three stages--initiation of cracks, slow propagation of cracks, and rapid crack growth leading to fracture[6]. If one considers the total fatigue life, these three stages are combined into one quantitative value. Investigating the influences of various material parameters on the total fatigue life may result in misleading conclusions as to the effects of such parameters on the individual states of initiation and propagation. Therefore, it is more prudent to examine directly the properties of interest such as crack propagation under fatigue loading. Fatigue crack growth data are used in a practical sense to estimate the remaining life of a cracked structure under known fatigue loading conditions.

The growth of existing cracks can occur as a result of cyclic loading of the body or test specimen containing the crack. Such crack growth for ductile metals has been described by Laird[7] in a "plastic blunting process" theory. According to this theory a tensile load applied to the crack forces the crack tip to be stretched and plastically deform to accommodate the tensile load. The plastic flow of material is accommodated by dislocation movement and intense slip along planes oriented at about 45^{o} to the plane of the crack. As the load decreases to its minimum value the previously deformed material is compressed by the closing crack and buckles and folds over resulting in an increment of crack growth. This compression of the crack tip material serves to resharpen the crack tip. Upon the next tensile load the crack tip is again blunted by plastic flow, and as the load is reduced the crack tip is resharpened. This process occurs over and over

again as a test specimen undergoes cyclic tensile loading. Crack growth in ductile materials therefore occurs by a crack tip blunting mechanism wherein crack growth rate is inversely proportional to crack tip blunting.

Since blunting and resharpening of the crack tip during cyclic loading occurs by plastic flow, the material characteristics influencing plastic flow are influenced by the extent of dislocation movement. Materials of high stacking fault energy are known to allow easy cross slip of dislocations[8, 9]. Cross slip occurs when dislocations being stopped or piled up shift or cross over from one slip plane to a differently oriented slip plane. Materials of low stacking fault energy usually have substantially greater amounts of alloying elements[10] and conversely do not permit easy cross slip of dislocations. These dislocations are then restricted to their original slip planes. Resistance to cross slip can result in differences in plastic flow properties of the material such as strain hardening. Materials with high resistance to cross slip generally exhibit a higher degree of strain hardening[11]. The strain-hardening exponent, n, in the stress-strain relationship, $\sigma = A\varepsilon^n$, would have high values for high resistance to cross slip and low values for low resistance to cross slip.

Stacking fault energy also manifests itself through the substructure arrangement of dislocations in plastically strained materials. The substructures of material near fatigue fracture surfaces and fatigue crack tips have been observed by transmission electron microscopy using carefully prepared thin films. High stacking fault energy materials generally exhibit cellular arrangements of dislocations[12]. The cells

are usually equiaxed with well-defined walls. Low stacking fault energy materials exhibit dislocation patterns in a more banded arrangement[13]. These bands constitute areas of intense slip activity. Dislocation densities are quite high in the walls of the cells of high stacking fault energy material and in the slip bands of low stacking fault energy material.

According to the theory of Laird the crack tip blunting and resharpening growth mechanism requires a sufficient number of dislocations to accommodate the plastic deformation at the crack tip. In materials permitting easy cross slip, the dislocations can move easily onto slip planes favorably oriented for the blunting process. If cross slip is difficult, as in the low stacking fault energy materials, dislocations are restricted to their original slip planes and are not as available to aid in the crack tip blunting process. Therefore, the level of stacking fault energy and subsequent ease of cross slip should have a reasonable effect on fatigue crack growth by influencing the number of dislocations available for the blunting process. Crack growth studies in Cu-Al and Cu-Ni alloys indicates a stacking fault energy influence. Low stacking fault energies resulted in low crack growth rates[14, 15]. Another influence of stacking fault energy on crack growth may be to provide paths of least resistance to crack growth. These paths would be the cell walls and slip bands of the substructure formed by cyclic loading. If such paths offered the least resistance, the crack could progress along them rather than across them.

The fatigue fracture surface often reveals a considerable amount of qualitative information and sometimes some quantitative data

concerning the fatigue crack growth process. This information is gathered by examining the fracture surfaces directly in a scanning electron microscope or examining carefully prepared replicas of the fracture surfaces on a scanning or transmission electron microscope[16]. The blunting and resharpening process described earlier results in striated markings observable at high magnifications on the fracture surface. Study of these striations indicates that each striation usually corresponds to one complete loading cycle. Based on this assumption, fatigue crack growth rates on a microscopic level have been determined by counting the number of striations over a given distance on the fracture surface. Fatigue fractures can exhibit other interesting features such as ductile dimples in highly stressed regions, cleavage fracture facets in brittle material and intergranular fracture in embrittled material. Griffiths, et al, have related fracture surface features, i.e., striations or ductile dimples, to the state of stress at that point[17]. The state of stress (plane stress or plane strain) in this referenced work was described by fracture surface orientation with respect to the tensile loading axis. Plane strain conditions usually exhibit a flat fracture plane oriented perpendicular to the loading axis, and plane stress conditions usually exhibit fracture surfaces oriented about 45^{o} to the loading axis. Striations were detected in plane strain regions while plane stress regions exhibited mostly ductile dimple microvoid coalescence failure. The reader is referred to an ASTM STP 436 for basic discussion of fractographic features[18]. Reference has also been made in the literature about a "structure sensitive fatigue fracture" in FCC materials[19]. A sensitivity of fatigue fracture appearance to microstructure has been

described for low carbon steel, O.F.H.C. copper, and a commercial 18/8 (Type 304) stainless steel. Certain fracture surface features correspond to grain boundaries or twin boundaries. This sensitivity seems to be most pronounced at low crack growth rates.

The question of influence of grain size on fatigue crack growth has been addressed only briefly by a few investigators. These investigations have been limited to only a few metals and alloys in the face centered cubic crystal system. Fatigue studies on copper[20], a high stacking fault energy material, indicated grain size influenced total fatigue life but apparently by influencing the number of cycles to initiate a crack rather than the crack growth properties. A recent study of fatigue crack growth by Thompson and Bucci in a copper-nickel alloy of low stacking fault energy indicated no difference in fatigue crack growth[21]. However, the specimens of various grain sizes exhibited different yield strengths. Therefore, they did not adequately account for variations in stress state which is influenced in thin sections by yield strength by assuming yield strength variations have no influence on crack growth.

The state of stress at the tip of a fatigue crack can be generally described as plane stress or plane strain or a mixture of these, and depends primarily on the thickness of the specimen, the yield strength of the material, and the stress intensity factor at the crack tip. The stress intensity factor is a single parameter describing the stress field at any point near a crack tip. A more detailed description of this factor is contained in the Appendix A. The case of

plane strain is one in which there is little or no plastic deformation through the specimen thickness and the triaxial stresses along the crack front are high. A state of plane stress results when there is gross yielding through the thickness of the specimen, and the triaxial stresses are low.

When a tensile stress is imposed on a specimen containing a crack, a small zone of plastically deformed material will be developed around the crack tip, and is surrounded by the elastically deformed bulk material[22].

The size of this plastic zone, r_p, can be calculated for cyclic loading by[23]:

$$r_p = \frac{1}{12\pi}\left(\frac{K}{\sigma_{YS}}\right)^2 \qquad \text{Equation 1}$$

Where r_p is the plastic zone size beyond the crack tip, K is the stress intensity factor during fatigue loading, σ_{YS} is the yield strength of the material. If r_p is small compared to the thickness of the specimen, the lateral contraction will be small, and the stress state at the crack tip approaches that of plane strain. If r_p is large compared to the specimen thickness, considerable lateral contraction occurs, and a state of plane stress exists.

The effect of stress state on fatigue crack growth has not been clearly examined, but there is some evidence that such an influence exists. The state of stress at the tip of a fatigue crack depends primarily upon specimen thickness, material yield strength, and stress

intensity factor. For given loading conditions, thick specimens or high strength material will be under plane strain conditions, while thin specimens or low strength material will be under plane stress conditions. Richards and Lindley[24] have examined the influence of specimen thickness and flow stress on fatigue crack growth in ferritic materials. Their studies indicate decreasing specimen thickness (moving toward plane stress) results in smaller amounts of flat fracture and higher crack growth rates. However, this influence seems to be most prominent at high fatigue loads near general yield of the material, while little or no effect is seen at low loads. Further, they comment that increasing the flow stress (moving toward plane strain) results in a decrease in crack growth rates. In general, when stress state conditions tend toward plane stress, increased rates of crack growth are observed as McEvily and Johnston[25] described for fatigue crack growth in sheet specimens of two aluminum alloys. As the cracks grew longer in these materials, the plane of the crack turned from normal to the loading axis (indicative of plane strain) to an angle of about 45^{o} to the loading axis (plane stress). They indicated the transition was related to size of the plastic zone with respect to the specimen thickness. By their analysis, however, the crack growth rates were lower in plane stress than in plane strain. This is in contrast with the work of Richards and Lindley. The foregoing evidence indicates there seems to be a decided influence of stress state on fatigue crack growth. Therefore, analysis of fatigue crack growth data for thin specimens should rightly include consideration of the stress state at the crack tip.

The fatigue studies conducted on materials of the face centered cubic systems have led to various theories concerning influence of stacking fault energy and grain size on fatigue properties, although these influences in the fatigue crack growth area are not well understood. There has been little work done in this area on materials of the hexagonal close packed crystal system. Although a number of fatigue studies have been conducted on titanium alloys, few have considered grain size influences on fatigue crack growth.

Our work was conducted on materials from both the face centered cubic and hexagonal close packed crystal systems. Moreover, the material choices were made to represent both high and low stacking fault energy materials. The data from the FCC materials serve to support or oppose the existing theories on fatigue crack growth. The work on HCP materials is virtually the first of its kind for fatigue crack growth. Analysis of the data from both crystal systems will provide an opportunity to test the theories developed for FCC materials on HCP materials. This examination of the data from HCP materials will indicate the possible universality of fatigue crack growth theories.

The choice of materials was limited to single phase metals to avoid any problems inherent with multiphase microstructures. The work was limited to two materials (high and low stacking fault energy) from each crystal system and three grain sizes for each material. Pure aluminum and Type 304 stainless steel were chosen from the FCC system to represent high and low stacking fault energies respectively. These energies have been experimentally determined by others as about 280 ergs/cm^2 for aluminum[26] and about 13 ergs/cm^2 for stainless

steel[8] using transmission electron microscopy. Pure titanium and a titanium-8% aluminum alloy were chosen from the hexagonal close packed system. Stacking fault energies of these materials have not been experimentally determined, but the relative levels of these energies are revealed by two independent investigations on the dislocation substructure of the materials. Mackay and Tiner examined a series of Ti-Al alloys and detected a change in substructure from cellular at low aluminum levels to banded at a high aluminum level with the change occurring at about 4% to 5% aluminum[27]. Mauney, et al, described a banded dislocation substructure in a Ti-8% Al alloy[28]. On the basis of this evidence combined with the knowledge that alloying generally reduces stacking fault energy (at least in the FCC system), pure titanium was chosen for the high stacking fault energy material and a Ti-8% Al alloy for the low energy material.

The general approach of this work is to produce different grain sizes in each material by cold working and heat treating the FCC materials and heat treating the HCP materials. The tensile and fatigue crack growth properties were determined for each condition. These properties were then analyzed as a function of grain size, stacking fault energy, and crystal system. The fatigue crack growth data were reduced and analyzed using fracture mechanics principles. Consideration of stress state was included in this analysis. The fatigue fracture process was studied by examining the fatigue fracture surfaces directly on a scanning electron microscope. Dislocation substructure of each material was studied using transmission electron microscopy to examine thin film specimens taken from near the fatigue fracture surface.

CHAPTER II

EXPERIMENTAL PROCEDURE

Materials

The chemical compositions of the materials used for this work are contained in Table 1.

TABLE 1

CHEMICAL ANALYSIS OF MATERIALS

Aluminum:	99.99% Al (melting stock)
Type 304 Stainless Steel:	.063% C, 1.70% Mn, .016% S, .028% P, .57% Si, 18.55% Cr, 10.48% Ni, balance Fe
Commercially Pure Titanium:	.02% C, .014% N_2, .35% Fe, .322% O_2, 45 ppm H_2, balance Ti
Ti-8% Al Alloy:	.01% C, .009% N_2, .03% Fe, 7.7% Al, .066% O_2, 38 ppm H_2, balance Ti

The pure aluminum material was induction melted, cast, and forged to 5/8 inch thick plate. The austenitic stainless steel was obtained in 2-1/2 inch diameter bar stock and forged to 5/8 inch thick plate. The

commercially pure titanium (CPTi) was obtained as hot rolled, annealed sheet .162 inches thick. The titanium-8% aluminum alloy (Ti-8Al) was obtained as hot rolled sheet about .120 inches thick. These titanium materials were chemically cleaned to remove oxygen contaminated surfaces developed during hot rolling and annealing.

In order to obtain the desired grain sizes in the FCC materials, the 5/8 inch thick plates were cold rolled to about .25 inches for a total reduction of about 60% and then heat treated for relatively long periods of time. All rolling was done in one direction with no intermediate annealing. The HCP materials were not cold rolled since they have much less capacity for cold work. The commercially pure titanium can be cold reduced but, requires high rolling pressures. The Ti-8Al alloy has very little capacity for cold work. Preliminary heat treatment studies were conducted on small coupons of the cold-rolled FCC material and the as-received HCP material with various time-temperature combinations to obtain a range of grain sizes. After heat treatment, the coupons were cut in half and the transverse plane (parallel to the rolling direction and perpendicular to the surface of the sheet) was polished for metallographic examination.

Metallographic Investigation

The metallographic specimens were prepared by conventional metallographic procedures of mounting in bakelite, grinding on a successively finer series of silicon carbide papers, and polishing to a fine finish with 6μ diamond paste in oil followed by 0.25μ alumina

powder in water. Since four different materials were studied, different etchants were employed to reveal microstructure; these are listed in the following table:

TABLE 2
METALLOGRAPHIC ETCHES

Aluminum	0.5% HF 99.5% H_2O	Immersion Etch
Stainless Steel	Oxalic Acid Water	Electrolytic Etch Stainless Steel Cathode 6 volts
Titanium Titanium-8% Aluminum	10% HF 5% HNO_3 85% H_2O	Immersion Etch

Preliminary grain size measurements were made by comparison with an ASTM grain size chart to determine the proper heat treatment cycles to produce the desired grain sizes. The final grain sizes were determined for both longitudinal and transverse metallographic specimens taken adjacent to the fatigue fracture surfaces. These grain sizes were measured by a standardized procedure specified by ASTM[29]. The step-by-step procedure is as follows: (1) cursory examination of the structure and estimation of the equivalent ASTM grain size number using the comparison method; (2) selection of a magnification to yield approximately 100 intercepts for a 50 cm circular "bull's-eye" test pattern;

(3) selection of five areas for counting and determination of average number of intercepts; (4) conversion of average number of intercepts to equivalent Heyn grain size (mean linear intercept grain size) in microns. The average grain diameter is hereafter given either in microns or in inches. The following Table 3 describes the heat treatment cycles for each material:

TABLE 3

HEAT TREATMENTS

Material	Fatigue Spec. No.	Heat Treatment
Aluminum[a]	AF-1	800F-17 Hr
	AF-7	800F-28 Hr; 1000F-20 Hr
	AF-3	650F-24 Hr; 700F-24 Hr; 750F-9 Hr; 800F-6 Hr; 1230F-4 Hr
Type 304 Stainless Steel[a]	SF-5	1700F-20 Hr
	SF-6	1800F-16 Hr
	SF-1	2000F-15 Hr
Pure Titanium[b]	PTF-1	As Received
	PTF-3	1500F-18 Hr
	PTF-6	1550F-93 Hr
Titanium-8% Aluminum[c]	ATF-2	1600F-2 Hr
	ATF-6	1700F-12 Hr
	ATF-4	1800F-36 Hr

[a] Initial condition - cold rolled about 60%

[b] Initial condition - hot rolled and annealed

[c] Initial condition - hot rolled

Substructure Studies

A study of the substructure developed in the plastic zone of the fatigue crack for each material was made through the examination of thinned metal foils in the transmission electron microscope. For this study, one grain size sample for each material was selected. Thin strips of metal were cut from fatigue specimens AF-3, SF-6, PTF-3, and ATF-6 by means of a Buehler Isomet low speed diamond saw. These cuts were made parallel to the fatigue fracture plane and were nominally 0.025-inch in thickness.

Thin strips were ground on the fracture surface sides just sufficiently to create a planar surface; further grinding was done on the reverse side to reduce the nominal thicknesses to 0.008-inch. Discs of 0.125-inch diameter were punched from these strips for subsequent preparation by electropolishing.

Thinned foils suitable for transmission electron microscopical examination were prepared by electropolishing in two stages. A commercial Polaron electropolishing unit was used to profile the thin discs by jet polishing concave depressions on both sides. Final thinning was done in a separate cell where the electropolishing process could be monitored using an optical microscope. Thinning was terminated when foil perforation was observed.

The specimens were electropolished using an electrolyte consisting of 10 v/o perchloric acid and 90 v/o methanol. Profiling was done at an applied potential of 40 volts while final thinning was done

over a range of applied potentials (6 to 12 volts) with an optimum potential determined experimentally for each material.

Thinned specimens were examined in a Jeolco JEM-6A transmission electron microscope using an accelerating potential of 100 kv. Examination was performed over a range of magnifications (∿5000X to ∿30,000X) and representative electron micrographs were recorded on electron image plates. Photographic enlargements of typical substructural conditions observed in each material are presented in the results.

Mechanical Testing

Tensile and fatigue crack growth test specimen blanks were cut from each material either as cold rolled or as received, machined as illustrated in Figure 1, and heat treated in vacuum using the heat treatment cycles in Table 3. Vacuum annealing was used to minimize oxidation of the specimens. Tensile tests were conducted at room temperature on an Instron testing machine using a crosshead speed of about 0.05 inches per minute to maintain a constant strain rate. Strain was measured during the tensile test with a dual range extensometer which made possible the recording of load versus strain up to maximum load. A dual range extensometer measures strain during a tensile test first at high magnification (500:1) to record elastic modulus and yield data. This extensometer is then electronically switched to a low magnification (20:1) to record plastic flow data up to maximum load. From such a load-strain record, data were gathered for strain hardening exponent calculations. The strain hardening exponent was calculated by

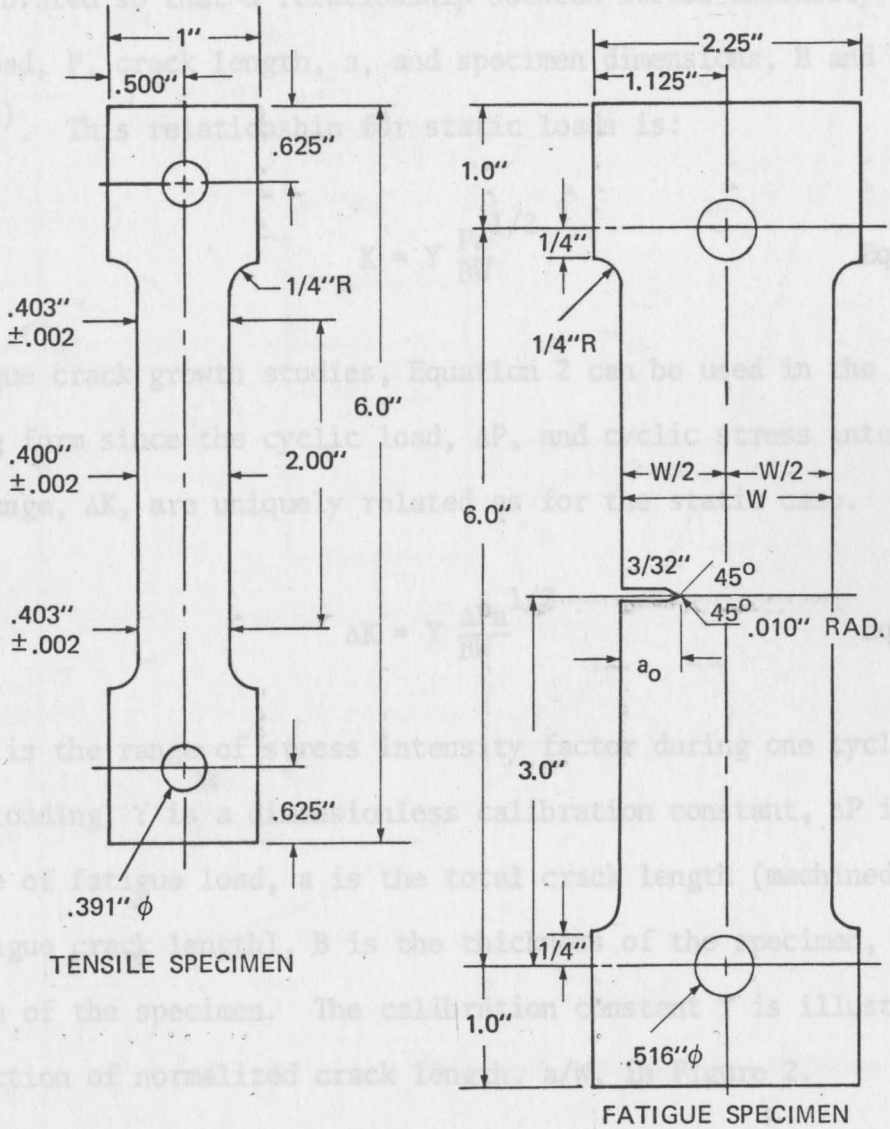

FIGURE 1 TEST SPECIMENS

determining a least-squares fit through the log stress-log strain data and calculating the slope of the line.

The single edge notched fatigue specimen used in this work has been calibrated so that a relationship between stress intensity factor, K, and load, P, crack length, a, and specimen dimensions, B and W, exists[30]. This relationship for static loads is:

$$K = Y \frac{Pa^{1/2}}{BW} \qquad \text{Equation 2}$$

For fatigue crack growth studies, Equation 2 can be used in the following form since the cyclic load, ΔP, and cyclic stress intensity factor range, ΔK, are uniquely related as for the static case.

$$\Delta K = Y \frac{\Delta Pa^{1/2}}{BW} \qquad \text{Equation 3}$$

Where ΔK is the range of stress intensity factor during one cycle of fatigue loading, Y is a dimensionless calibration constant, ΔP is the amplitude of fatigue load, a is the total crack length (machined notch plus fatigue crack length), B is the thickness of the specimen, W is the width of the specimen. The calibration constant Y is illustrated as a function of normalized crack length, a/W, in Figure 2.

Fatigue crack growth tests were conducted at room temperature on an MTS closed-loop, servo-controlled hydraulic test system. Fatigue cracks were initiated at the bottom of the machined notches under a constant cyclic load and grown at frequencies of 5 to 30 cycles per second. The fatigue load was reduced during the test so that failure

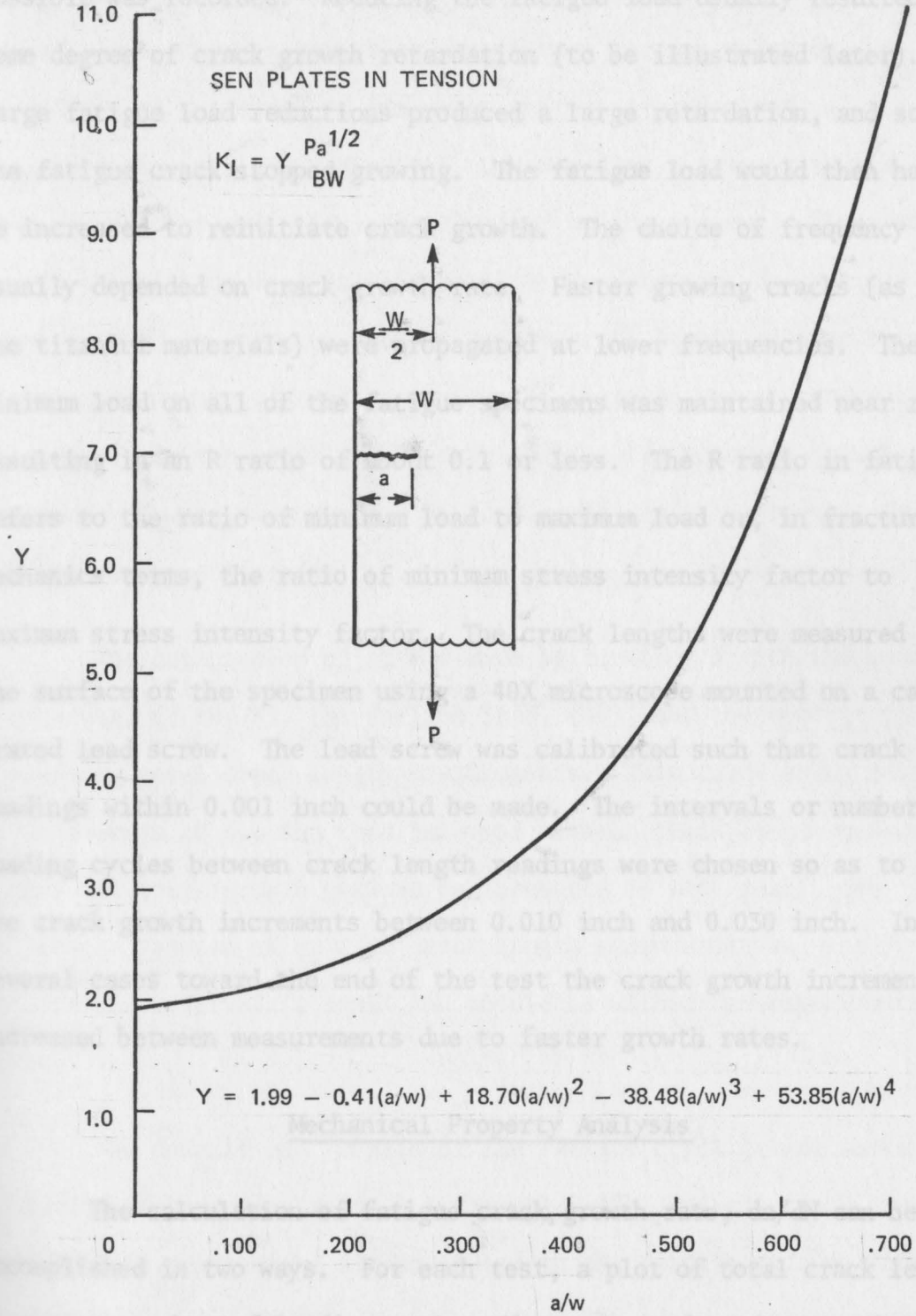

FIGURE 2 STRESS INTENSITY FACTOR CALIBRATION CURVE FOR SINGLE EDGE NOTCHED (SEN) PLATES LOADED IN TENSION

of the specimen would not occur before as much crack growth data as possible was recorded. Reducing the fatigue load usually resulted in some degree of crack growth retardation (to be illustrated later). Large fatigue load reductions produced a large retardation, and sometimes the fatigue crack stopped growing. The fatigue load would then have to be increased to reinitiate crack growth. The choice of frequency usually depended on crack growth rate. Faster growing cracks (as in the titanium materials) were propagated at lower frequencies. The minimum load on all of the fatigue specimens was maintained near zero resulting in an R ratio of about 0.1 or less. The R ratio in fatigue refers to the ratio of minimum load to maximum load or, in fracture mechanics terms, the ratio of minimum stress intensity factor to maximum stress intensity factor. The crack lengths were measured on the surface of the specimen using a 40X microscope mounted on a calibrated lead screw. The lead screw was calibrated such that crack length readings within 0.001 inch could be made. The intervals or number of loading cycles between crack length readings were chosen so as to keep the crack growth increments between 0.010 inch and 0.030 inch. In several cases toward the end of the test the crack growth increments increased between measurements due to faster growth rates.

Mechanical Property Analysis

The calculation of fatigue crack growth rate, da/dN can be accomplished in two ways. For each test, a plot of total crack length, a, against number of loading cycles, N, can be made and a smooth curve drawn through these points. This curve will typically be parabolic in form and the shape (steep or shallow) will depend on the cyclic load.

Figures 3 through 6 illustrate typical crack length-cycle curves for the materials in this work. Figures 3 and 6 illustrate crack growth retardation. The fatigue crack growth rate for any point on this curve is defined as the slope of the curve or the first derivative, da/dN, of the expression for the a-N curve. One may draw a tangent to the curve at a given point and calculate the slope of the tangent. The crack growth calculation used in this work was to determine the ratio of crack growth, Δa, between two successive crack length measurements to the elapsed number of loading cycles, ΔN, between the measurements. This ratio was the crack growth rate $\Delta a/\Delta N$. If the crack growth increment between measurements is kept small, $\Delta a/\Delta N$ approaches the derivative value of da/dN.

The calculation of ΔK was made by Equation 3 with the specimen dimensions, (B and W), the fatigue load, (ΔP), and the average of two successive total crack length measurements. This calculation results in an average ΔK for the test interval between crack length measurements. If crack growth between measurements is kept small, the difference between ΔK at each crack length measurement and the average ΔK over the interval is small and should be within the experimental error.

The details and results of the fatigue crack growth tests are contained in Appendix Tables B-1 through B-12. Fatigue crack growth curves for each specimen are presented in the Results section with crack growth rate, da/dN, plotted against the fatigue stress intensity range, ΔK, on log-log scales.

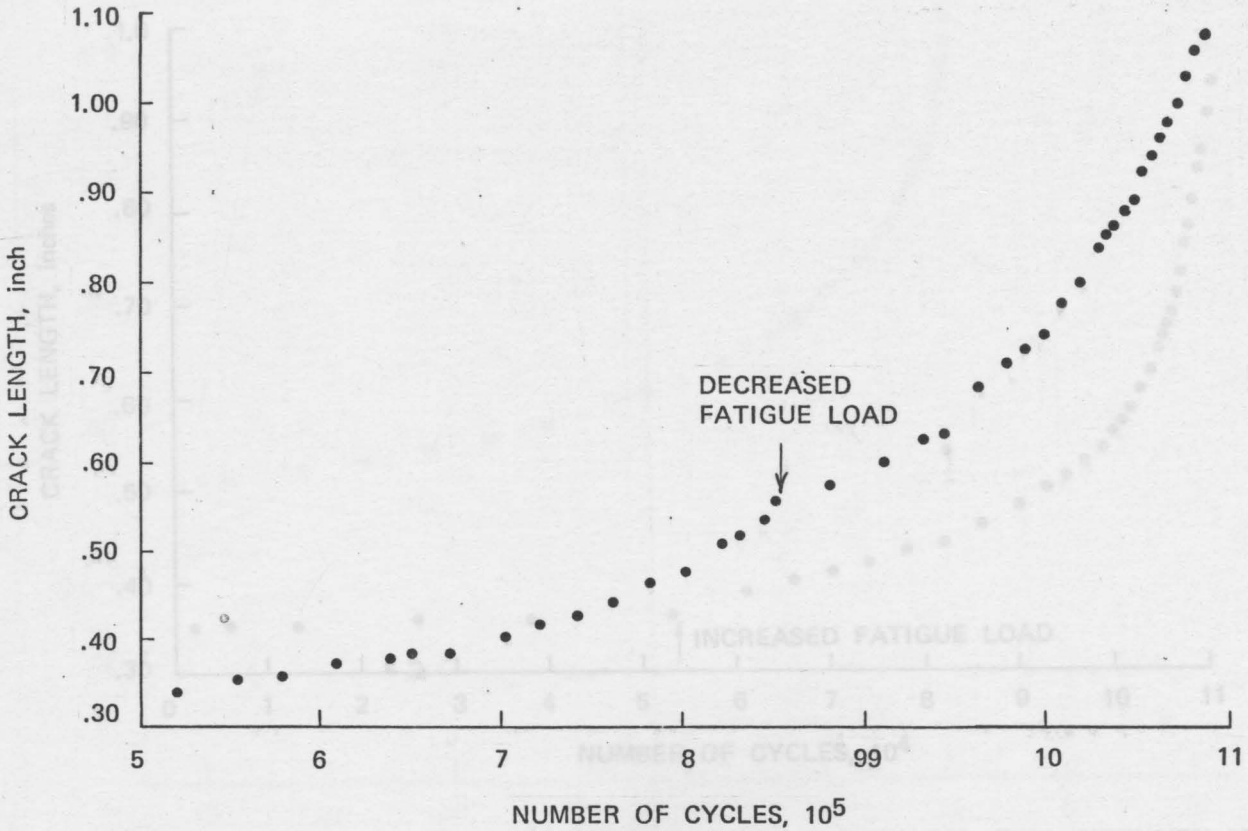

FIGURE 3 ' CRACK GROWTH CURVE FOR PURE ALUMINUM (SPECIMEN AF-7)

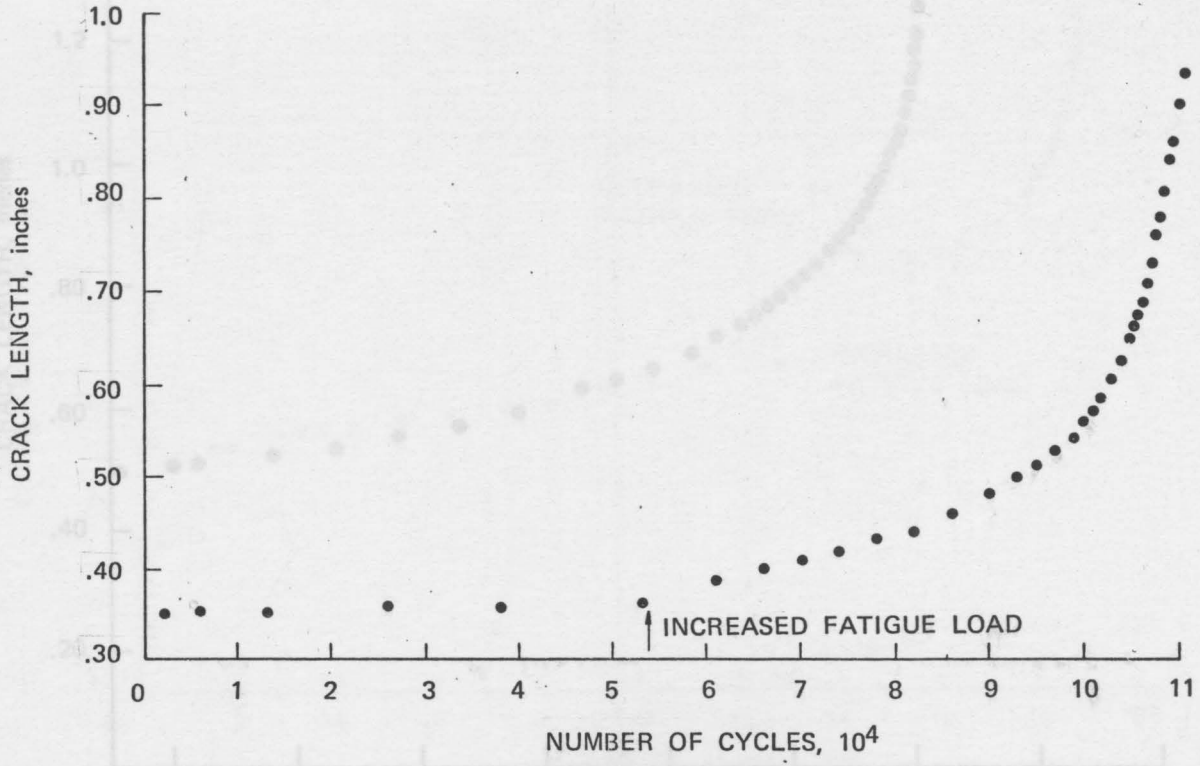

FIGURE 4 CRACK GROWTH CURVE FOR TYPE 304 STAINLESS STEEL (SPECIMEN SF-1)

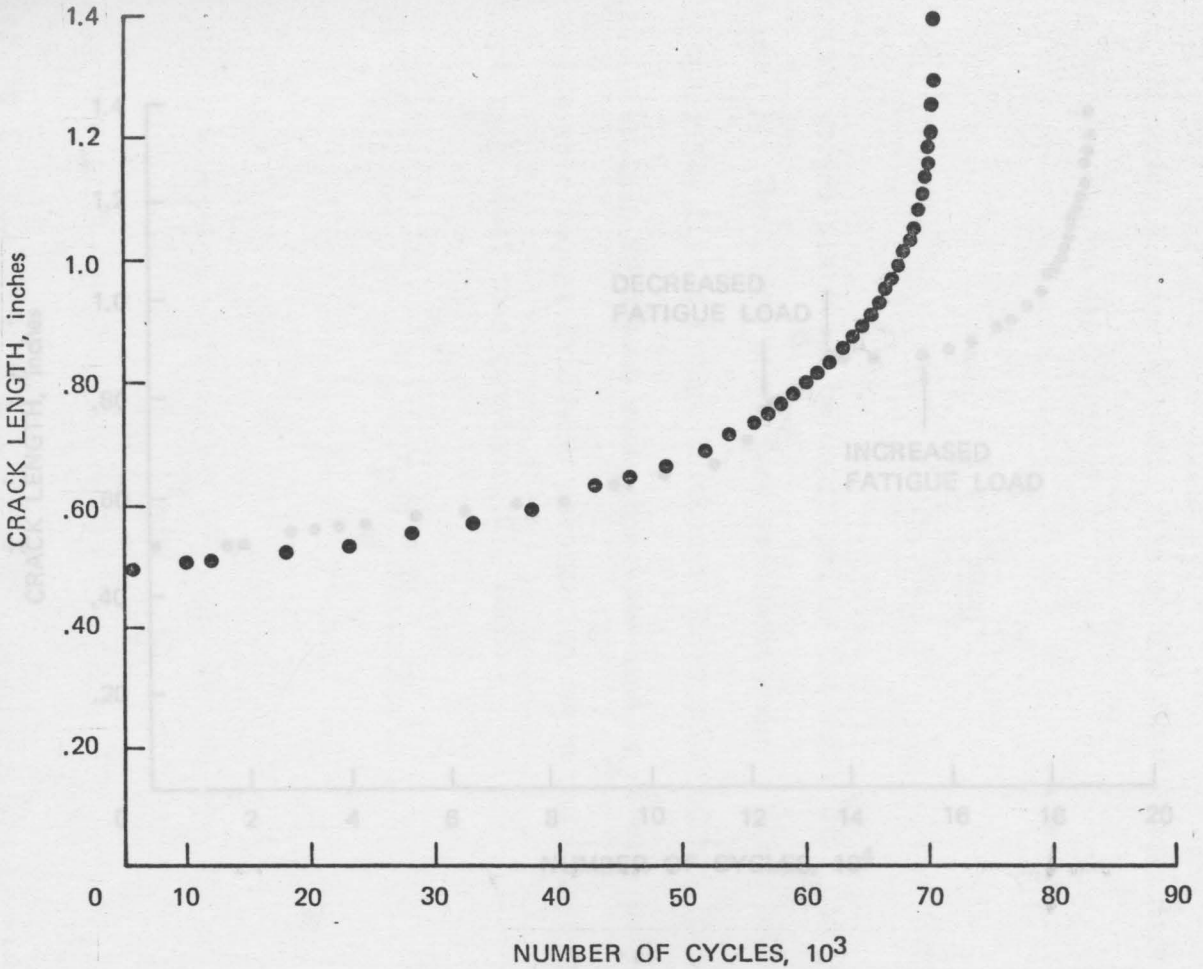

FIGURE 5 CRACK GROWTH CURVE FOR UNALLOYED TITANIUM (SPECIMEN PTF-6)

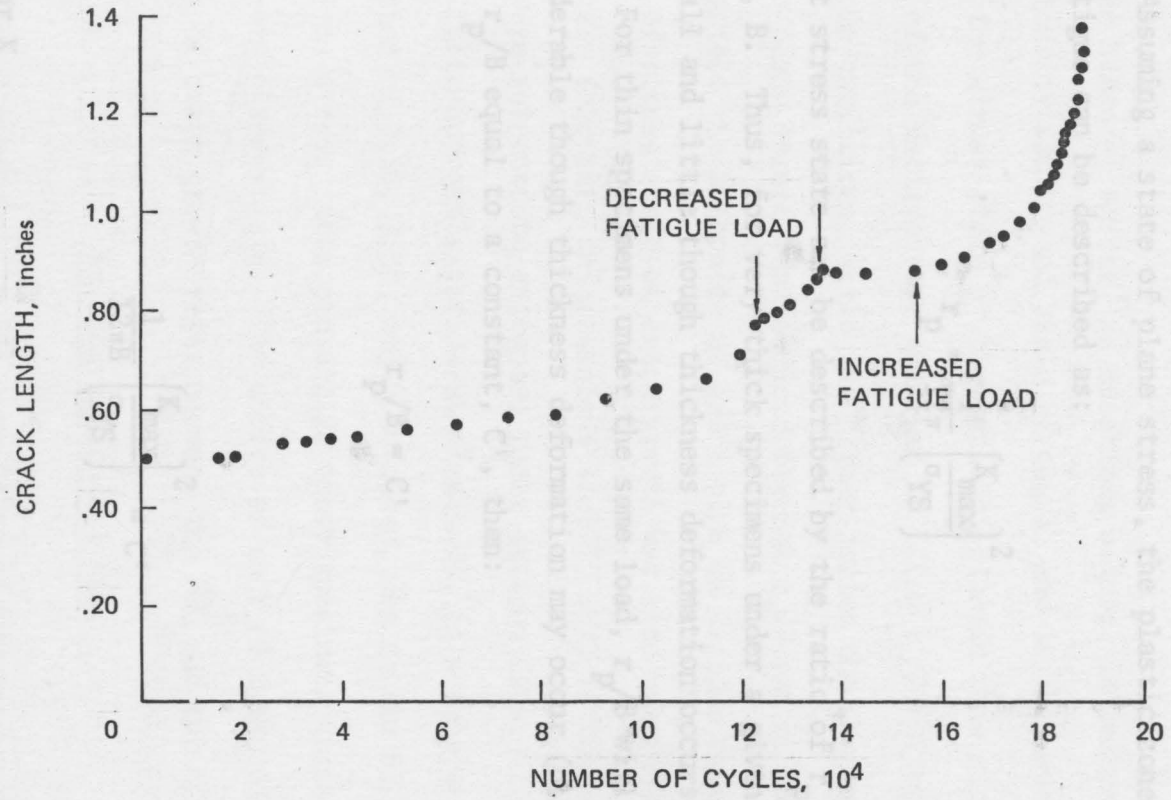

FIGURE 6 CRACK GROWTH CURVE FOR Ti-8% Al (SPECIMEN ATF-4)

When evaluating fatigue crack growth data as a function of grain size, changes in yield strength due to grain size differences should be taken into account. This can be accomplished by analyzing the fatigue data for a constant state of stress. Analysis of fatigue crack growth data by constant stress state is accomplished in the following manner. Assuming a state of plane stress, the plastic zone size, r_p, during fatigue can be described as:

$$r_p = \frac{1}{12\pi}\left(\frac{K_{max}}{\sigma_{YS}}\right)^2$$

A constant stress state can be described by the ratio of r_p to specimen thickness, B. Thus, for very thick specimens under a given load, r_p/B can be small and little though thickness deformation occurs (plane strain). For thin specimens under the same load, r_p/B will be large and considerable though thickness deformation may occur (plane stress). If we set r_p/B equal to a constant, C', then:

$$r_p/B = C'$$

or

$$\frac{1}{12\pi B}\left(\frac{K_{max}}{\sigma_{YS}}\right)^2 = C'$$

Solving for K_{max}

$$K_{max} = \sigma_{YS}\sqrt{12\pi BC'}$$

For R ratios near zero K_{max} will equal ΔK, and therefore:

$$\Delta K = \sigma_{YS} \sqrt{12\pi BC'}$$

This value of ΔK is that value at which the ratio r_p/B is equal to C' for a material of yield strength σ_{YS}.

The state of stress, as described before, is influenced by stress intensity factor and yield strength, and in this work, we have described the stress state by the ratio of plastic zone size, r_p, to the thickness of the fatigue test specimen, B. Low r_p/B ratios indicate plane strain conditions, while for higher ratios the stress state approaches plane stress conditions. Several r_p/B ratios were chosen in order to assess the influence of grain size on fatigue crack growth. The influence of stress state on crack growth was also examined. For the FCC materials (aluminum and stainless steel), r_p/B ratios of 0.50, 0.65, and 0.80 were selected to encompass their fatigue data. For the HCP materials (titanium and titanium-8% aluminum), it was necessary to select ratios of 0.10, 0.30, and 0.50 since, due to the higher yield strength, the stress state present in these specimens during testing tended toward plane strain. The choice of an r_p/B ratio of 0.50 allows comparison of crack growth rates between the FCC and the HCP systems.

Fractographic Analysis

Photomicrographs (≃4.5X) were taken of fracture surfaces typical of the aluminum, stainless steel, titanium, and titanium-8% aluminum fatigue specimens. These pictures illustrate the relative states of stress as revealed by flat or shear fracture and degree of through

thickness deformation present in the specimens. Fracture surfaces of fatigue test specimens were examined directly at high magnification using a Jeolco JSM-II scanning electron microscope. Fractographs (photomicrographs) depicting typical fracture surface features were taken at magnifications of 60, 100, and 1000 diameters. Direct measurements of interfatigue striation distances were recorded from the scanning electron microscope viewing screen at a magnification of 6000 diameters.

Fractographs were recorded from precisely located positions on the fatigue test specimens. Each fractograph in the Results contains an arrow indicating the direction of the macroscopic crack growth. Fractographs at 60 and 100 diameters magnification were taken at the notch area of the fatigue specimens and at 5 millimeter intervals, i.e., 0, 5, 10, 15, and 20 millimeter positions, measured from the notch root. These fractographs were illustrative of the variation in fracture mechanism as a function of fatigue stress intensity factor, which varied at these positions for the constant load fatigue tests. Fracture mechanism variations were catalogued with respect to fatigue stress intensity factor and grain size.

Fractographs at 1000 diameters were taken at the notch area of the fatigue specimens and at 2 millimeter intervals, i.e., 0, 2, 4, 6, 8, 10, 12, 14, 16, 18, 20, and 22 millimeter positions, measured from the notch root. These fractographs were illustrative of the variation in fine scale fatigue evidence, e.g., striation markings, which varied in size and spacing as a function of the fatigue stress intensity factor.

A measure of the rate of propagation of fatigue cracks on a microscale as a function of fatigue stress intensity factor was obtained for each specimen by determining the average spacing of fatigue striation markings at the appropriate positions. Averages were obtained by direct measure, at 6000 diameters magnification, on the scanning electron microscope screen at the notch area and at 1 millimeter intervals, measured from the notch root. Propagation rate as a function of stress intensity factor determined by this method was plotted and compared to similar results calculated from observations of macroscopic crack growth. Crack propagation data were also catalogued with respect to grain size.

For most materials there exists some continuum of stress intensity factors for which fatigue crack propagation is in essence a microplastic fracture process. This aspect of the fatigue process, for materials considered in this work, was investigated through the use of the high resolution technique of transmission electron fractography. Specifically, two comparisons between materials (including in this context comparison within materials between grain sizes) were made. These comparisons were a description of the nature and topology of fatigue striation markings for each material for (a) a condition of constant stress state (r_p/B, of 0.50), and (b) for constant crack propagation rate, i.e., 10^{-5} inches/cycle. The appropriate areas of fatigue fracture surfaces to be examined by transmission electron microscopy were selected on the basis of macroscopic crack propagation data.

Areas selected, using the preceding criteria, were replicated using 0.005-inch thick acetyl cellulose tape wetted with acetone. The

solvent used in replication was permitted to dry, then replica tapes were stripped from the fracture surfaces. To make a specimen suitable for examination in the transmission electron microscope, the replica tapes were "shadowed", then coated with approximately 1000 $\mathring{A}$ of carbon. The shadowing procedure consisted of deposition of a thin coating ($\sim$200 $\mathring{A}$) of palladium onto the replica tape surface at an angle of about 45°; the shadowing direciton was parallel to and in the direction of the macroscopic fatigue crack propagation direction--this provided a means of orientation in subsequent examination. Carbon coating was applied normal, or at an angle of 90°, to the shadowed replica tape while the replica tapes were rotated. A shadowed carbon replica fractograph was subsequently prepared after removing the primary acetyl cellulose replica material by dissolution and a series of washings in acetone. Replicas were examined in a Jeolco JEM 6-A transmission electron microscope using an accelerating potential of 50 kv over a range of magnifications (2000 to 10,000). Fractographs were taken at magnifications of 5000 diameters to show the microplastic detail of fatigue striations.

CHAPTER III

RESULTS

Microstructure

For this study three different grain sizes were produced in samples of each of the four materials, by heat treatment (see Procedure). These different microstructural conditions were sought for purposes of studying the effects of grain size on tensile and fatigue properties, ultimately seeking to determine grain size dependent fatigue crack propagation characteristics.

Each microstructural condition was analyzed metallographically to ascertain its general character. A mean linear intercept grain size was determined analytically for each condition for purposes of correlating mechanical properties and material grain size. Figures 7-10 illustrate the microstructural conditions which were employed in these studies of aluminum, stainless steel, titanium, and titanium-8% aluminum, respectively.

Grain sizes obtained are listed in the following table.

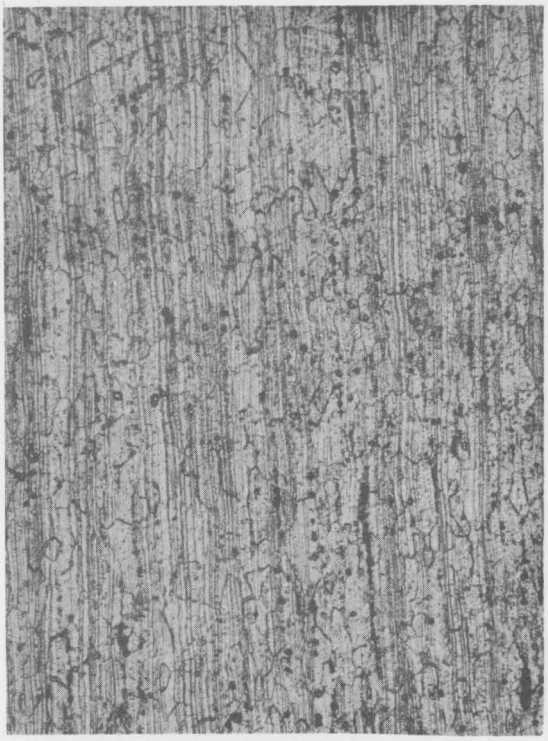

Grain Size = 20.4μm

Grain Size = 36.0μm

Grain Size = 81.8μm

Figure 7. Optical Photomicrographs Showing the Microstructure of Aluminum Fatigue Specimens.

(HF Etch)

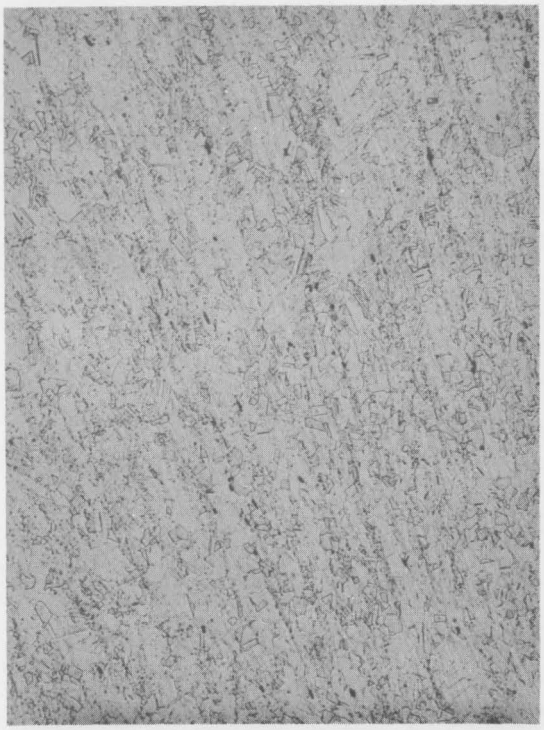

Grain Size - 11.0μm

Grain Size - 47.7μm

Grain Size = 79.6μm

Figure 8. Optical Photomicrographs at 100X Showing the Microstructure of Stainless Steel Fatigue Specimens.

(Electrolytic Oxalic Acid Etch)

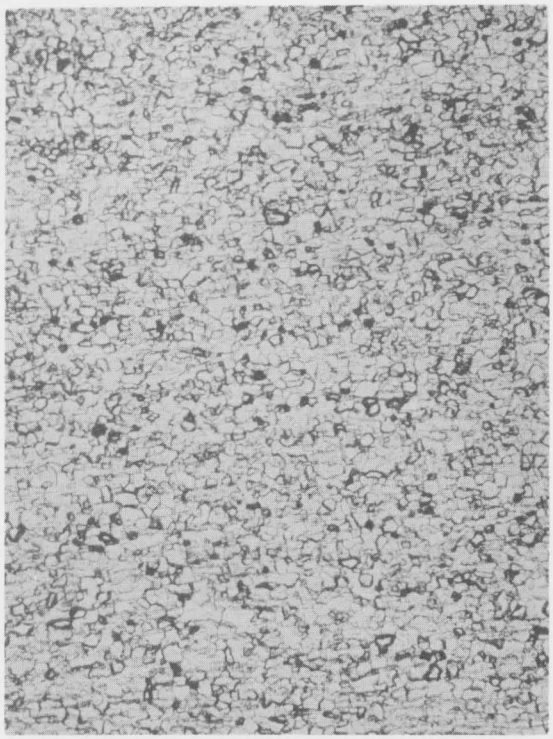

Grain Size = 11.7μm

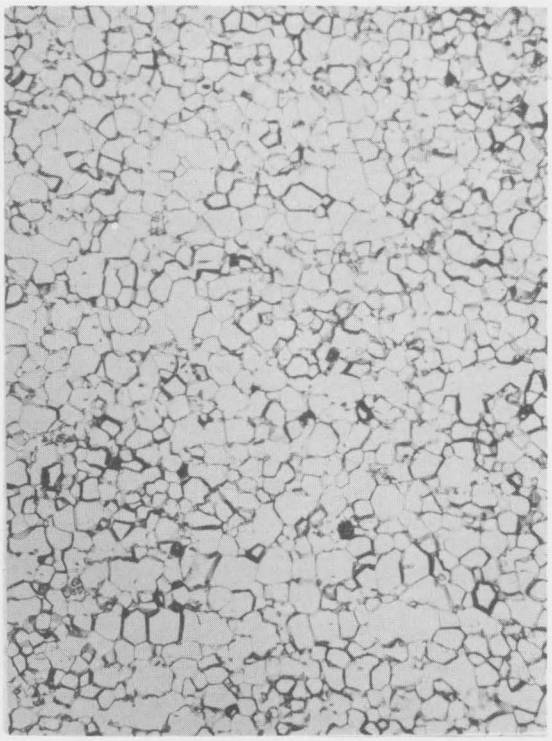

Grain Size = 23.1μm

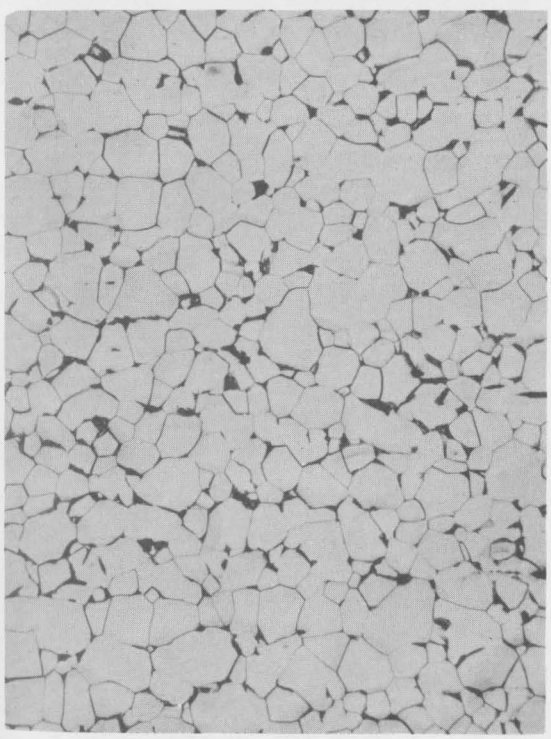

Grain Size = 35.4μm

Figure 9. Optical Photomicrographs at 100X Showing the Microstructure of Titanium Fatigue Specimens.

($HF-HNO_3$ Etch)

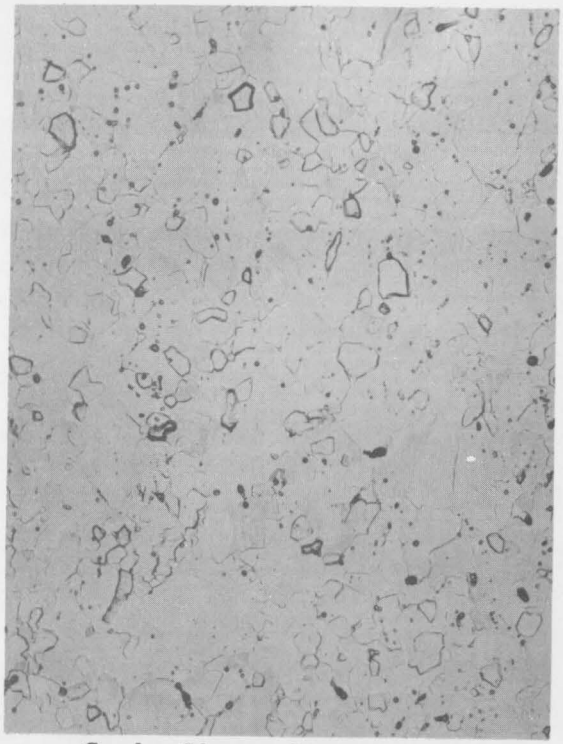

Grain Size = 29.4μm

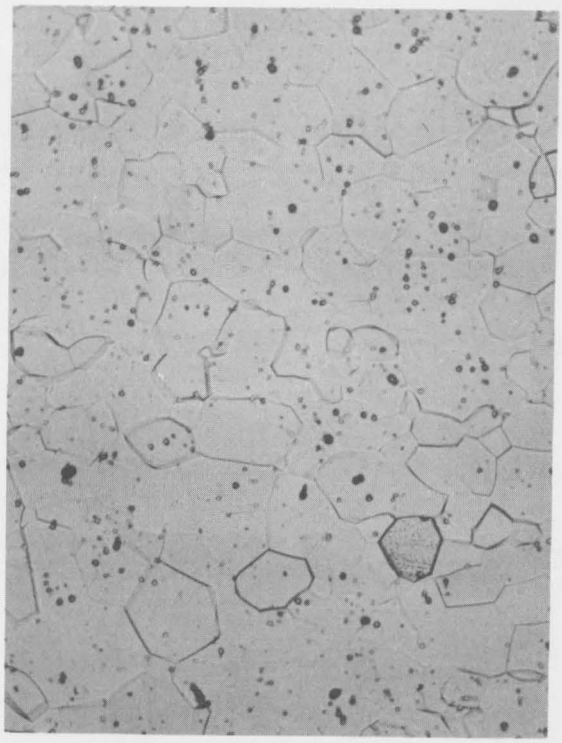

Grain Size = 60.1μm

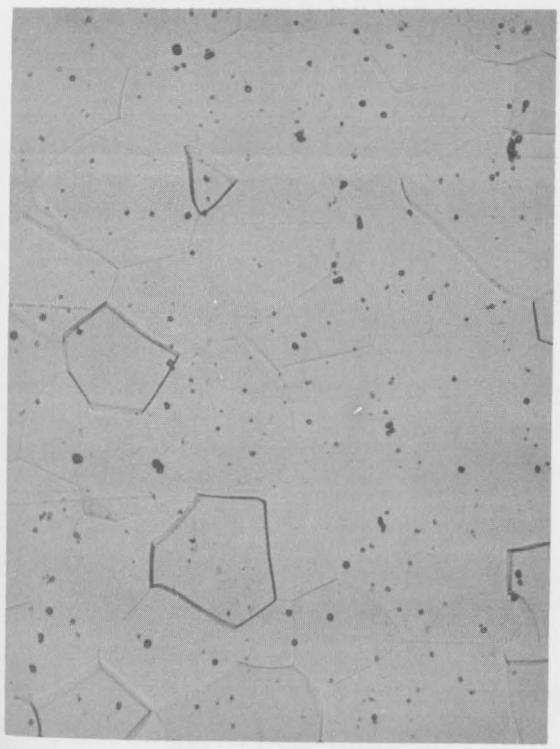

Grain Size = 137.5μm

Figure 10. Optical Photomicrographs at 100X Showing the Microstructure of Titanium-8% Aluminum Alloy Fatigue Specimens.

($HF-HNO_3$ Etch)

TABLE 4

MATERIAL GRAIN SIZES

Material	Small Grain Size (Microns)	Medium Grain Size (Microns)	Large Grain Size (Microns)
Aluminum	20.4	36.0	81.8
Stainless Steel	11.0	47.7	79.6
Titanium	11.7	23.1	35.4
Titanium-8% Aluminum	29.4	60.1	137.5

It should be observed that regions of grain size overlap were obtained for all materials. Thus, comparisons for constant grain size were possible through interpolation of data.

The maximum grain size obtainable in titanium was restricted due to a limited amount of stored energy of cold work in the "as received" condition. This material was purchased from Reactive Metals, Inc. in a heat-treated condition. The titanium-8% aluminum was obtained in a hot-rolled condition containing sufficient stored energy for substantial grain growth by further heat treatment. Aluminum and stainless steel were heavily cold-worked then heat treated to derive a large range of grain sizes.

Microstructural Analysis

Aluminum

All microstructures prepared in aluminum were fully recrystallized and consisted of relatively equiaxed grains. Some tendency toward

duplex grain size was exhibited in the larger grained specimens. It should be noted that the inclusion content of this material was relatively high, in spite of the fact that high purity melt stock was used in the preparation. X-ray analysis of the inclusions by electron microprobe showed that they were relatively high in iron content. It is believed that this iron contamination was picked up in the melting practice since the facility employed had previously been used in melting ferrous alloys. No other unusual microstructural features were noted in the aluminum. Mechanical polishing resulted in the superficial cold work effects noticeable in Figure 7.

Stainless Steel

All microstructures were fully recrystallized, however grain size distributions varied between the small and the two larger grain size specimens. The small grain specimen exhibited a duplex grain phenomenon with grains in some portions of the microstructure in more advanced stages of growth than others. All grains exhibited twinning. In addition to these microstructural aspects, a heavy dispersion of random chromium carbides was observed distributed throughout the microstructure. The carbide dispersion apparently resulted from heat treatment near the carbide solvus temperature.

In contrast to the fine-grained stainless steel the large-grained specimens exhibited little dispersed chromium carbide in their microstructures. The latter were heat treated at higher temperatures (above the carbide solvus temperature) resulting in substantially

greater grain growth. Both of these conditions exhibited some tendency toward duplex grain structure (endemic to stainless steels) and considerable twinning.

The grain sizes measured for stainless steel samples were based on both twin boundary and grain boundary content. This procedure is recommended by investigators[31] who suggest that both twin (low angle) and grain (high angle) boundaries should be considered in attempts to correlate mechanical properties and grain size.

Titanium

All titanium microstructures were fully recrystallized and exhibited essentially equiaxed grains, with little duplex grain structure. Microstructures of the two smallest grain size conditions were clearly single phase and all were low in inclusion content. The largest grained specimen exhibited some secondary phase separation at grain boundaries; this phase was not identified but was thought to be transformed β-phase titanium.

Titanium-8% Aluminum

All titanium-8% aluminum microstructures were fully recrystallized. The smallest grain size sample exhibited an irregular and somewhat duplexed grain structure which may be the result of prior hot working history. The two larger grain size samples, on the other hand, exhibited quite equiaxed grain structure and little duplex grain structure. All microstructures exhibited a random dispersion of either secondary phase or inclusion particles. These were not identified.

Substructure

It is generally held that subgrain structures in materials contribute substantially to controlling their fatigue crack propagation rates. Depending upon material, different characteristic substructure configurations are possible; thus, variance in slip band character and dislocation densities and arrangements occur. The precise substructure array in a given material is determined by its basic property of stacking fault energy which is a function of crystal structure and the sizes and arrangements of atoms in the crystal.

Substructures form as a result of plastic deformation of the crystal, such as in the plastic zone at the tip of fatigue cracks. Subsequently, as fatigue cracks proceed through the substructures of the plastic zones, the nature and geometrical aspects of this substructure exerts some influence on the kinetics of crack propagation. This control is thought to be through a process of plastic blunting of the crack tip. Two modes by which control might be exerted involve (1) propagation through preferred substructural paths and (2) propagation interrupted by intersection of substructure. In either event it is believed that substructural dislocation arrangements tend to interact with the propagating fatigue crack.

Thus, it is important to determine the nature of substructure in the materials under study to provide some qualitative means of interpreting differences in crack propagation rate due to substructural differences. Numerous research papers have been published on this subject[32, 33, 34, 35, 36].

Thin foil specimens were prepared from the fatigue crack plastic zones which had formed during tests of each of the four materials studied. The specimens were examined extensively by transmission electron microscopy. The areas selected for study were representative of portions of the fatigue specimen exhibiting flat fracture surfaces.

Aluminum

Aluminum plastic zone substructure consisted of a cellular arrangement of dislocations. See Figure 11. There were no slip bands in evidence. Tangled dislocations were present in cell boundaries and cell interiors exhibited generally low dislocation density. These findings can be considered consistent with the classical deformation patterns in aluminum[37] and indicative of relatively high characteristic stacking fault energy. Further, the cellular arrangement and absence of slip band substructure imply that easy cross slip of dislocations occurred in the plastic zone of the fatigue cracks in aluminum.

Stainless Steel

The dislocation substructure of the plastic zone of stainless steel contrasted markedly to that of aluminum. See Figure 12. It should be noted that many persistent slip bands of various orientations were formed in the stainless steel. Dislocations were for the most part confined to slip bands. These observations may also be considered classical evidence indicative of a relatively low stacking fault energy[37]. The fact that dislocations were confined to slip bands implies that cross slip was difficult in the plastic zones of fatigue cracks of this material.

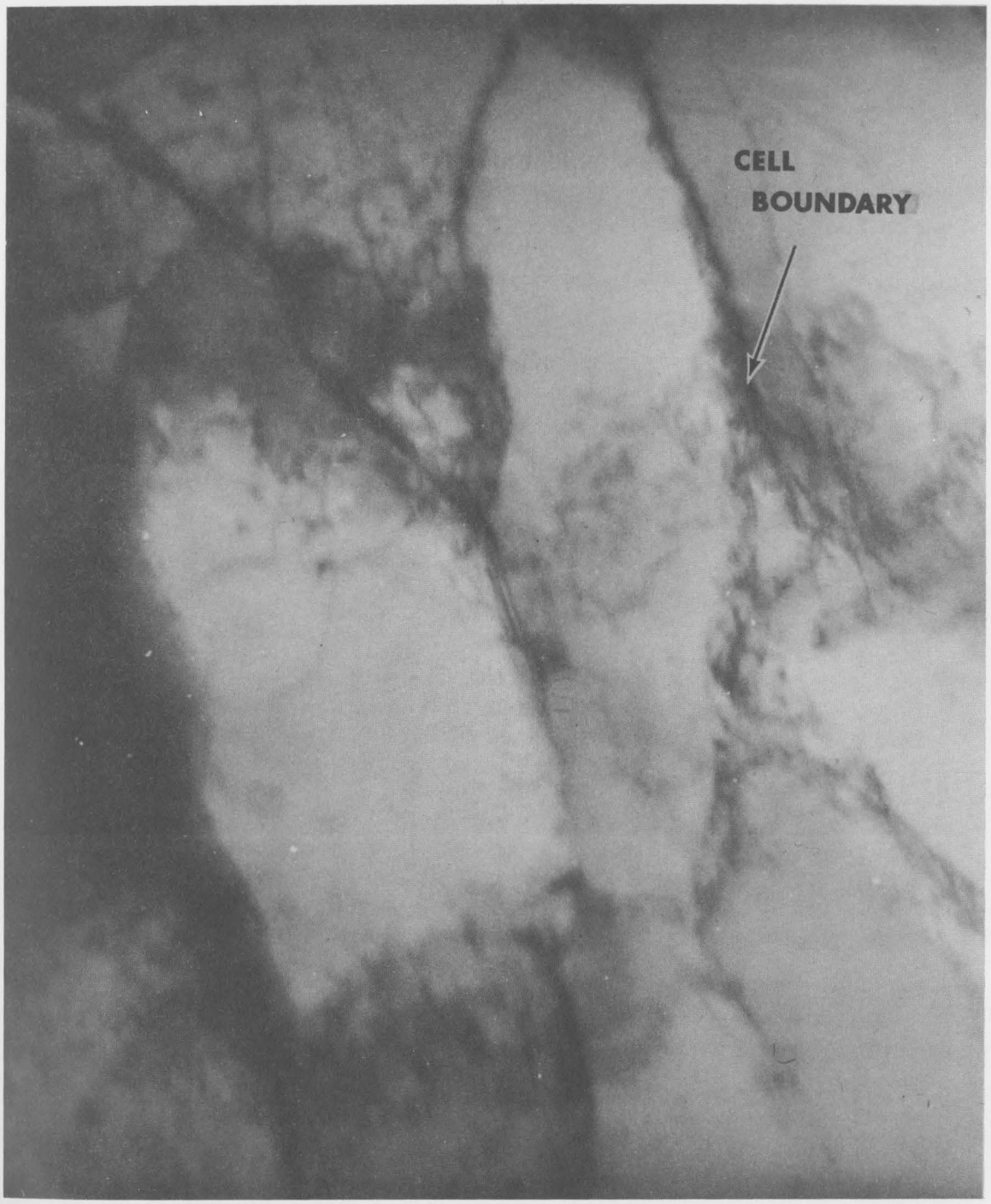

Figure 11. Transmission Electron Microscope Photomicrograph of Thinned Foil from Aluminum Specimen at 40,000X Showing Dislocation Arrangements in the Plastic Zone of the Fatigue Crack.

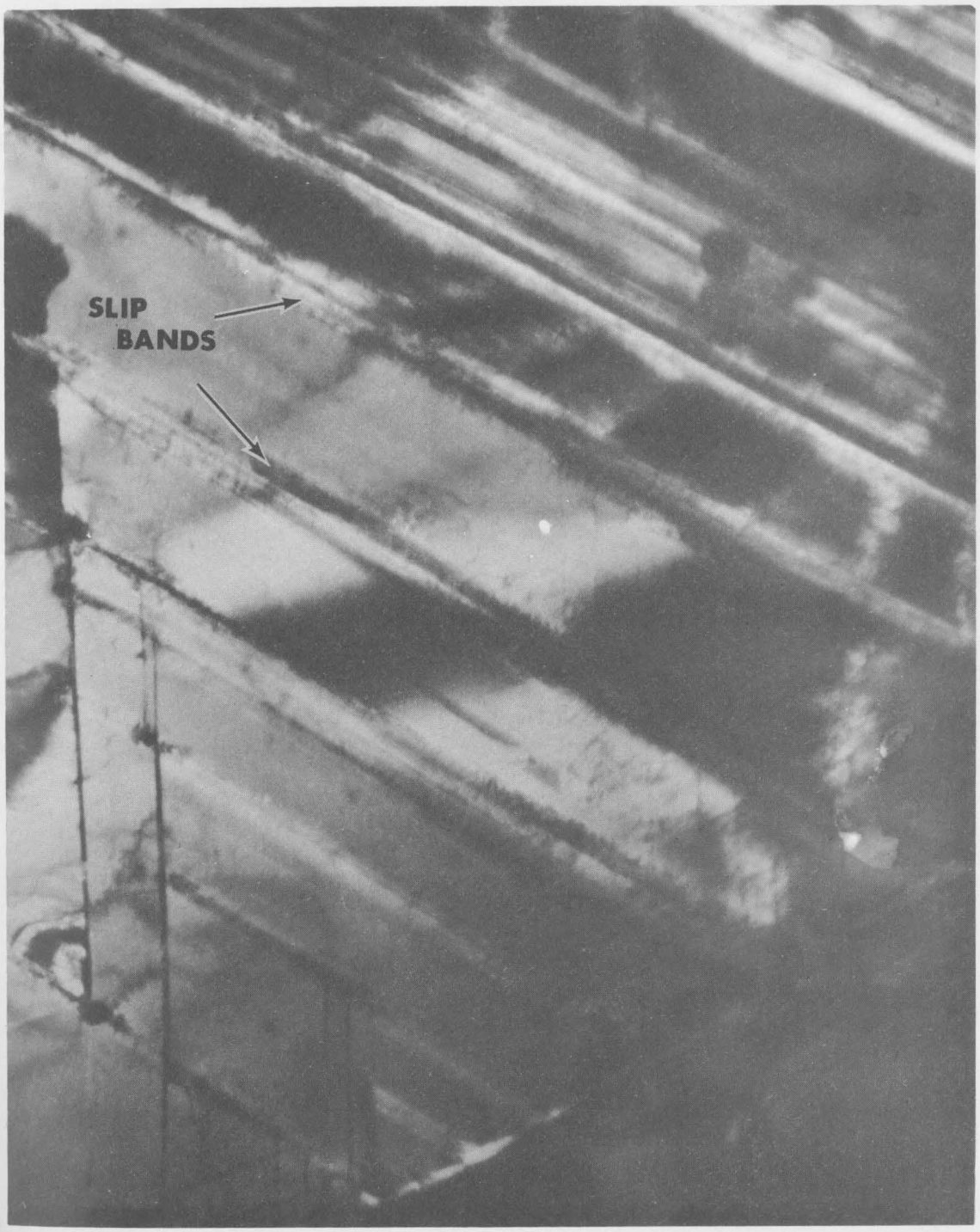

Figure 12. Transmission Electron Microscope Photomicrograph of Thinned Foil from Stainless Steel Specimen at 25,000X Showing Dislocation Arrangements and Substructure in the Plastic Zone of the Fatigue Crack.

Titanium

Much less is known of the deformation substructures of HCP materials as compared to FCC substructures. In titanium, we observed that dislocations were arrayed in a network configuration, consisting of mutually perpendicular dislocations. See Figure 13. There were indications of linear substructural features of relatively small mutual misorientation as indicated by differences in diffraction contrast, but no tendency toward dislocation sub-boundary formation or of persistent slip band formation. The dislocation network appeared to be a quite stable planar configuration, suggesting that component dislocations were sessile in character. It was not possible to assess the relative stacking fault energy on the basis of comparison to literature examples as was possible for the FCC materials. However, the apparently sessile dislocation configuration suggested the probability that cross slip would be difficult and from this it may be inferred that stacking fault energy was probably relatively low.

Titanium-8% Aluminum

Titanium-8% aluminum exhibited a fatigue crack plastic zone substructure which in some respects resembled that formed in stainless steel. See Figure 14. Close inspection showed that indeed substantial numbers of slip bands had formed, and that dislocations were present in the slip bands and also in irregular network arrangements. There was a significant difference in the slip band dislocation geometry as compared to that in stainless steel. In titanium-8% aluminum, dislocations were oriented either at an angle to or parallel to the axis of

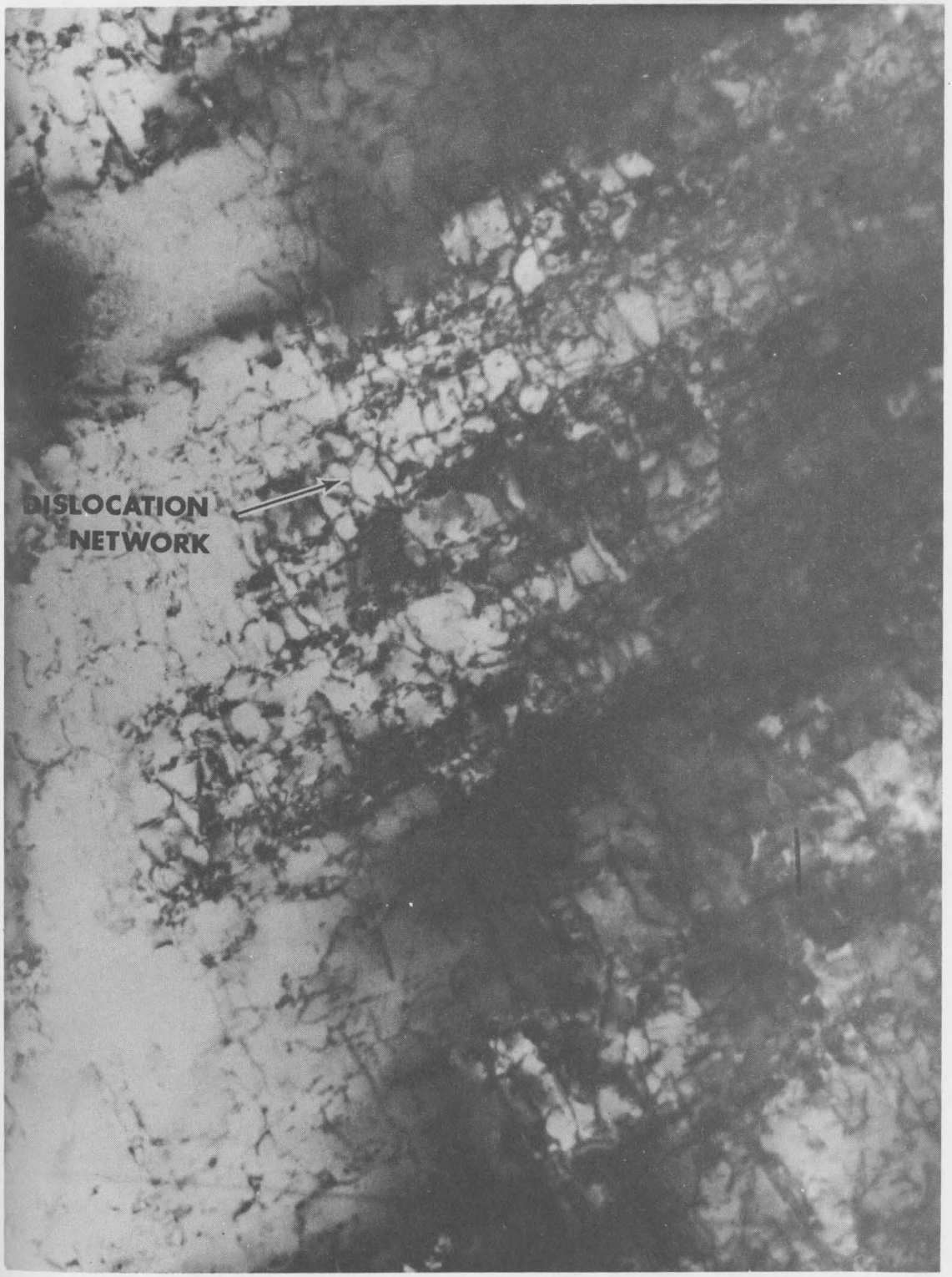

Figure 13. Transmission Electron Microscope Photomicrograph of Thinned Foil from Titanium Specimen at 26,000X Showing Dislocation Arrangements in the Plastic Zone of the Fatigue Crack.

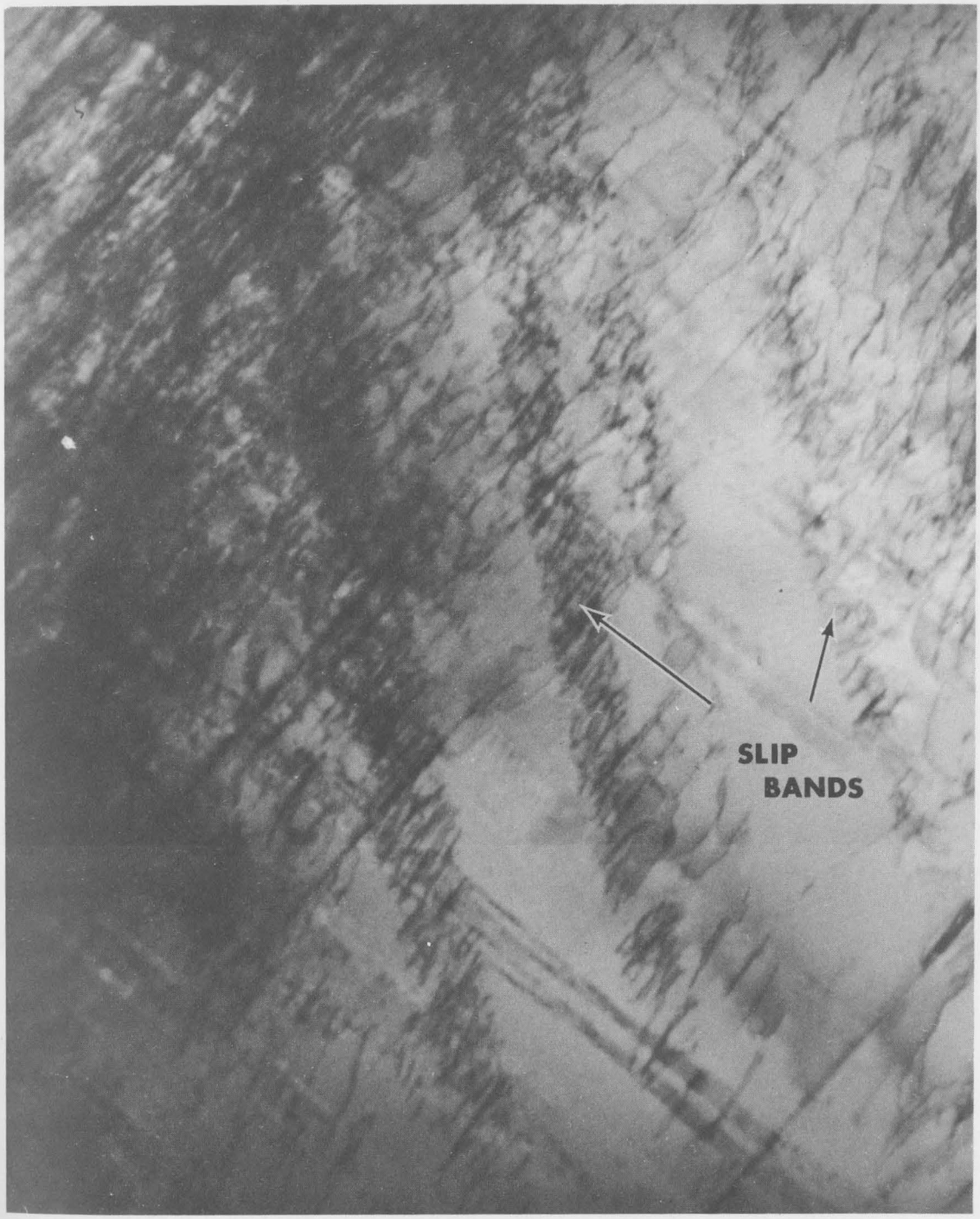

Figure 14. Transmission Electron Microscope Photomicrograph of Thinned Foil from Titanium - 8% Aluminum Specimen at 18,000X Showing Dislocation Arrangements in the Plastic Zone of the Fatigue Crack.

the slip bands, and apparent dislocation interactions were noted. Whereas in stainless steel the dislocations tended to be isolated and oriented perpendicular to the axes of slip bands.

Clearly the substructure of titanium-8% aluminum was for the most part planar and there was little evidence of cross slip of dislocations. Therefore, we conclude that the stacking fault energy of the alloy was somewhat lower than that of the pure titanium.

Tensile Properties

In order to ultimately apply the desired fracture mechanics and plastic zone size analysis to fatigue data it was necessary to obtain tensile yield stress data for each of the material conditions studied. This was done by running tensile tests for each grain size condition for each material. In addition to the readily obtained tensile data, the strain hardening exponent was derived for each tensile test condition. Strain hardening exponent is a relatively sensitive indicator of material deformation character. Since fatigue is essentially a microdeformation process, strain hardening exponent was sought as an independent indicator of potential material performance.

All tensile test data are presented in the following Table 5.

TABLE 5

TENSILE PROPERTIES

Material	Grain Size, in.	UTS psi	0.2% YS psi	Elong %
Type 304 Stainless Steel	4.33×10^{-4} (48.0) [a]	90,200	34,200	59.5
	18.8×10^{-4} (23.1)	87,100	27,000	74.2
	31.3×10^{-4} (17.9)	82,100	25,500	78.0
Pure Aluminum	8.03×10^{-4} (35.3)	11,600	5,500	50.0
	14.2×10^{-4} (26.6)	11,200	5,700	50.0
	32.2×10^{-4} (17.6)	11,200	5,900	50.0
Ti-8% Al	11.6×10^{-4} (29.4)	107,800	102,900	16.8
	23.7×10^{-4} (20.6)	99,600	97,500	13.8
	54.1×10^{-4} (13.6)	95,000	93,300	8.0
Unalloyed Titanium	4.61×10^{-4} (46.6)	94,500	80,600	50.0
	9.09×10^{-4} (33.2)	91,800	75,100	26.8
	13.9×10^{-4} (26.8)	91,800	73,200	24.0

[a] Number in parentheses is $d^{-1/2}$

There is a well known relationship between grain size and tensile properties established by Hall and Petch wherein an essentially linear relationship exists between properties and the inverse square root of grain size, $d^{-1/2}$. Thus, we show in Figures 15 through 18 the

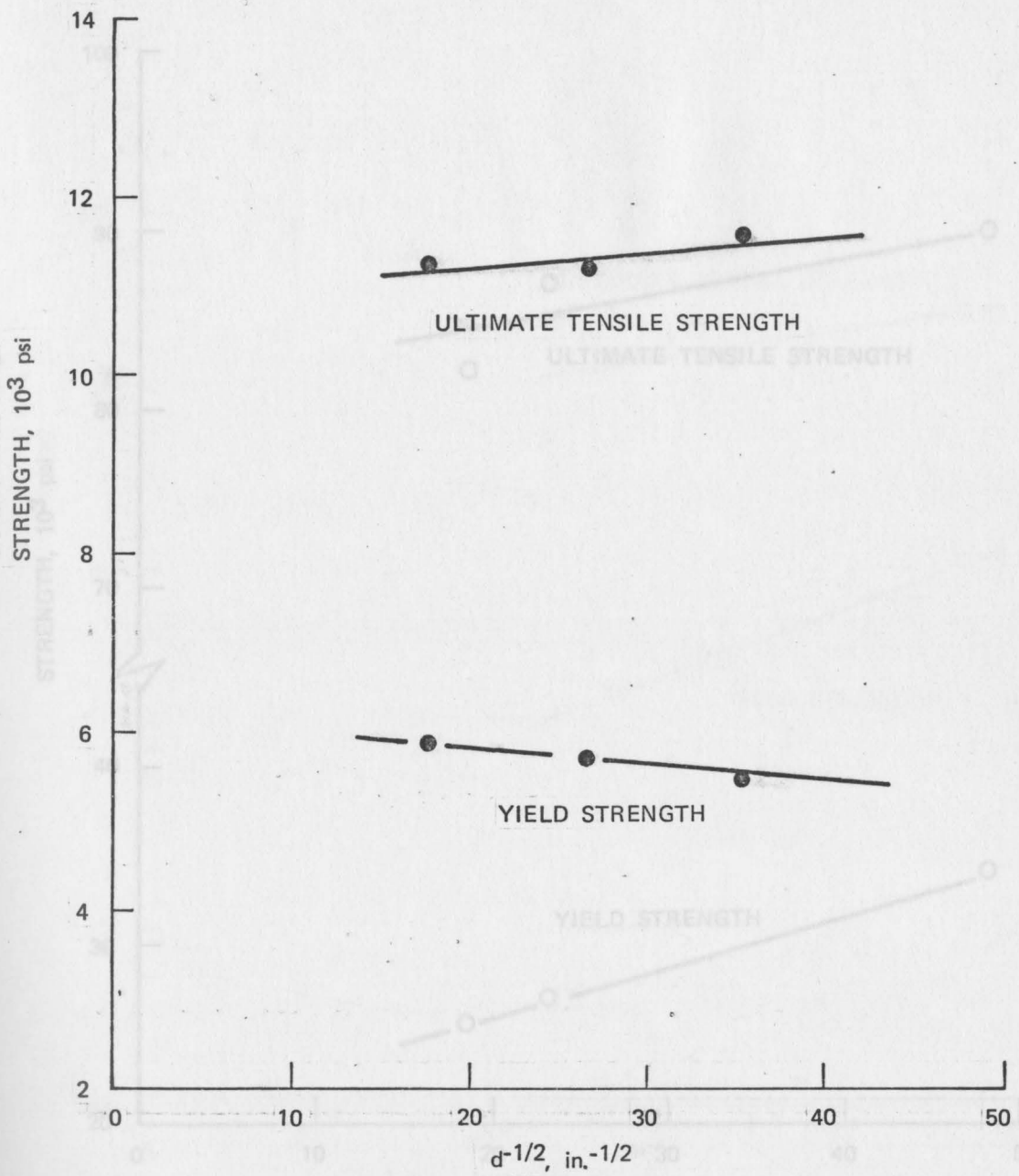

FIGURE 15 INFLUENCE OF GRAIN SIZE ON THE TENSILE PROPERTIES OF ALUMINUM

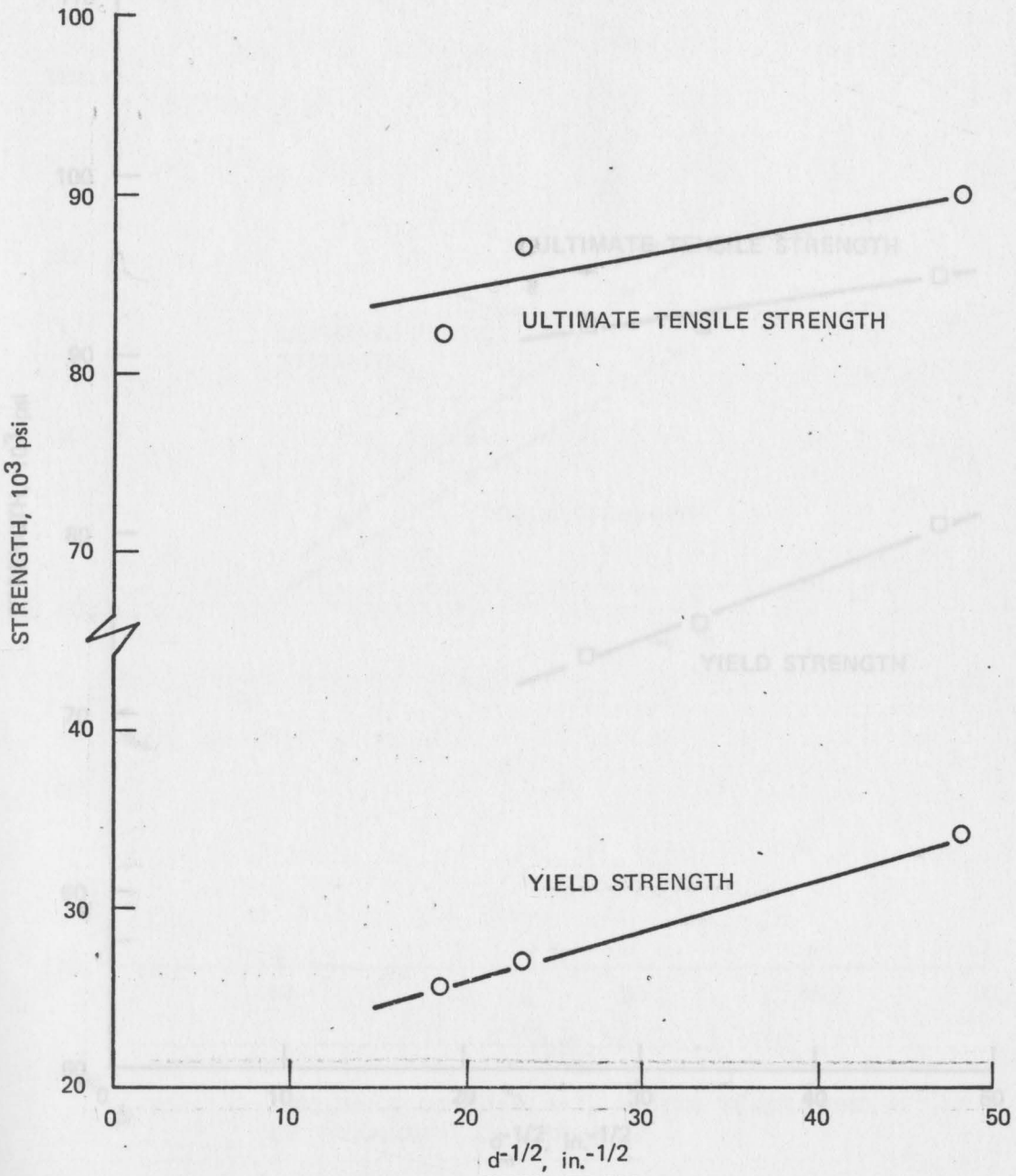

FIGURE 16 INFLUENCE OF GRAIN SIZE ON THE TENSILE PROPERTIES OF STAINLESS STEEL

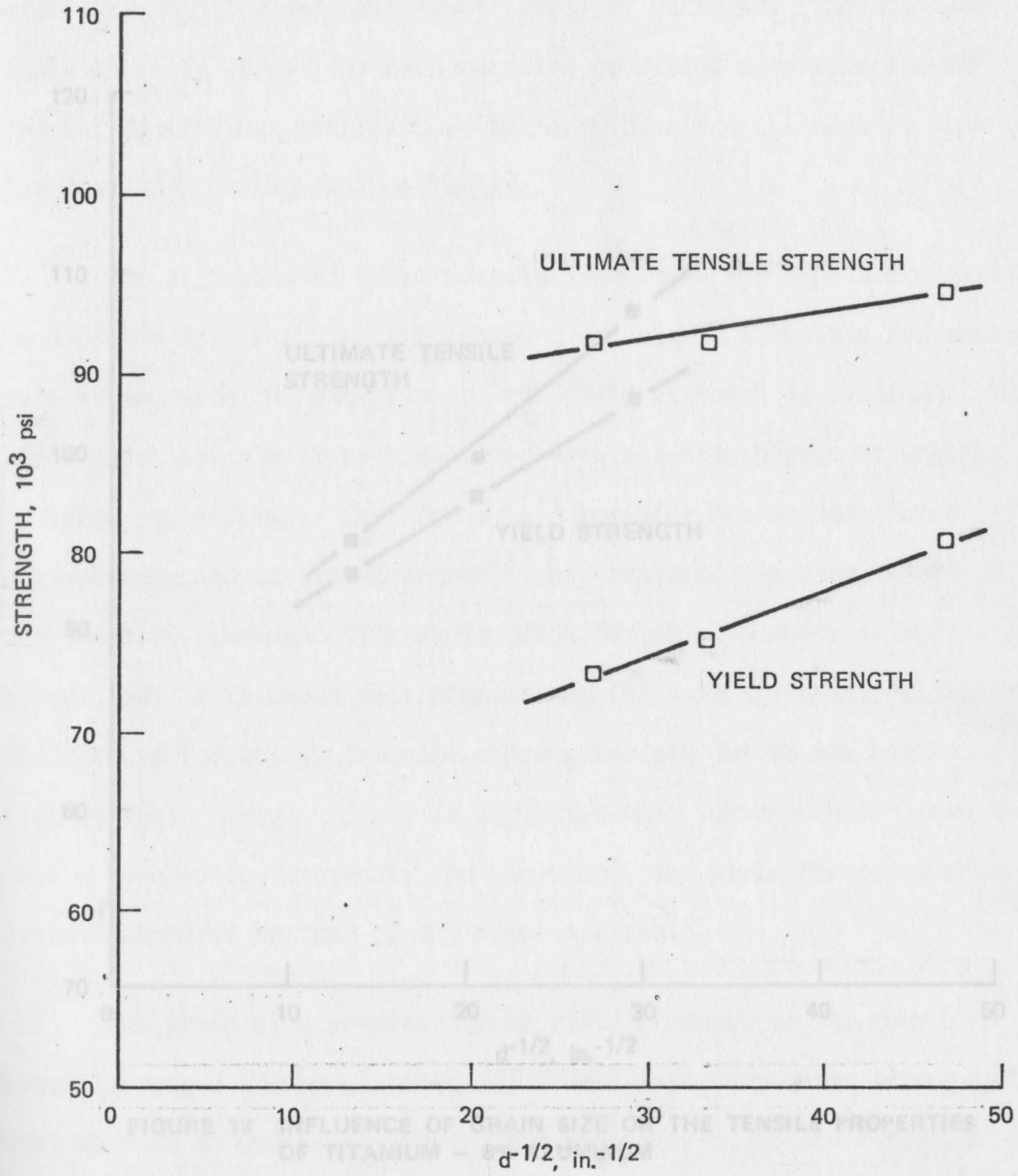

FIGURE 17 INFLUENCE OF GRAIN SIZE
ON THE TENSILE PROPERTIES OF TITANIUM

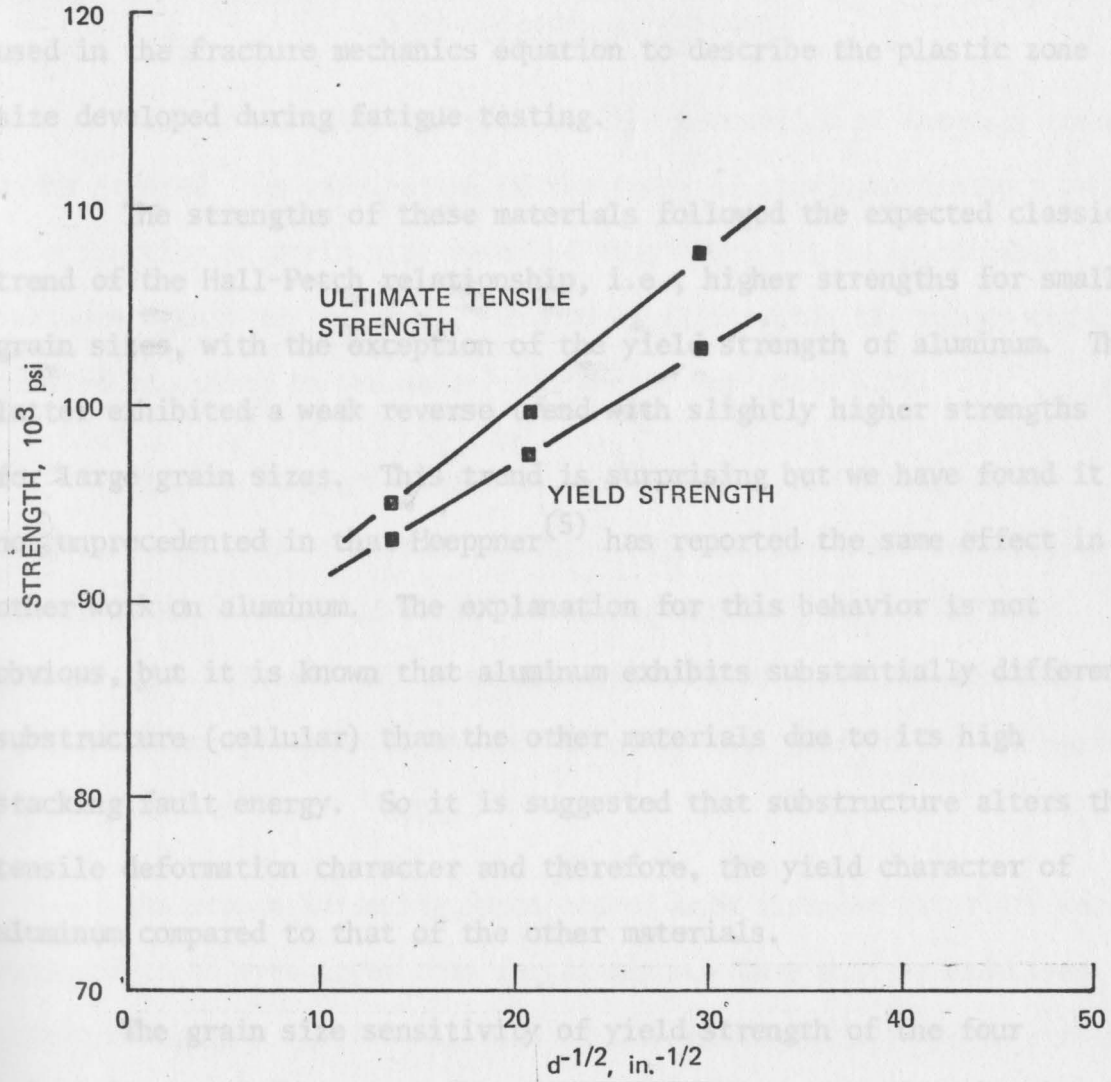

FIGURE 18 INFLUENCE OF GRAIN SIZE ON THE TENSILE PROPERTIES OF TITANIUM – 8% ALUMINUM

relationship between grain size and both ultimate and 0.2% off-set yield strength of aluminum, stainless steel, titanium, and titanium-8% aluminum, respectively. These figures show that the four different materials exhibit widely different levels of strength. The absolute levels of yield stress for each material condition were subsequently used in the fracture mechanics equation to describe the plastic zone size developed during fatigue testing.

The strengths of these materials followed the expected classical trend of the Hall-Petch relationship, i.e., higher strengths for smaller grain sizes, with the exception of the yield strength of aluminum. The latter exhibited a weak reverse trend with slightly higher strengths for large grain sizes. This trend is surprising but we have found it not unprecedented in that Hoeppner[5] has reported the same effect in other work on aluminum. The explanation for this behavior is not obvious, but it is known that aluminum exhibits substantially different substructure (cellular) than the other materials due to its high stacking fault energy. So it is suggested that substructure alters the tensile deformation character and therefore, the yield character of aluminum compared to that of the other materials.

The grain size sensitivity of yield strength of the four materials ranged from negligible for aluminum to strong for titanium-8% aluminum with moderate sensitivity for stainless steel and titanium. McEvily and Johnston have recently reported that for increased difficulty of cross slip in materials, the slope of yield stress/grain size curves increase[25]. Their findings are reflected precisely in our results of Figures 15 through 18. Here it is observed that there is no

strong yield stress/grain size dependency in the easy cross slip material (aluminum), but a tendency for increasing slopes reflecting a stronger dependency for the difficult cross slip materials; stainless steel, titanium, and titanium-8% aluminum, in that order.

Strain Hardening Exponent

Table 6 contains the plastic flow properties of material conditions studied. An examination of the value of strain hardening exponent as a function of grain size revealed that there was no appreciable variance within any material. Figure 19 illustrates the values obtained plotted according to the Hall-Petch method for grain size.

Of greater significance in these data is the difference in relative magnitude of strain hardening exponent for these materials. Generally high values of strain hardening exponent imply difficult plastic flow. Therefore, in comparing stainless steel and aluminum strain hardening exponents one may conclude that plastic flow is easier in the aluminum (lower value).

The strain hardening exponents of both titanium materials were observed to be even lower than for aluminum. Care must be exercised in interpreting this result. In view of the relatively high yield stress values for titanium materials compared to both aluminum and stainless steel, it would seem that the appropriate interpretation could be: once yielding is initiated, plastic flow is easier in the titanium materials but at much higher stress levels. This must be a rather localized plastic deformation phenomenon in titanium materials due to

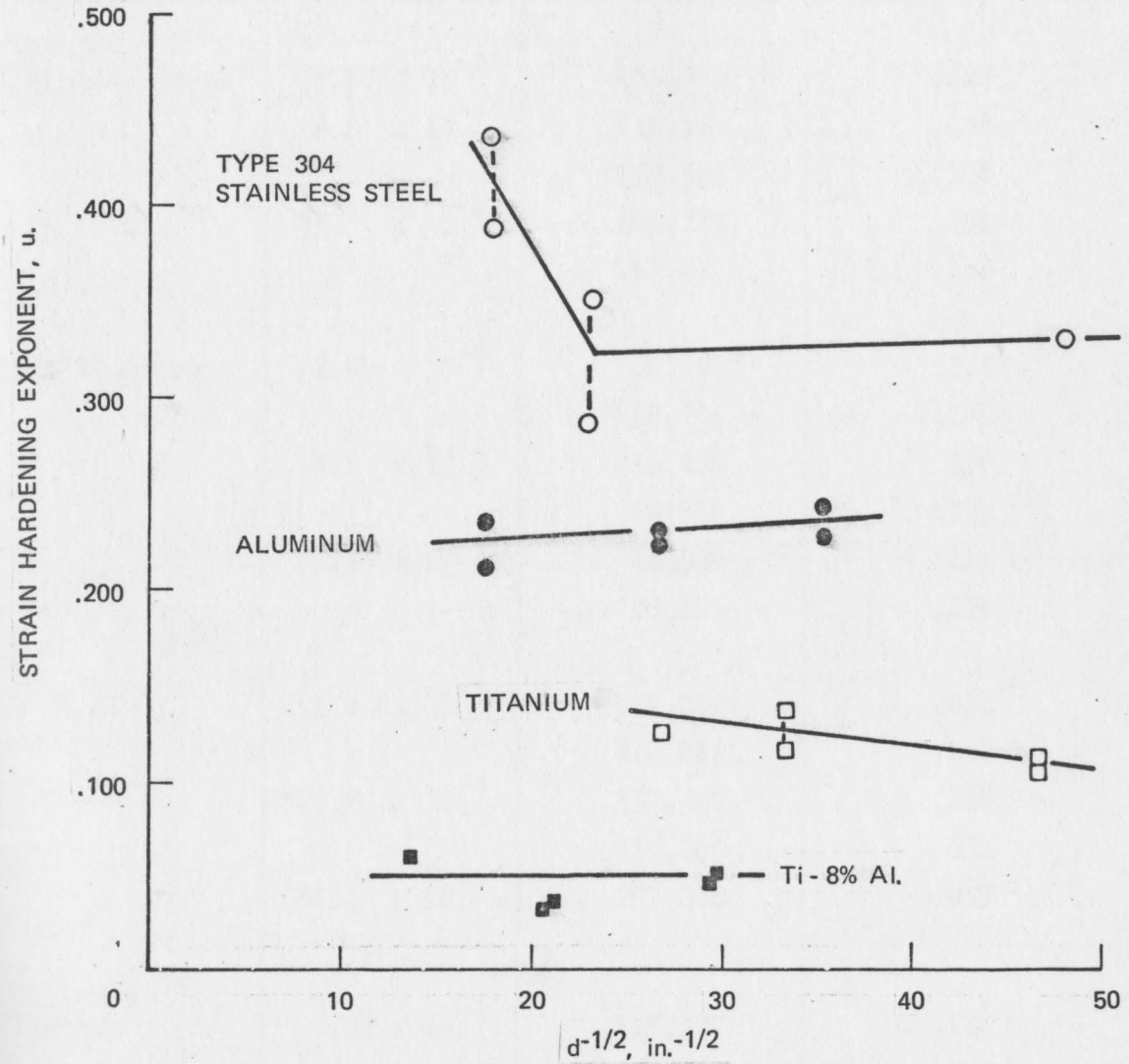

FIGURE 19 INFLUENCE OF GRAIN SIZE ON STRAIN HARDENING EXPONENT

their limited number of possible slip systems. It is also of interest to note that the strain hardening exponent for titanium was greater than for titanium-8% aluminum, implying easier plastic deformation in the latter material, in spite of its higher yield stress.

TABLE 6

PLASTIC FLOW PROPERTIES[a]

Material	Grain Size, in.	Strength Coefficient, A	Strain Hardening Exponent, n
Type 304 Stainless Steel	4.33×10^{-4}	163,962	.329
	18.8×10^{-4}	118,828	.286
		139,586	.350
	31.3×10^{-4}	166,236	.434
		147,472	.388
Pure Aluminum	8.03×10^{-4}	20,208	.225
		20,706	.242
	14.2×10^{-4}	19,430	.229
		19,550	.221
	32.2×10^{-4}	18,608	.211
		20,103	.234
Ti-8% Al	11.6×10^{-4}	132,227	.053
		128,911	.045
	23.7×10^{-4}	117,406	.038
		114,306	.032
	54.1×10^{-4}	117,318	.059
Unalloyed Titanium	4.61×10^{-4}	133,202	.110
		131,702	.104
	9.09×10^{-4}	137,274	.136
		132,107	.115
	13.9×10^{-4}	134,918	.124

[a] From strain hardening equation $\sigma = A\varepsilon^n$

The indications of relative plastic character within crystal systems, i.e., stainless steel < aluminum for the FCC system, and titanium < titanium-8% aluminum for the HCP system according to strain hardening exponent value, were in fact demonstrated in their relative fatigue crack propagation rate data which reflects the microplastic deformation character of the materials. However, the strain hardening exponent values were not useful indicators of relative plasticity as regards fatigue propagation in contrasts made between the two crystal systems. As is discussed in more detail later, this fact is attributed to the very marked difference in character of FCC and HCP crystal structures.

Macroscopic Crack Growth

Fatigue crack growth data were obtained for each grain size condition of each material using single edge notched (SEN) fatigue crack propagation specimens. In such tests the fracture mechanics approach has been widely used to analyze fatigue crack propagation. The crack propagation rate (da/dN) and stress intensity factor range (ΔK) are found to be related by a power relationship for intermediate growth rates[38]:

$$da/dN = C\ (\Delta K)^m$$

where

da/dN = fatigue crack propagation rate

ΔK = stress intensity range

C, m = constants

Due to the form of the preceding relationship, it is possible to plot log da/dN versus log ΔK and obtain a linear relationship.

Figures 20 through 31 show log-log plots of da/dN versus ΔK for the 12 material conditions (3 grain sizes each for 4 materials) investigated. It should be noted that portions of the data for each specimen lay along a straight line, reflecting obedience of the power law, and usually this occurred over the higher range of ΔK values for each specimen.

Fractographic studies of these fatigue specimens (see Fractography section) showed that all experienced a transition in fracture character as ΔK was increased. The range of ΔK over which the power law was observed to apply corresponded to that realm in which crack propagation by a process of fatigue striation formation was prominent. For lower values of ΔK, where the power law previously described did not apply, the fractographic evidence suggested that crack propagation process was more material structure sensitive and less prone to fatigue striation formation.

The data did, in fact, suggest the possibility that most of the material conditions obeyed two different crack propagation power laws over different stress intensity factor ranges. There were relatively few data points with which to formulate a power law curve applicable to lower ΔK values, but one must note the decided trend toward linearity in this region of the data. These fractographic observations described may be viewed as supporting evidence for a dual fracture mechanism responsible for the crack growth behavior observed.

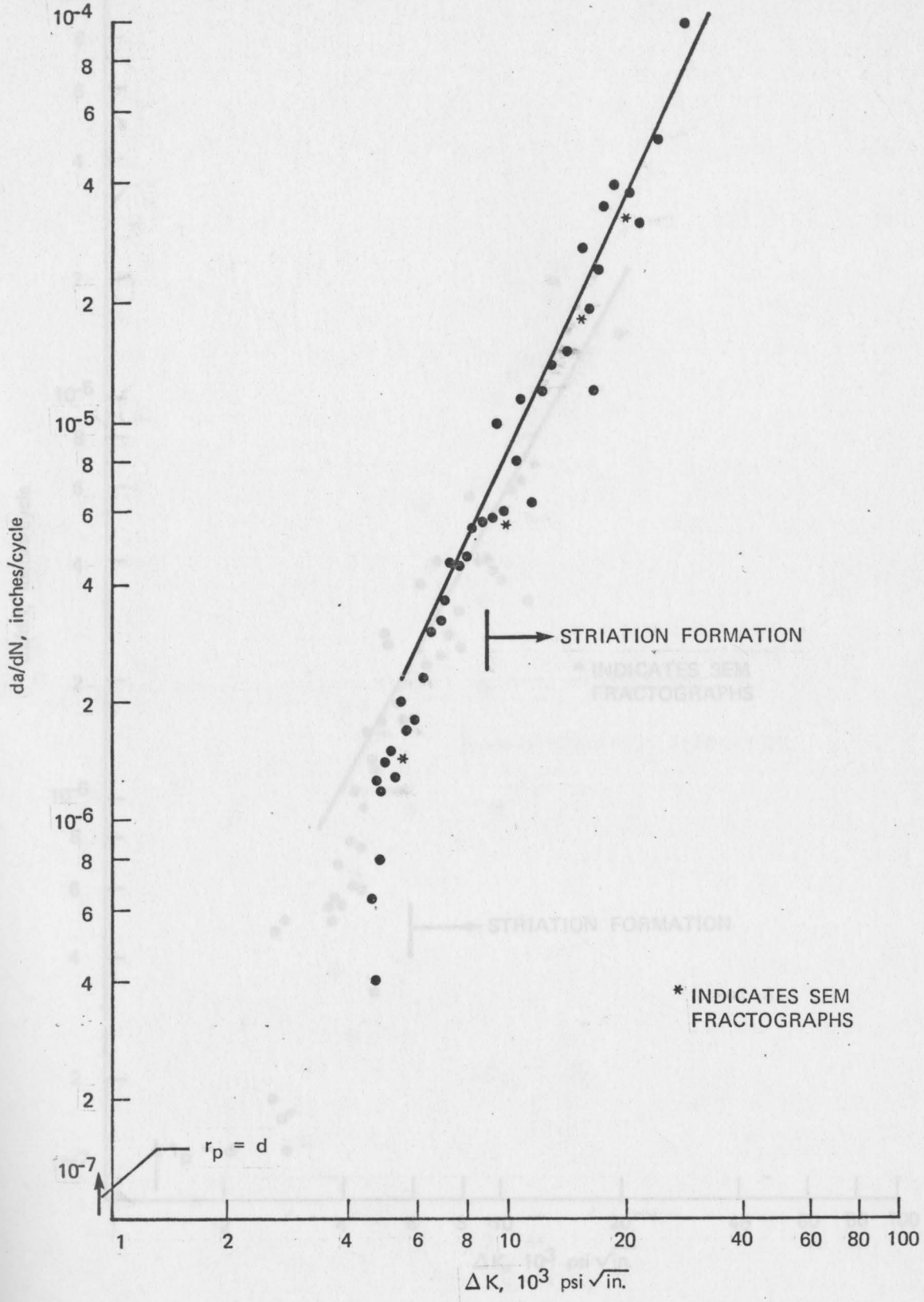

FIGURE 20 FATIGUE CRACK GROWTH DATA FOR ALUMINUM SPECIMEN AF-1 (GRAIN SIZE 20.4μ)

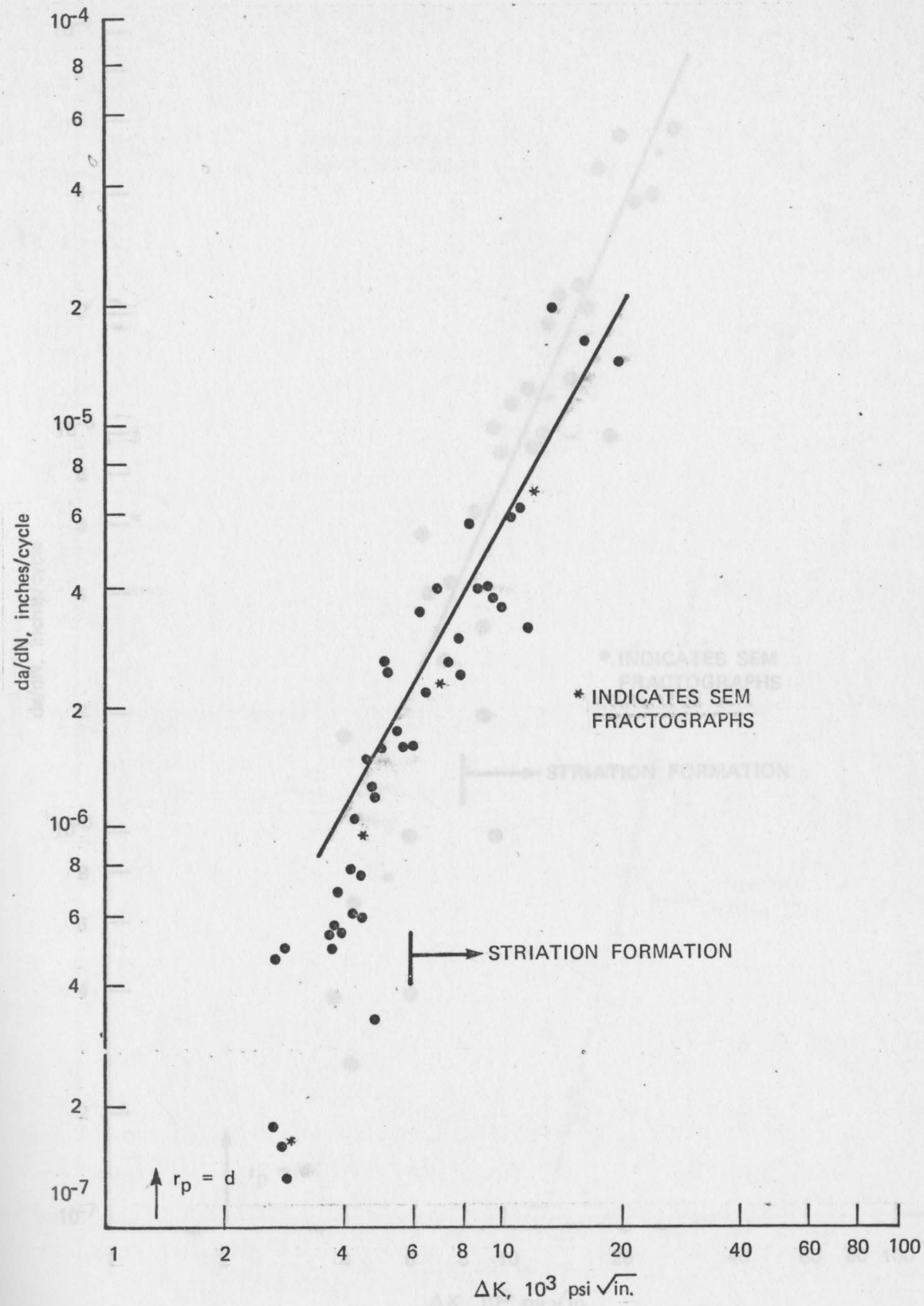

FIGURE 21 FATIGUE CRACK GROWTH DATA FOR ALUMINUM SPECIMEN AF-7 (GRAIN SIZE 36.0 μ)

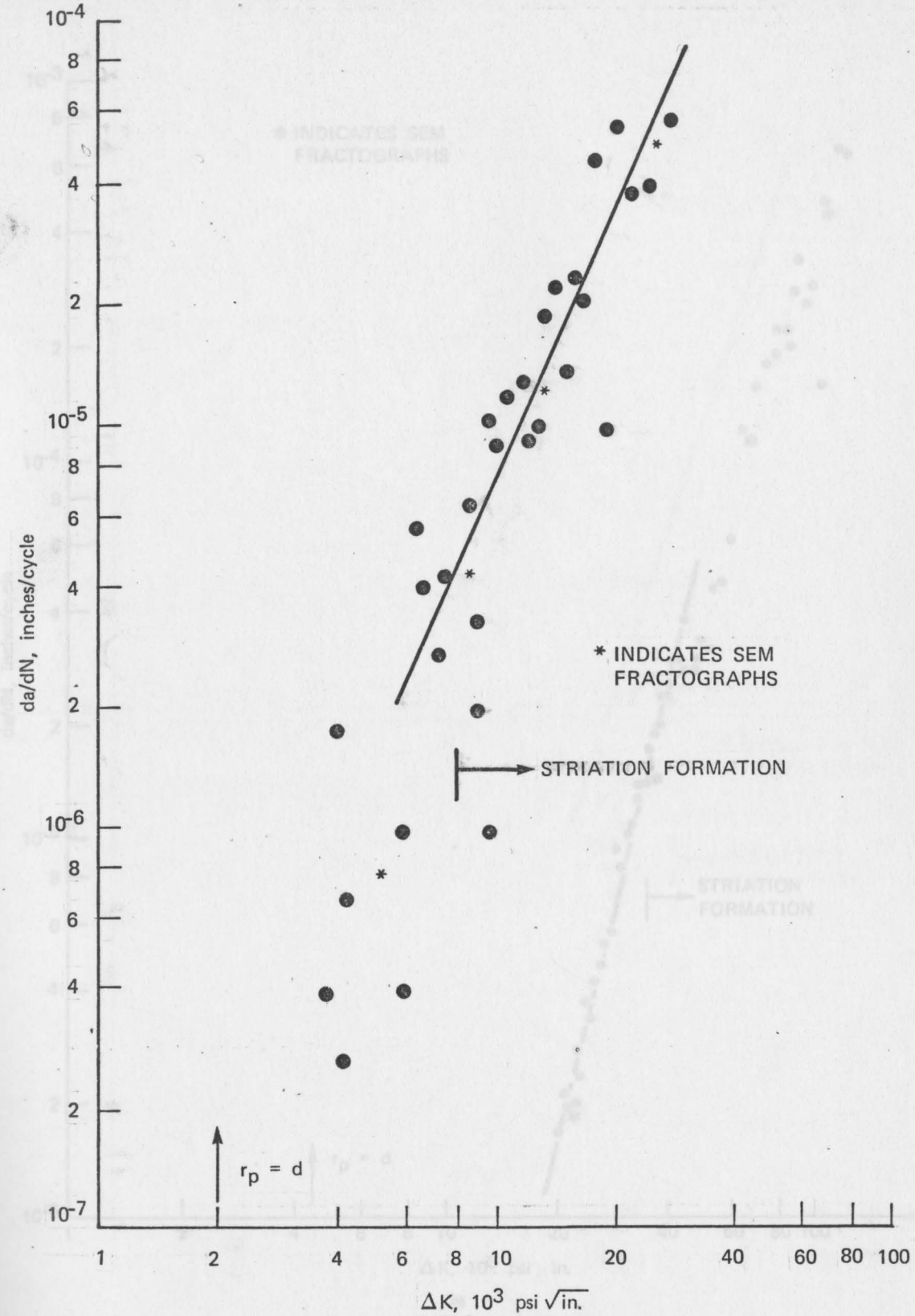

FIGURE 22 FATIGUE CRACK GROWTH DATA FOR ALUMINUM SPECIMEN AF-3 (GRAIN SIZE 81.8μ)

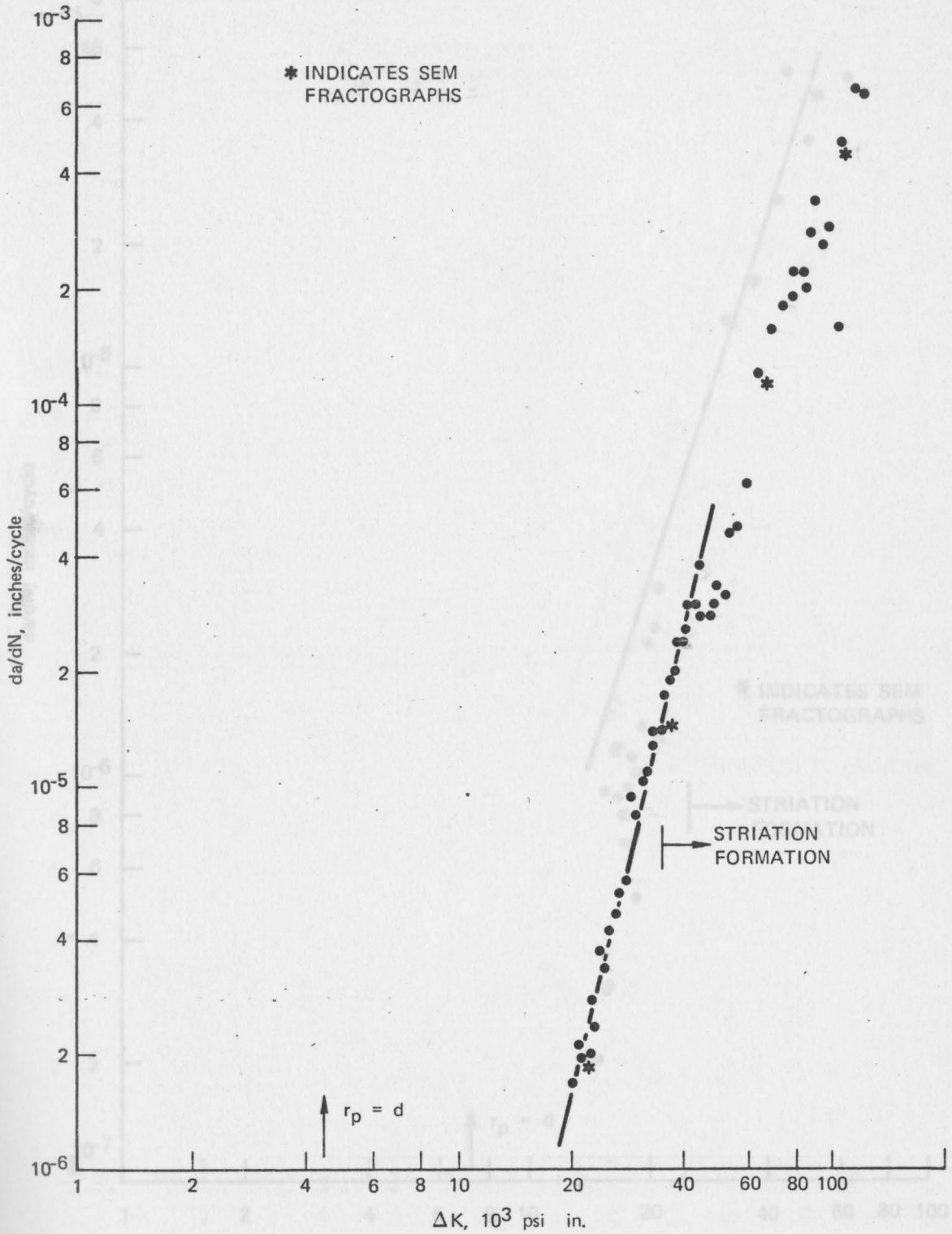

FIGURE 23 FATIGUE CRACK GROWTH DATA FOR TYPE 304 STAINLESS STEEL SPECIMEN SF-5 (GRAIN SIZE 11.0 μ)

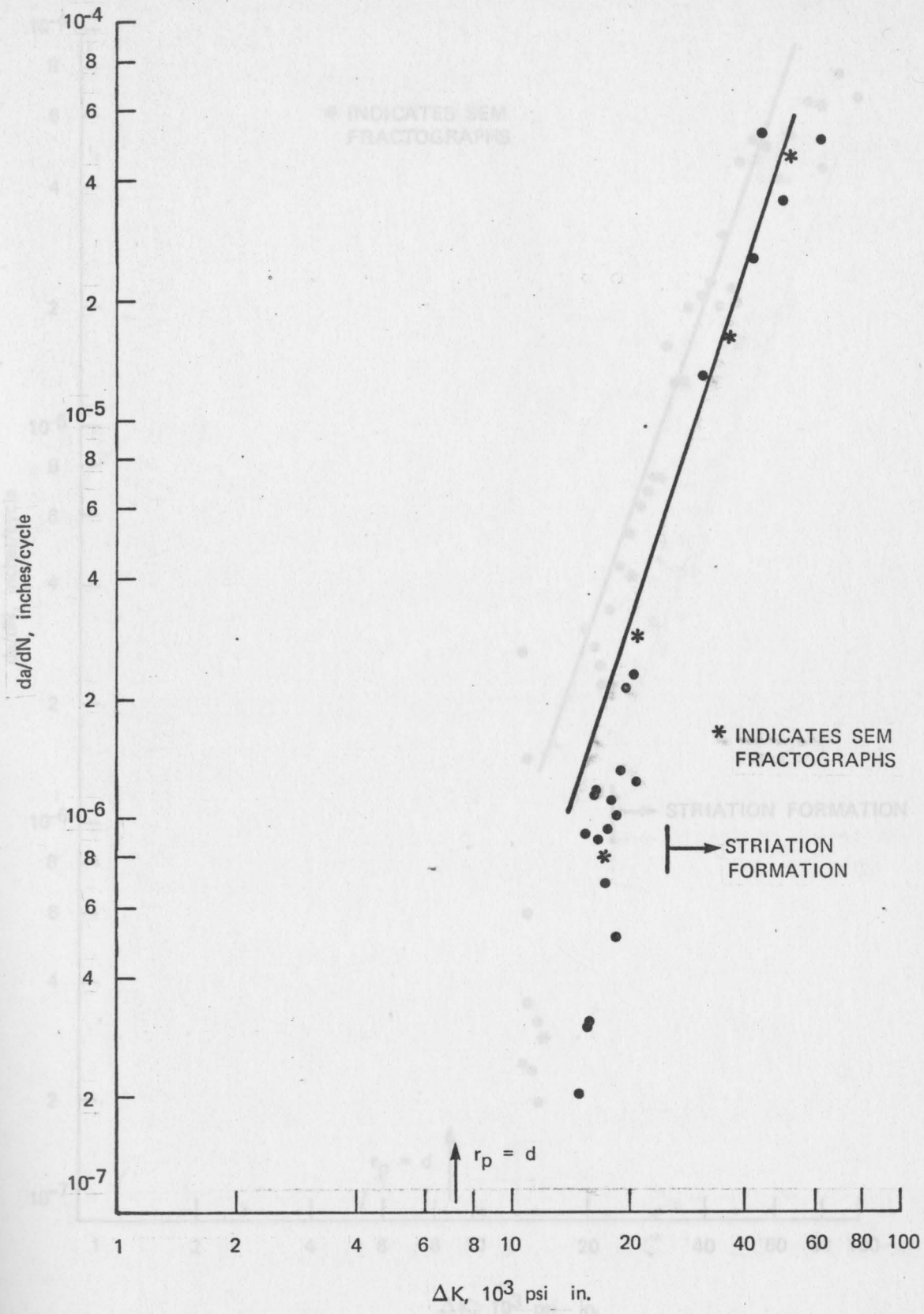

FIGURE 24 FATIGUE CRACK GROWTH DATA FOR TYPE 304 STAINLESS STEEL SPECIMEN SF-6 (GRAIN SIZE 47.7 μ)

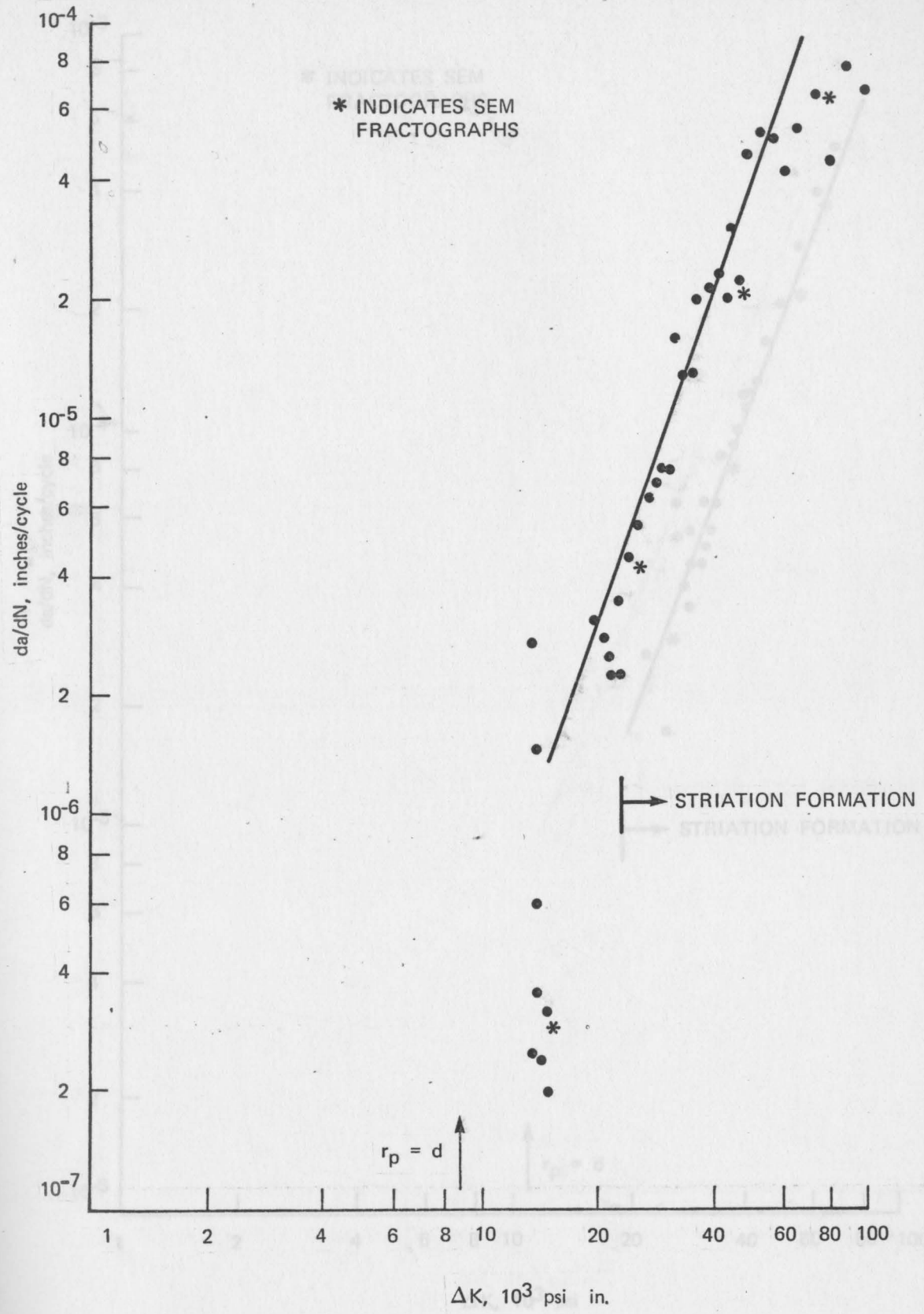

FIGURE 25 FATIGUE CRACK GROWTH DATA FOR TYPE 304 STAINLESS STEEL SPECIMEN SF-1 (GRAIN SIZE 79.6 μ)

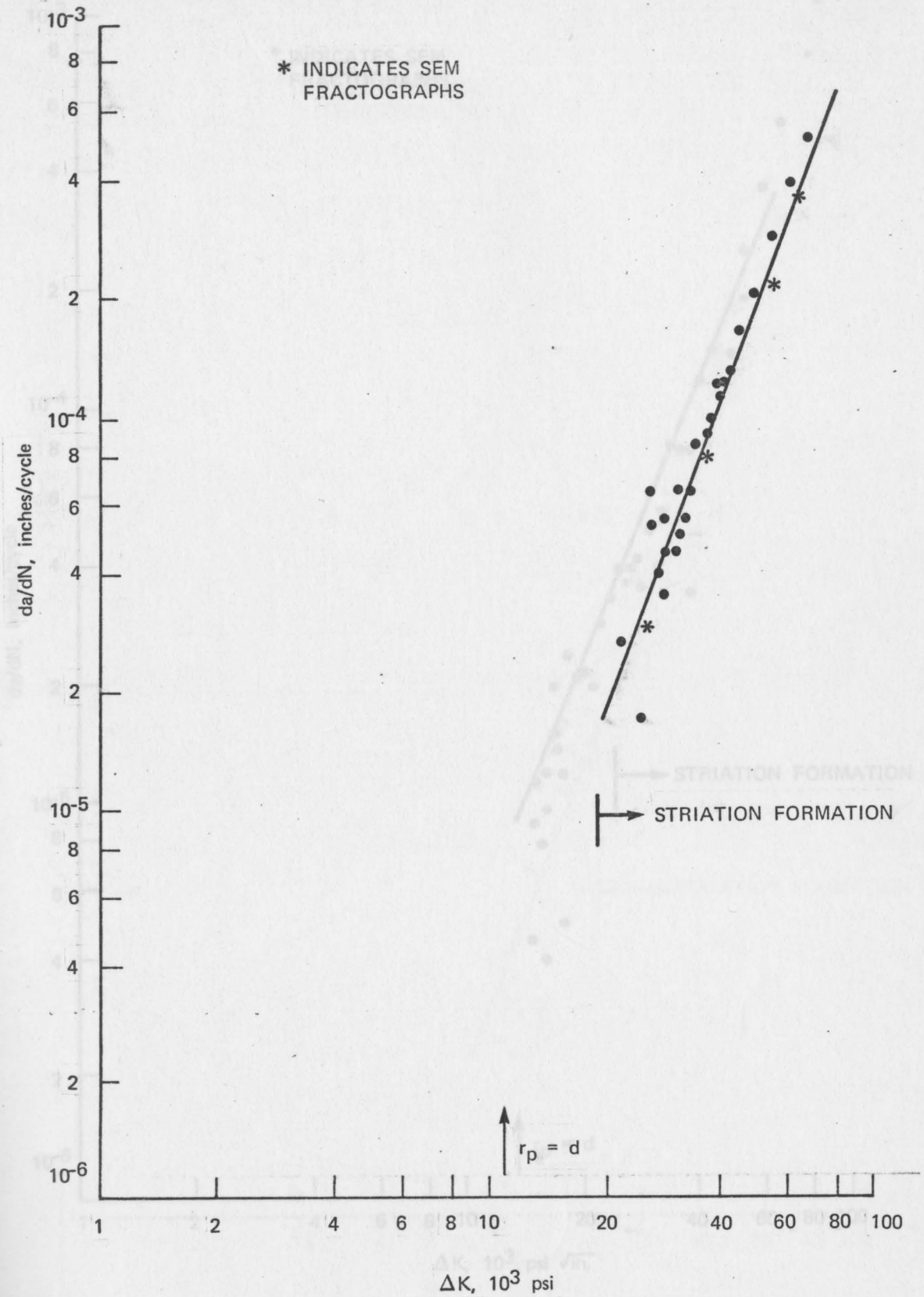

FIGURE 26 FATIGUE CRACK GROWTH DATA FOR TITANIUM SPECIMEN PTF-1 (GRAIN SIZE 11.7 μ)

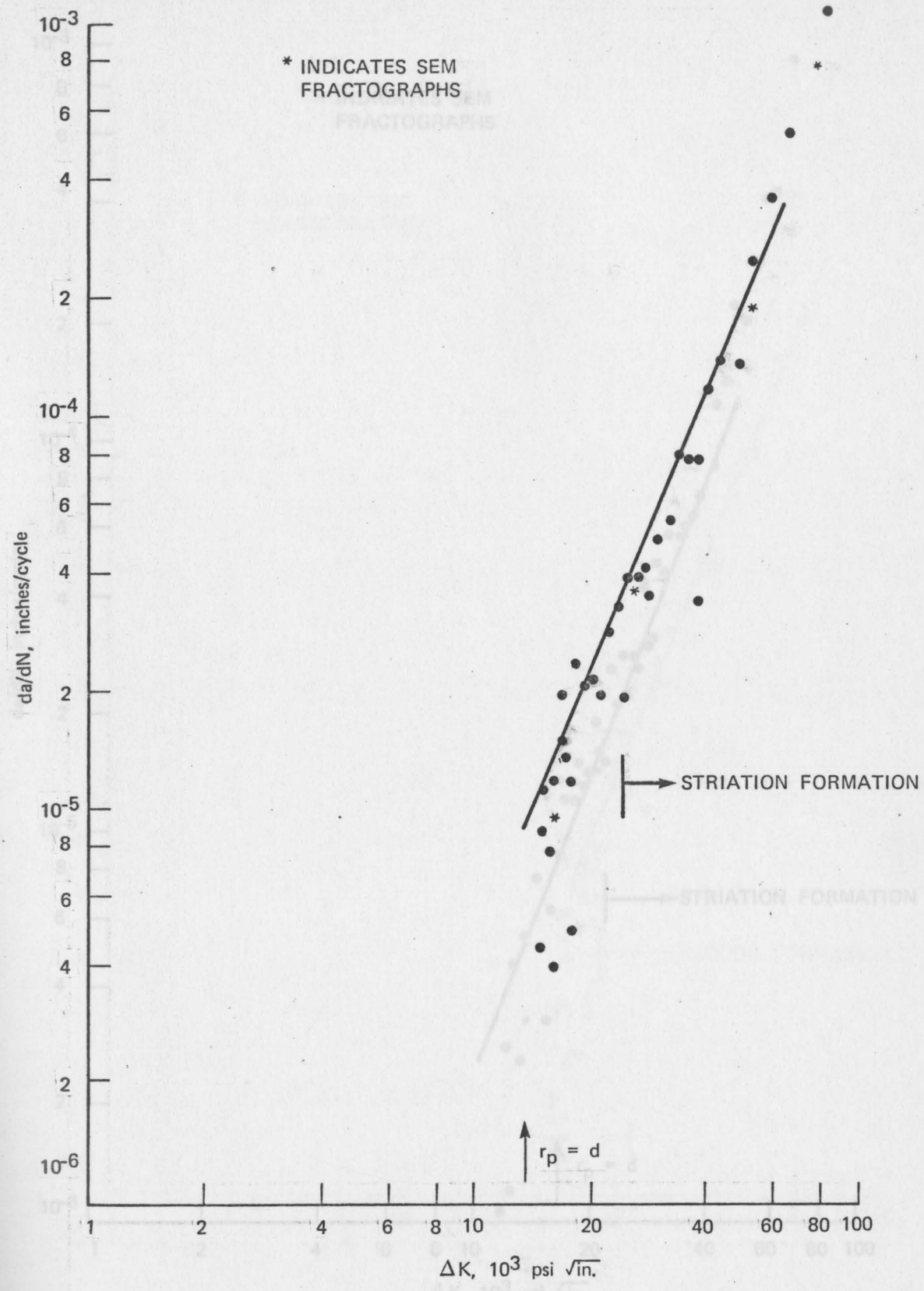

FIGURE 27 FATIGUE CRACK GROWTH DATA FOR TITANIUM SPECIMEN PTF-3 (GRAIN SIZE 23.1 μ)

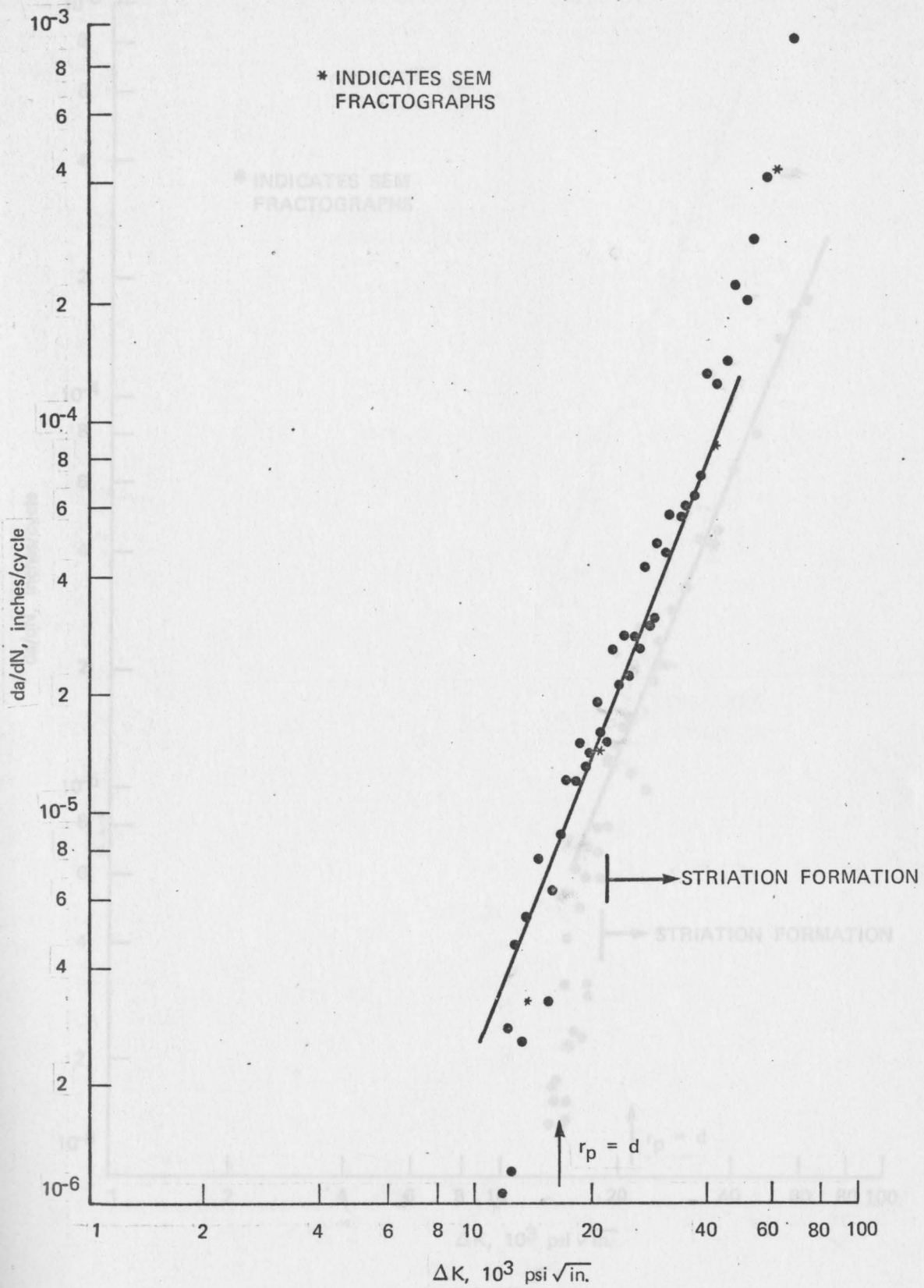

FIGURE 28 FATIGUE CRACK GROWTH FOR TITANIUM SPECIMEN PTF-6 (GRAIN SIZE 35.4 μ)

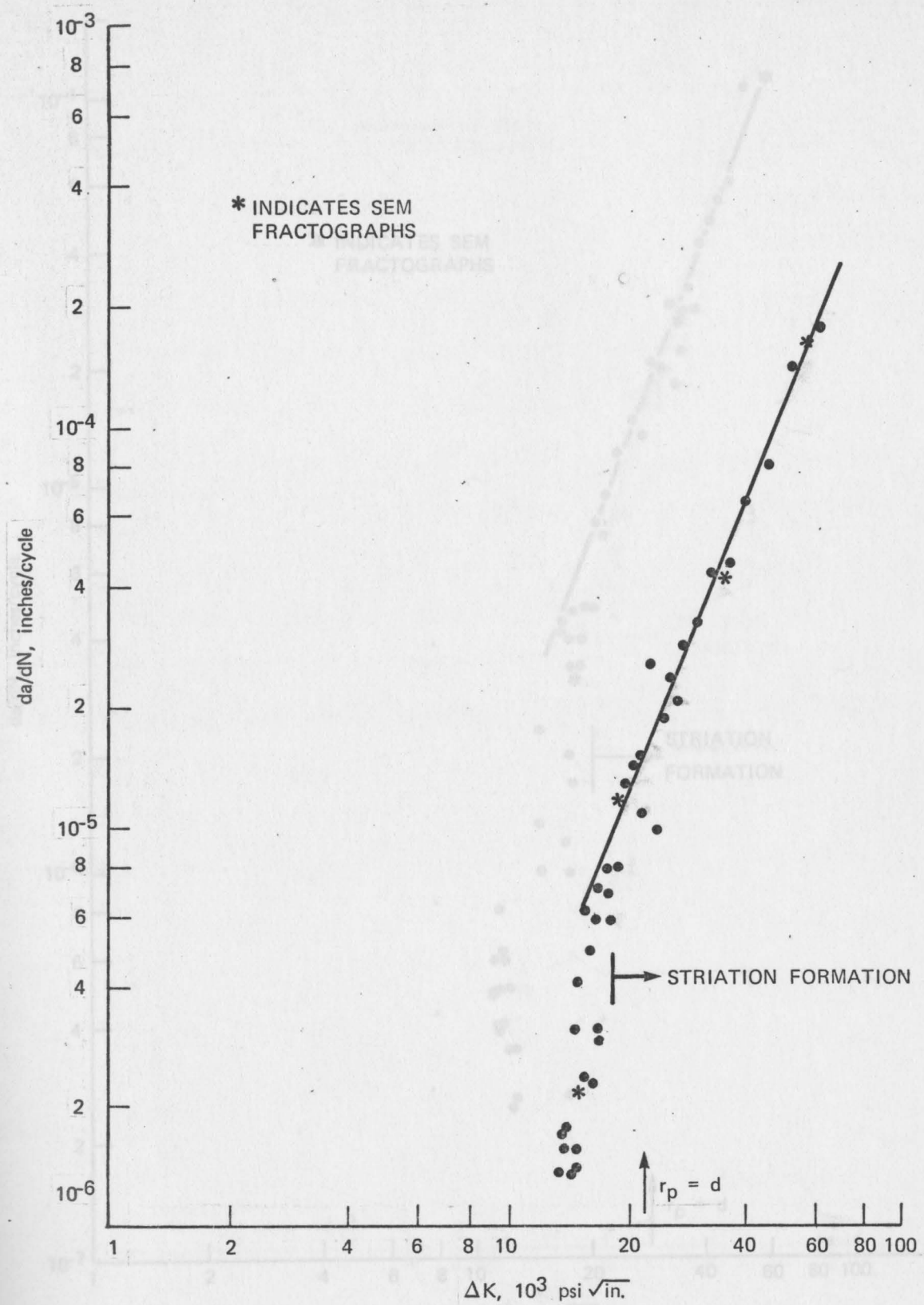

FIGURE 29 FATIGUE CRACK GROWTH DATA FOR Ti - 8Al SPECIMEN ATF-2 (GRAIN SIZE 29.4 μ)

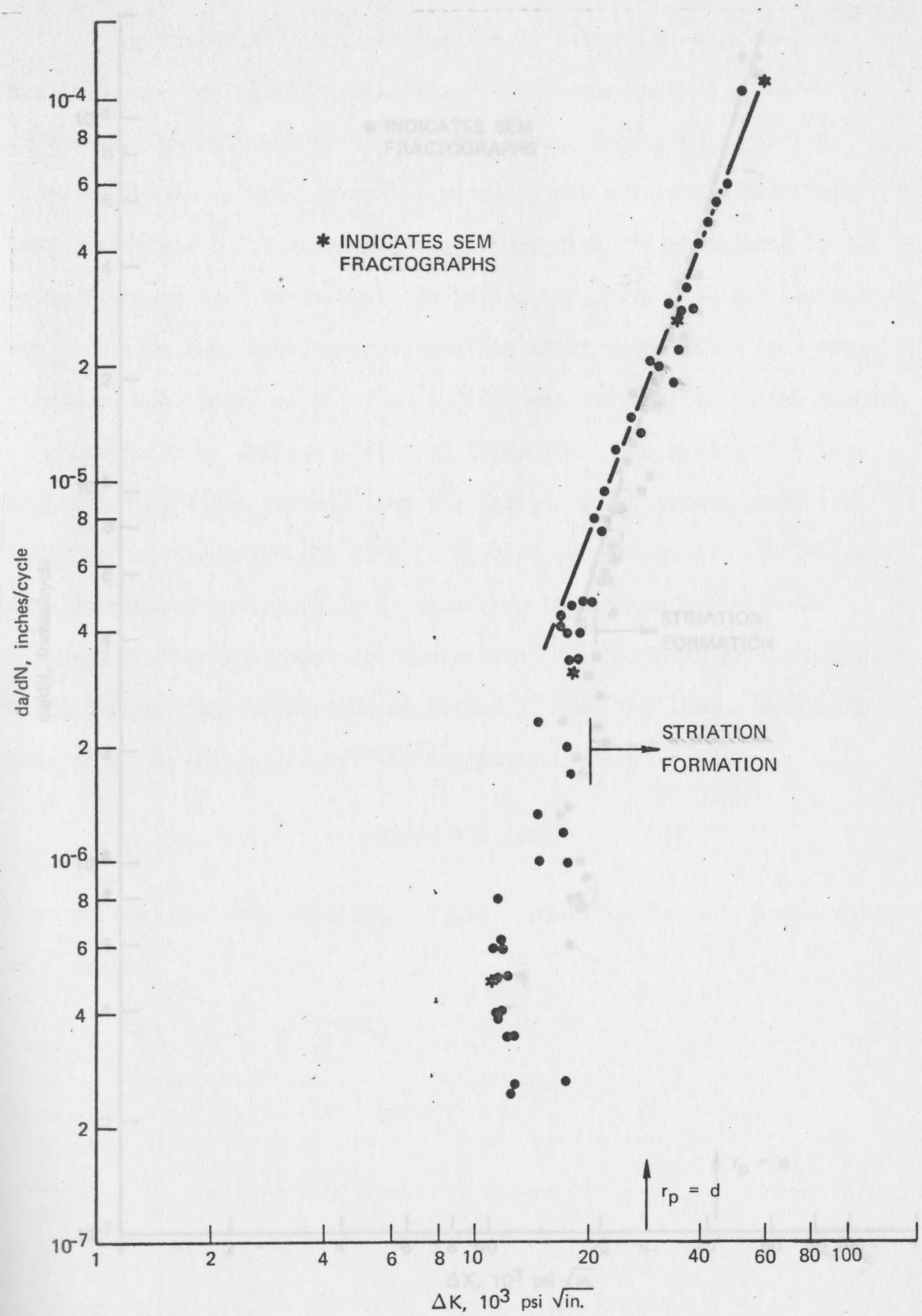

FIGURE 30 FATIGUE CRACK GROWTH DATA FOR Ti-8Al SPECIMEN ATF-6 (GRAIN SIZE 60.1 μ)

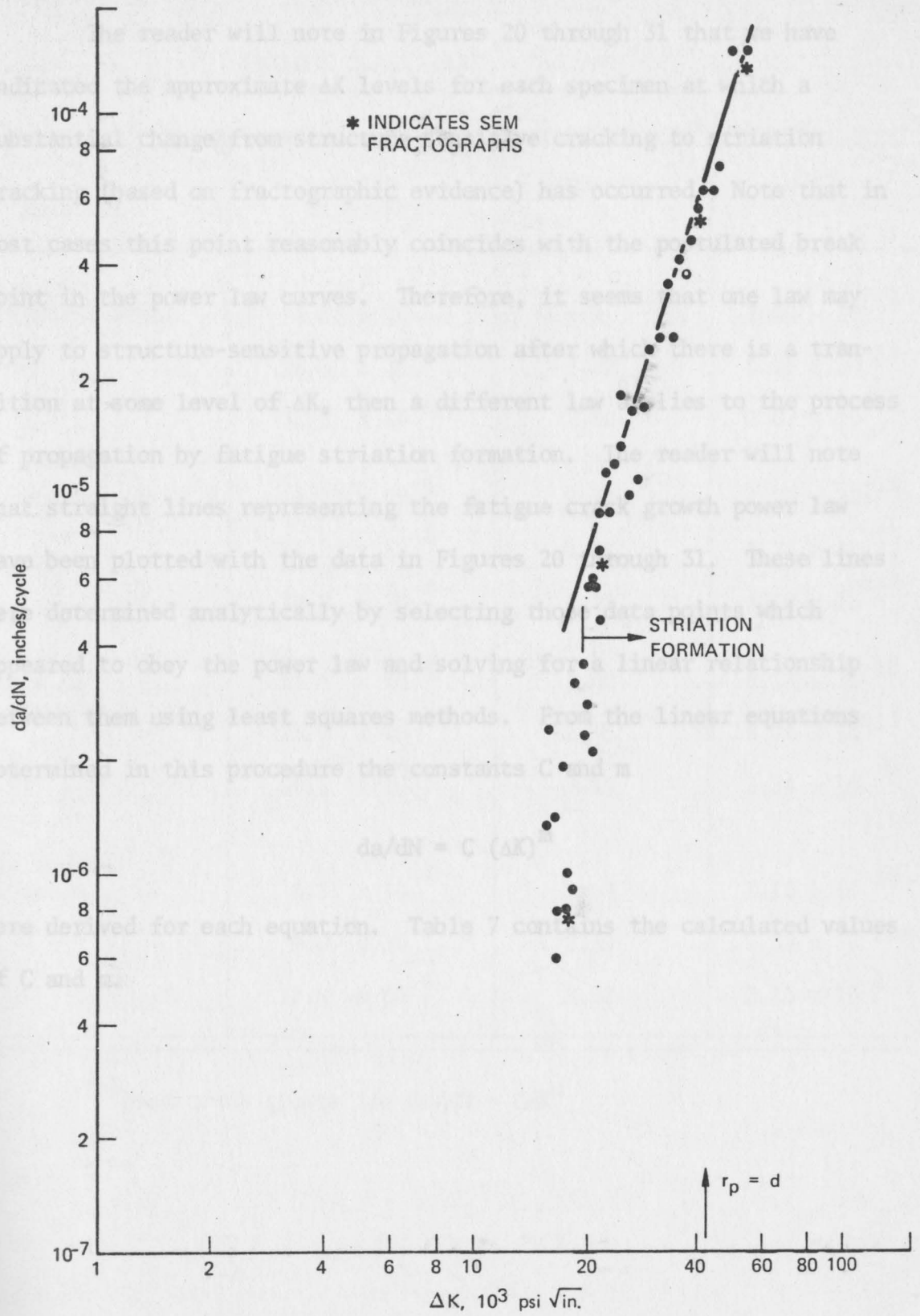

FIGURE 31 FATIGUE CRACK GROWTH DATA FOR Ti - 8Al SPECIMEN ATF-4 (GRAIN SIZE 137.5 μ)

The reader will note in Figures 20 through 31 that we have indicated the approximate ΔK levels for each specimen at which a substantial change from structure-sensitive cracking to striation cracking (based on fractographic evidence) has occurred. Note that in most cases this point reasonably coincides with the postulated break point in the power law curves. Therefore, it seems that one law may apply to structure-sensitive propagation after which there is a transition at some level of ΔK, then a different law applies to the process of propagation by fatigue striation formation. The reader will note that straight lines representing the fatigue crack growth power law have been plotted with the data in Figures 20 through 31. These lines were determined analytically by selecting those data points which appeared to obey the power law and solving for a linear relationship between them using least squares methods. From the linear equations determined in this procedure the constants C and m

$$da/dN = C\ (\Delta K)^m$$

were derived for each equation. Table 7 contains the calculated values of C and m.

TABLE 7

FATIGUE CRACK GROWTH CONSTANTS[(a)]

Material	Grain Size, in.	Exponent m	Constant C
Type 304 Stainless Steel	4.33×10^{-4}	4.10	4.01×10^{-24}
	18.8×10^{-4}	2.91	9.55×10^{-19}
	31.3×10^{-4}	2.80	3.02×10^{-18}
Pure Aluminum	8.03×10^{-4}	2.14	2.23×10^{-14}
	14.2×10^{-4}	1.81	3.32×10^{-13}
	32.2×10^{-4}	2.28	6.10×10^{-15}
Ti-8% Al	11.6×10^{-4}	2.40	6.15×10^{-16}
	23.7×10^{-4}	2.55	8.24×10^{-17}
	54.1×10^{-4}	3.10	3.34×10^{-19}
Unalloyed Titanium	4.61×10^{-4}	2.60	1.16×10^{-16}
	9.09×10^{-4}	2.39	1.35×10^{-15}
	13.9×10^{-4}	2.52	2.16×10^{-16}

(a) From crack growth law $da/dN = C\Delta K^m$

It would be desirable to attach some physical significance to the values of the constants derived for the power law equations descriptive of the crack propagation data. This is difficult to do, per se, but by analogy one may recognize the similarity of the crack propagation equation and the tensile flow equation and the further analogy between strain hardening exponent (n) in the latter and the power constant (m) of the former. This is not too surprising in that both equations describe types of plastic flow situations. Actually, the power constant seems the most important aspect of the crack propagation equation because da/dN is by definition a more sensitive function of m than of C. Examination of a possible relationship between the power constant (m) and strain hardening exponent (n) revealed no sensible correlation.

Figures 32 and 33 show plots of the power constant m versus Hall-Petch grain size ($d^{-1/2}$). In Figure 32 for FCC materials it is seen that grain size has no effect on m for aluminum, but for stainless steel the values of m are higher for smaller grain size. Higher values of m indicate a tendency toward higher crack growth rates. However, such indications must be considered tentative at best, because of the additional dependency of growth rates on the constant C (which decreased in value for increasing grain size, a trend counter to that of m).

For the hexagonal materials, Figure 33, titanium showed little influence of grain size on m. Titanium-8% aluminum showed some dependency of m on grain size, with a trend opposite to that exhibited for stainless steel, i.e., high values of m for large grain size material. The effect in titanium-8% aluminum, like that in stainless steel, was confounded by the fact that as values of the power constant

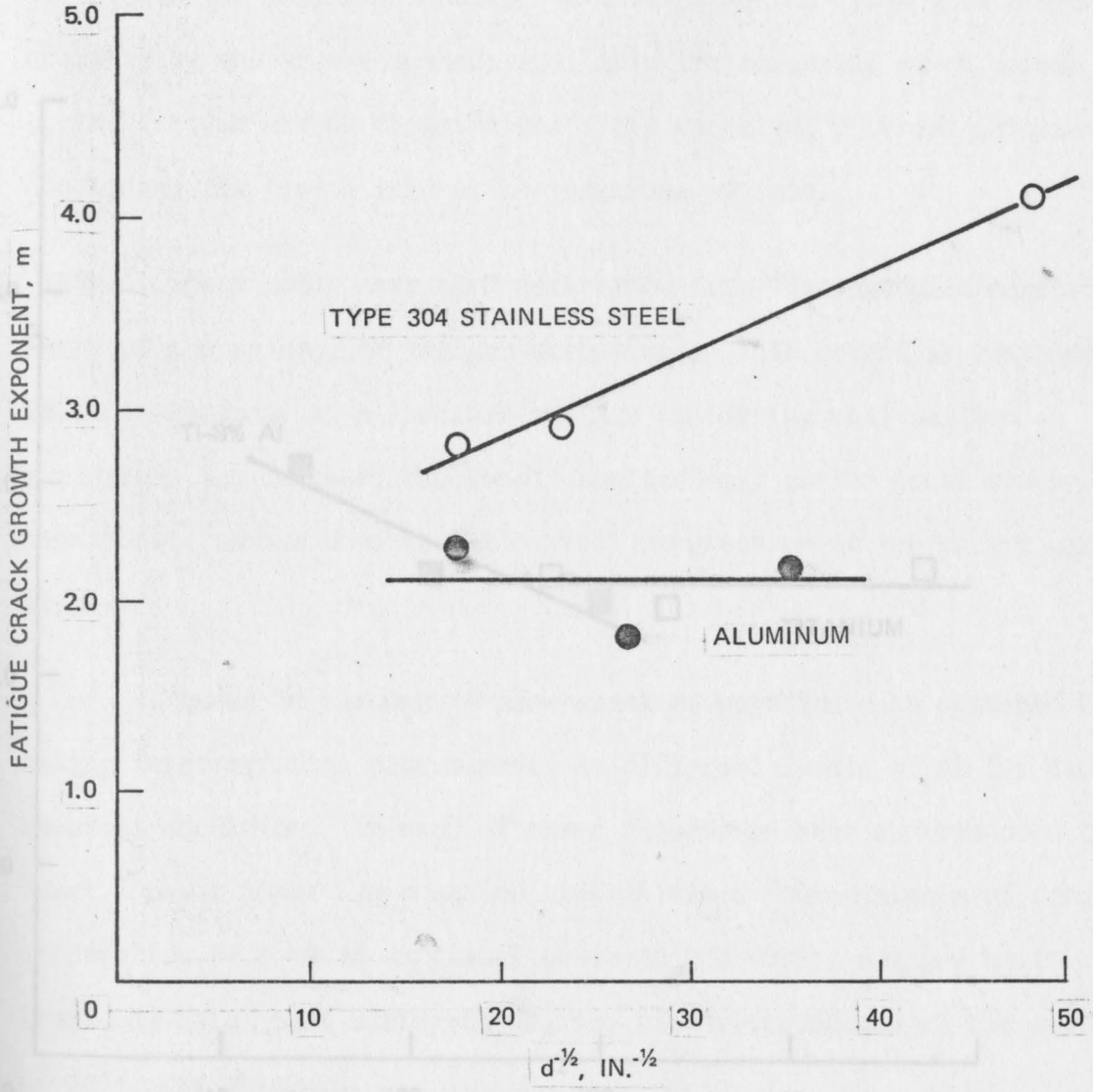

FIGURE 32 INFLUENCE OF GRAIN SIZE ON FATIGUE CRACK GROWTH EXPONENT FOR FCC METALS

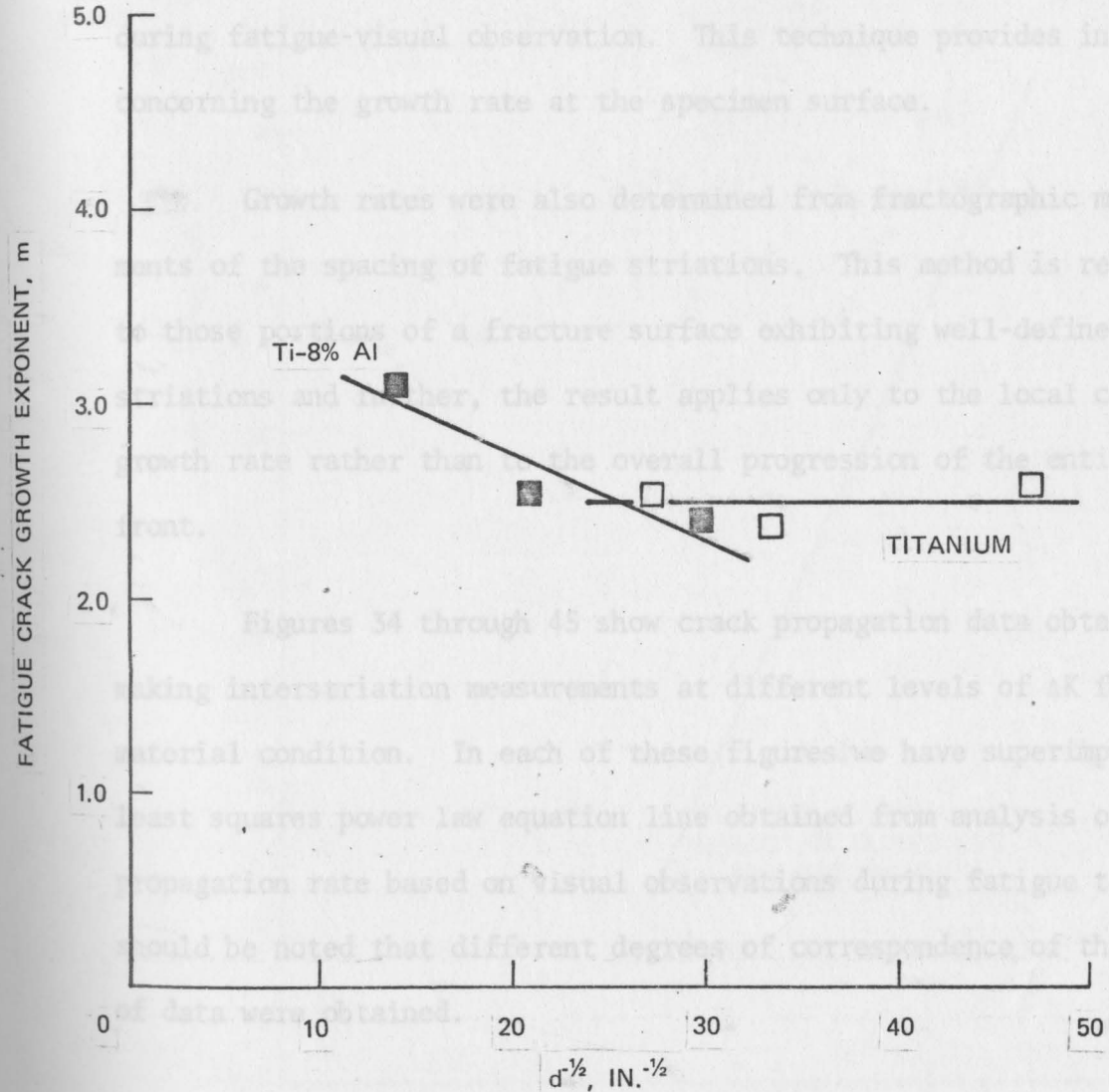

FIGURE 33 INFLUENCE OF GRAIN SIZE ON FATIGUE CRACK GROWTH EXPONENT FOR HCP METALS

m were increasing, values of the scalar C were decreasing. Therefore, it is not certain that higher values of m imply higher crack growth rates.

Microscopic Fatigue Crack Growth

In the previous results, we have presented crack growth data obtained by one of the methods available for measuring crack growth during fatigue-visual observation. This technique provides information concerning the growth rate at the specimen surface.

Growth rates were also determined from fractographic measurements of the spacing of fatigue striations. This method is restricted to those portions of a fracture surface exhibiting well-defined striations and further, the result applies only to the local crack growth rate rather than to the overall progression of the entire crack front.

Figures 34 through 45 show crack propagation data obtained by making interstriation measurements at different levels of ΔK for each material condition. In each of these figures we have superimposed the least squares power law equation line obtained from analysis of crack propagation rate based on visual observations during fatigue tests. It should be noted that different degrees of correspondence of the two sets of data were obtained.

For aluminum (Figures 34 through 36) it should be noted that generally higher rates of propagation were predicted based on fractographic data. Agreement tended to be better at higher levels of ΔK.

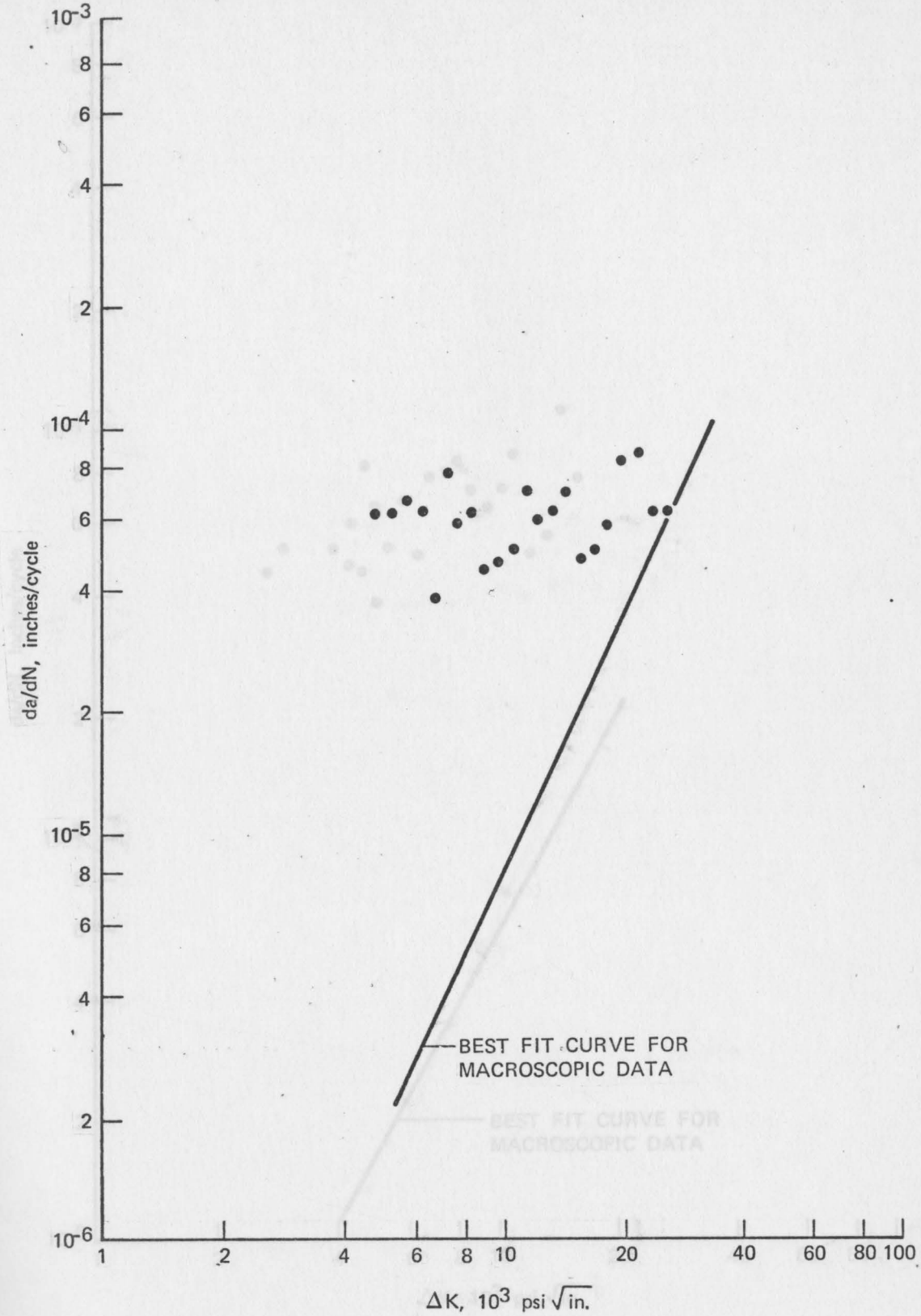

FIGURE 34 FATIGUE CRACK GROWTH DATA FROM STRIATION MEASUREMENTS FOR ALUMINUM SPECIMEN AF-1 (GRAIN SIZE 20.4 μ)

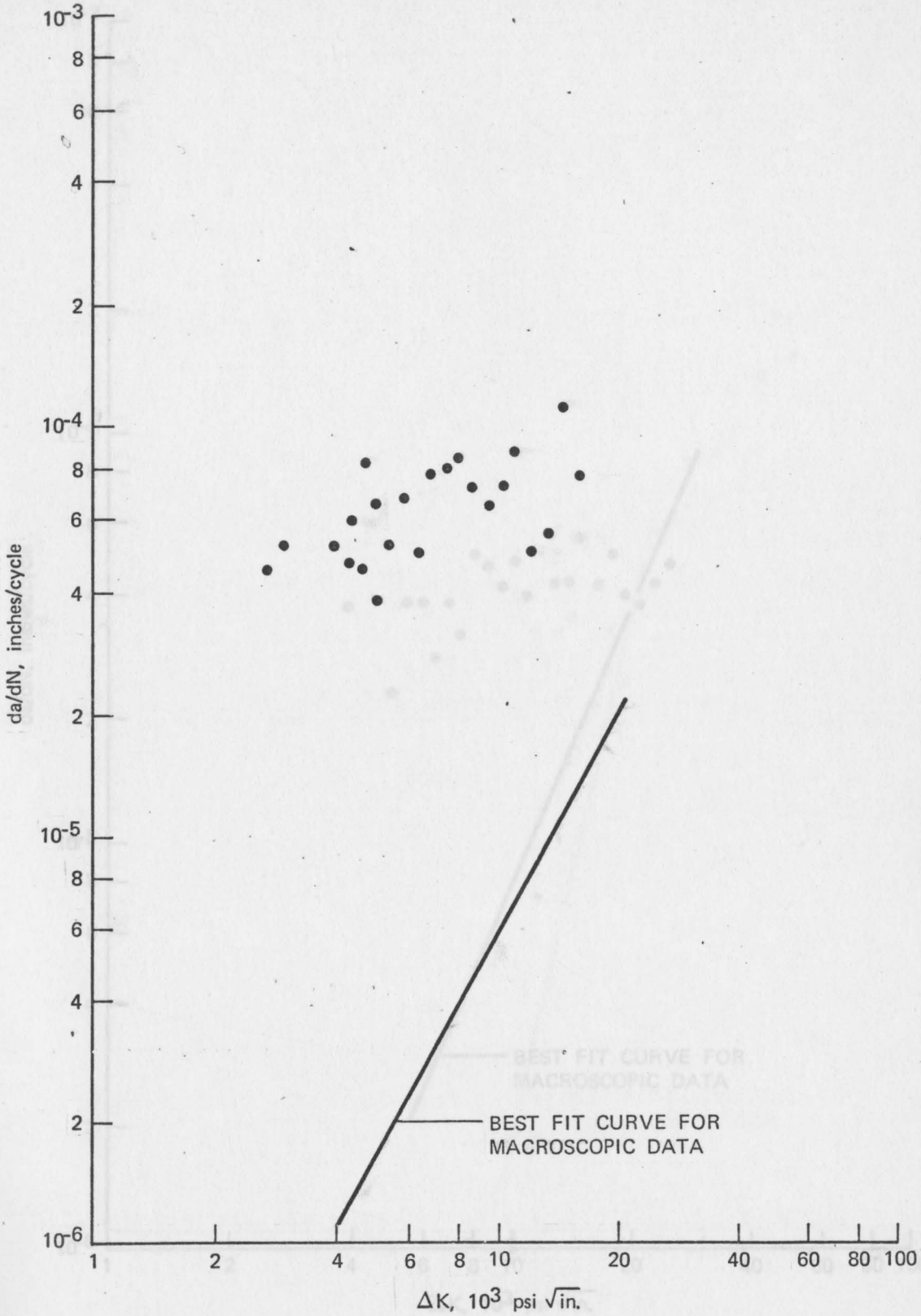

FIGURE 35 FATIGUE CRACK GROWTH DATA FROM STRIATION MEASUREMENTS FOR ALUMINUM SPECIMEN AF-7 (GRAIN SIZE 36.0 μ)

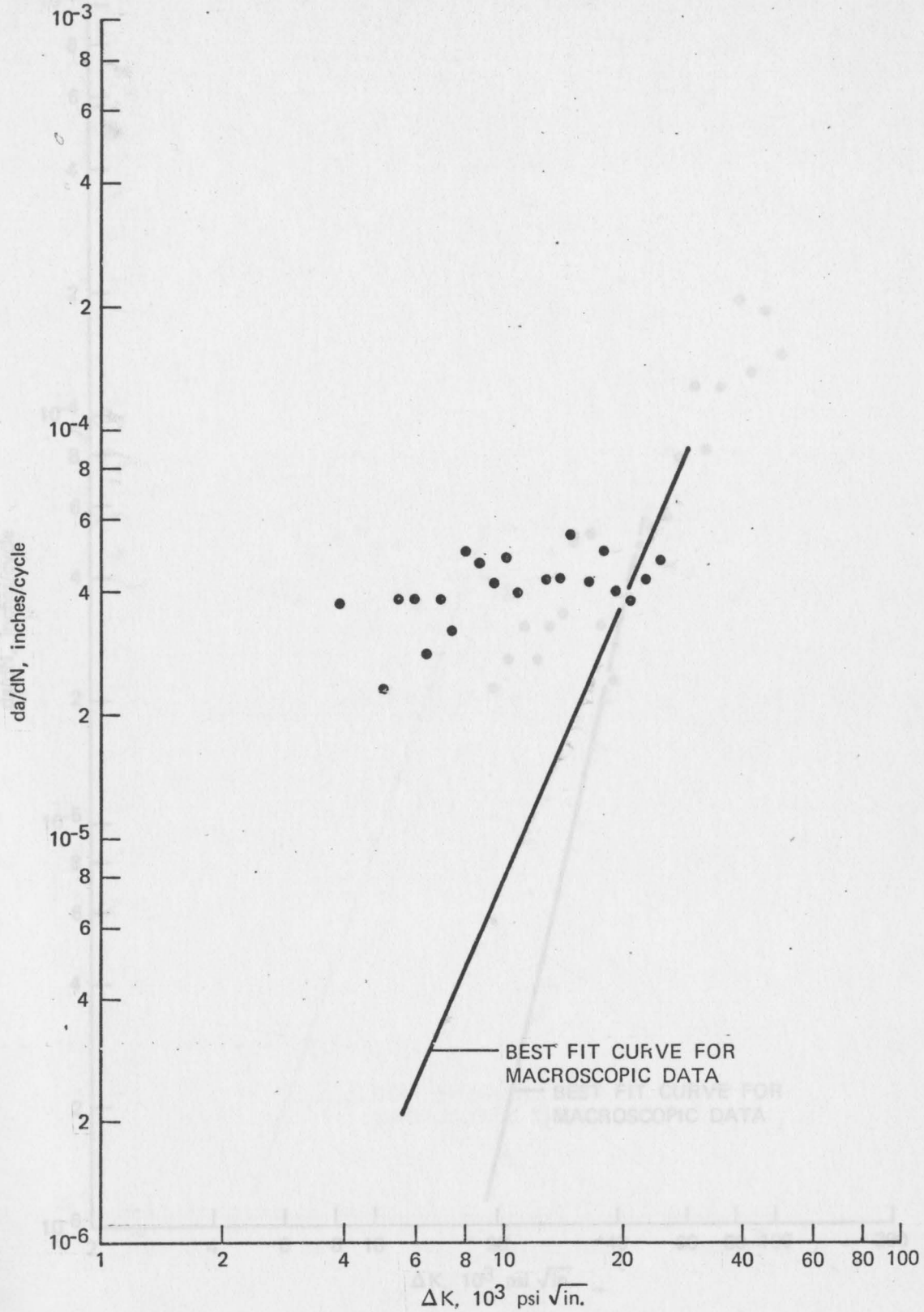

FIGURE 36 FATIGUE CRACK GROWTH DATA FROM STRIATION MEASUREMENTS FOR ALUMINUM SPECIMEN AF-3 (GRAIN SIZE 81.8 μ)

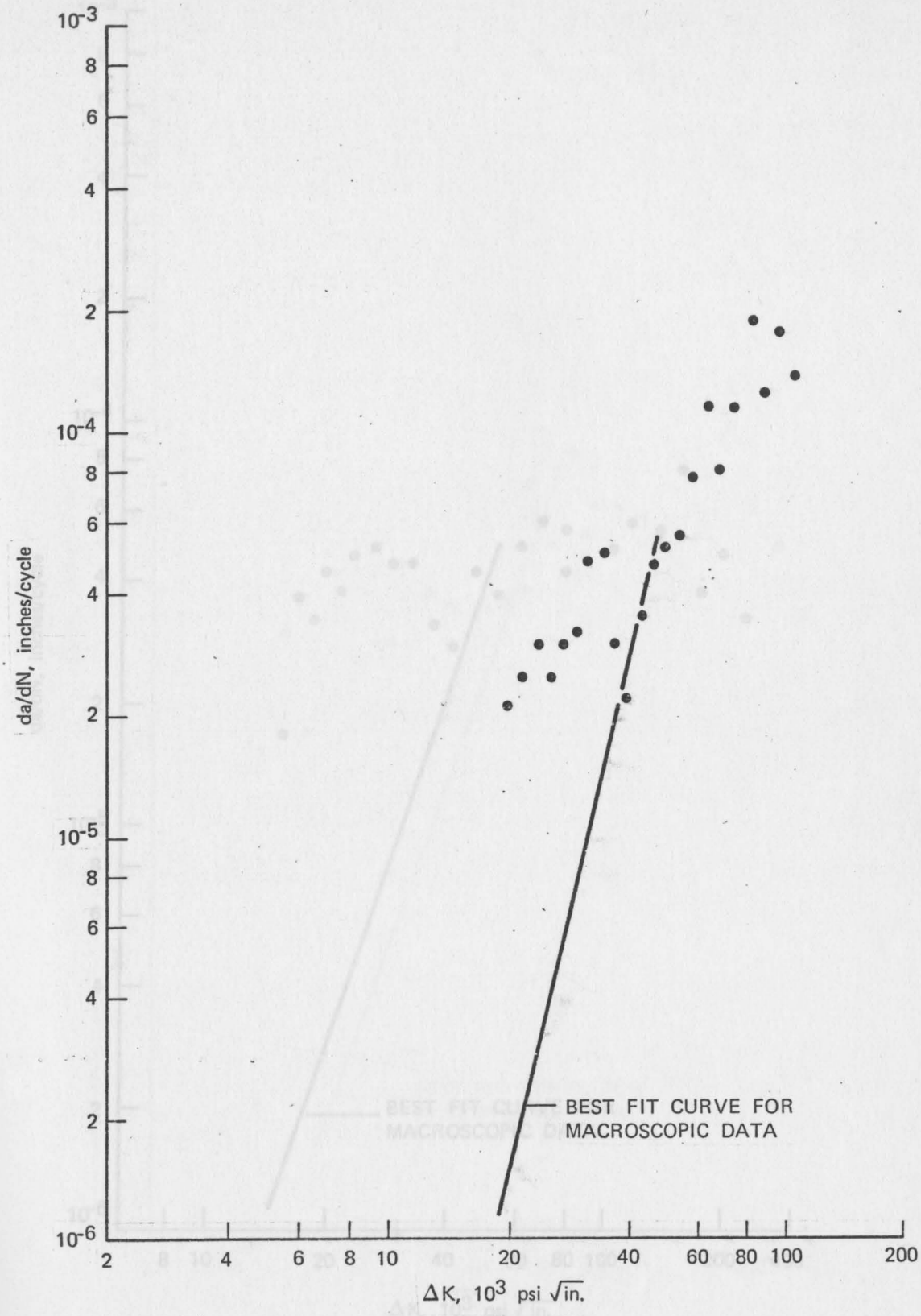

FIGURE 37 FATIGUE CRACK GROWTH DATA FROM STRIATION MEASUREMENTS FOR STAINLESS STEEL SPECIMEN SF-5 (GRAIN SIZE 11.0 μ)

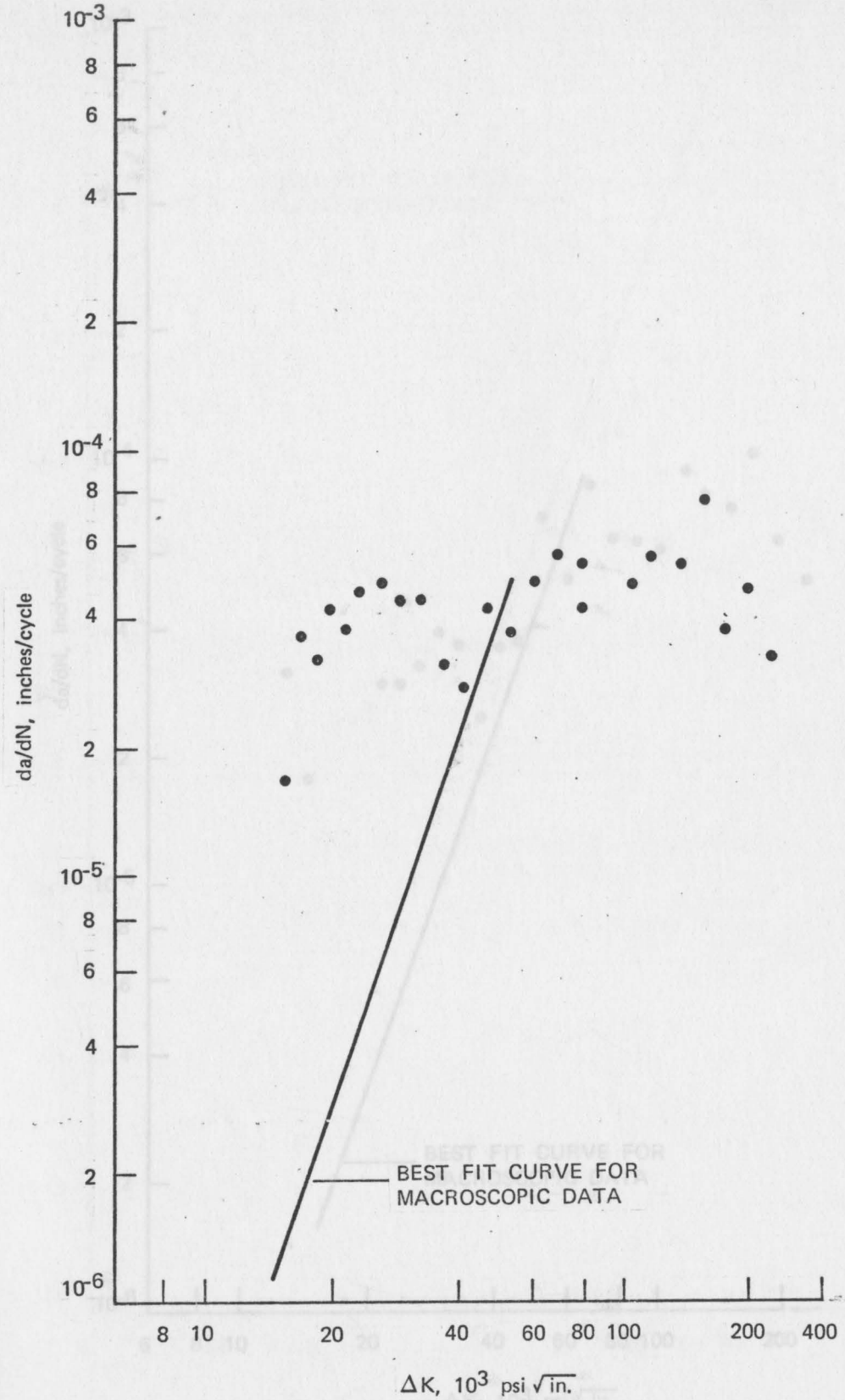

FIGURE 38 FATIGUE CRACK GROWTH DATA FROM STRIATION MEASUREMENTS FOR STAINLESS STEEL SPECIMEN SF-6 (GRAIN SIZE 47.7 μ)

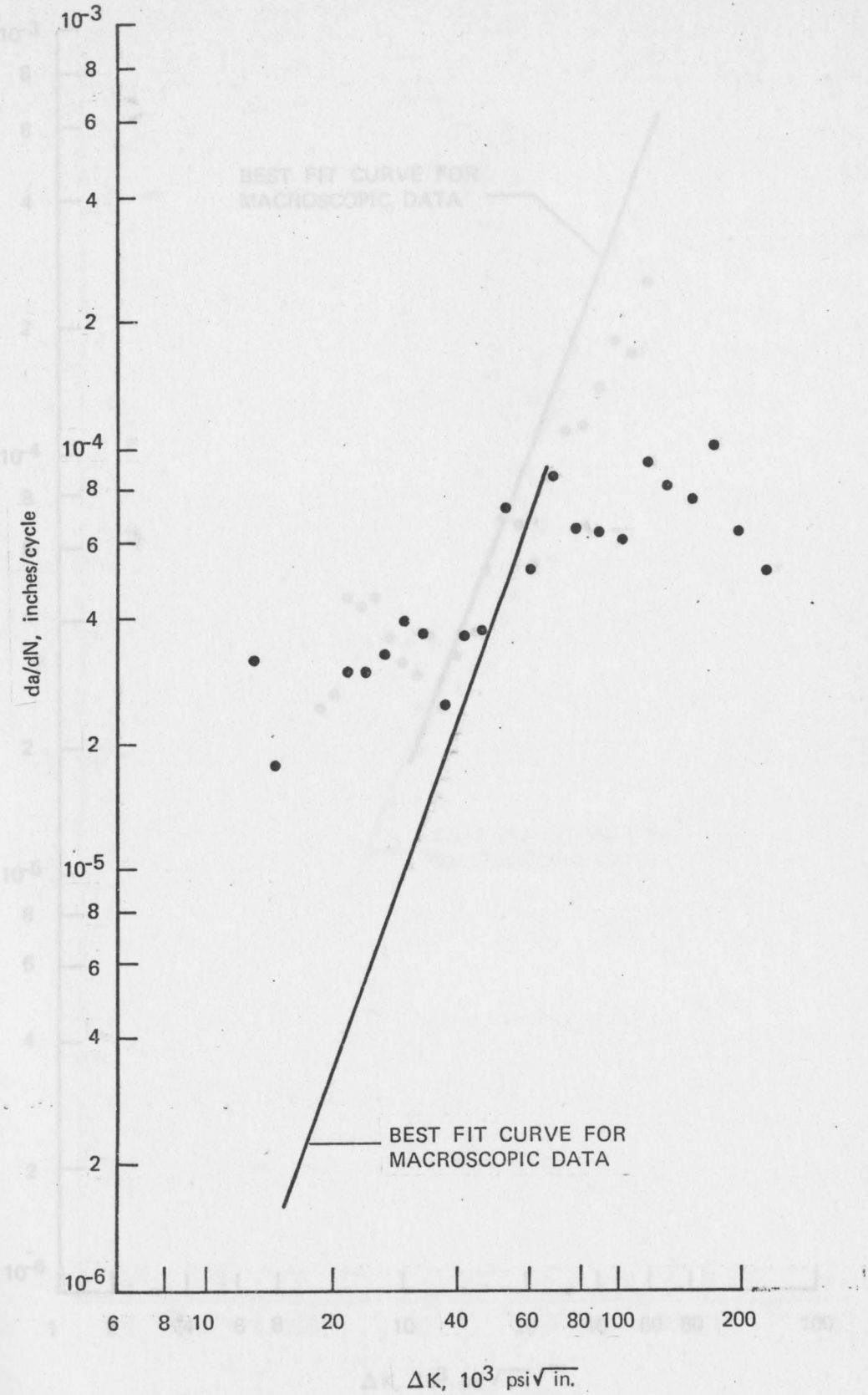

FIGURE 39 FATIGUE CRACK GROWTH DATA FROM STRIATION MEASUREMENTS FOR STAINLESS STEEL SPECIMEN SF-1 (GRAIN SIZE 79.6 μ)

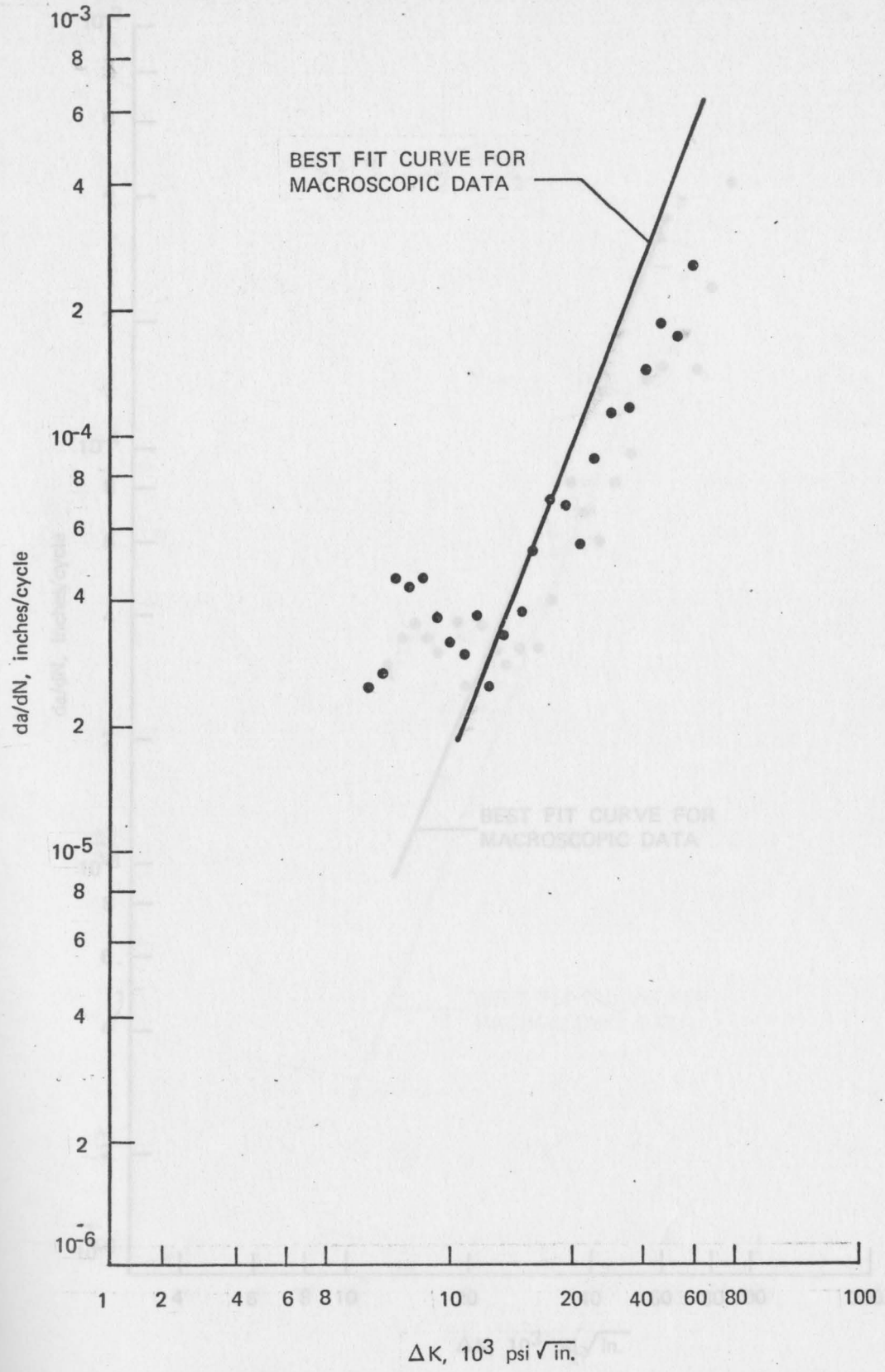

FIGURE 40 FATIGUE CRACK GROWTH DATA FROM STRIATION MEASUREMENTS FOR TITANIUM SPECIMEN PTF-1 (GRAIN SIZE 11.7 μ)

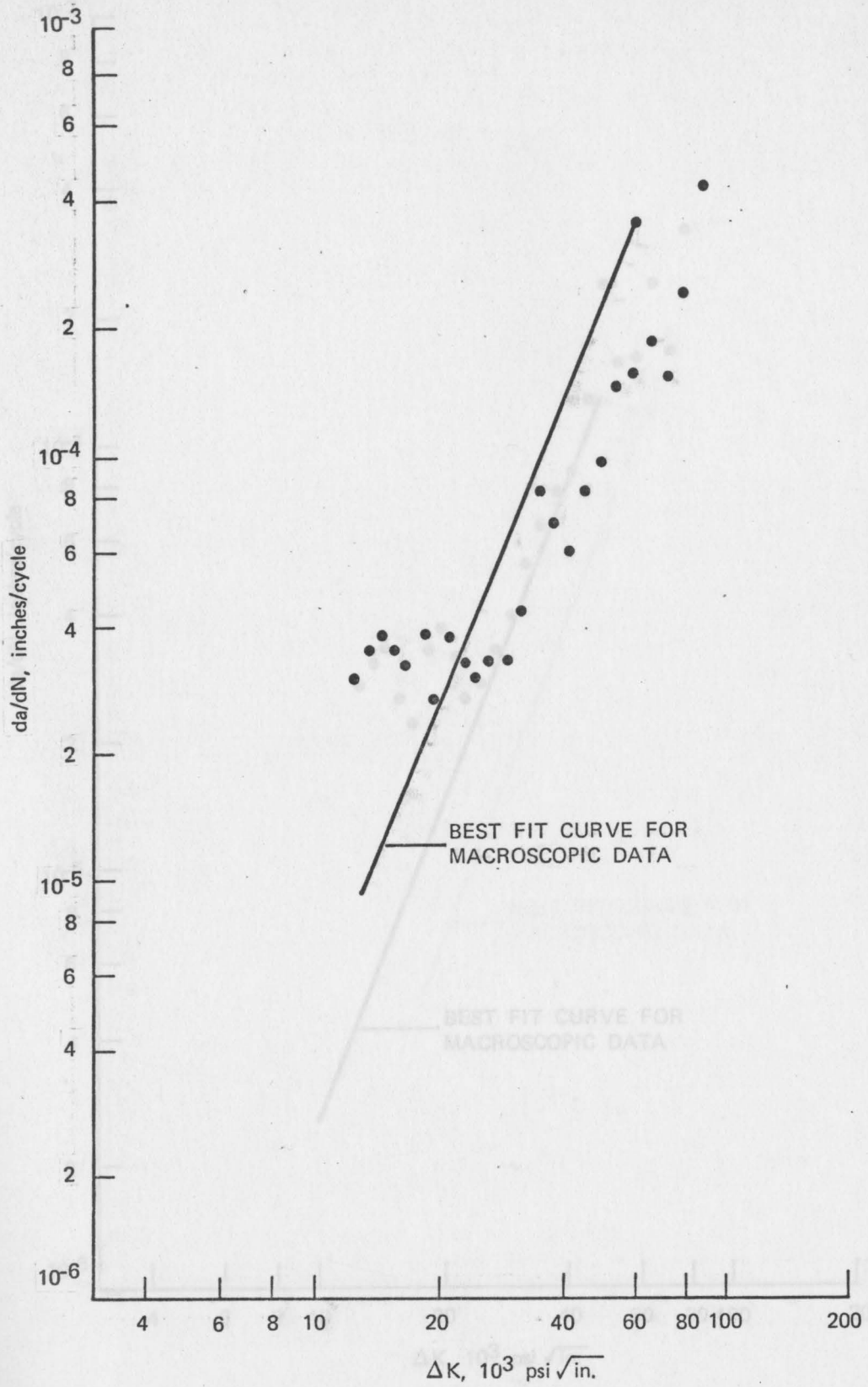

FIGURE 41 FATIGUE CRACK GROWTH DATA FROM STRIATION MEASUREMENTS FOR TITANIUM SPECIMEN PTF-3 (GRAIN SIZE 23.1 μ)

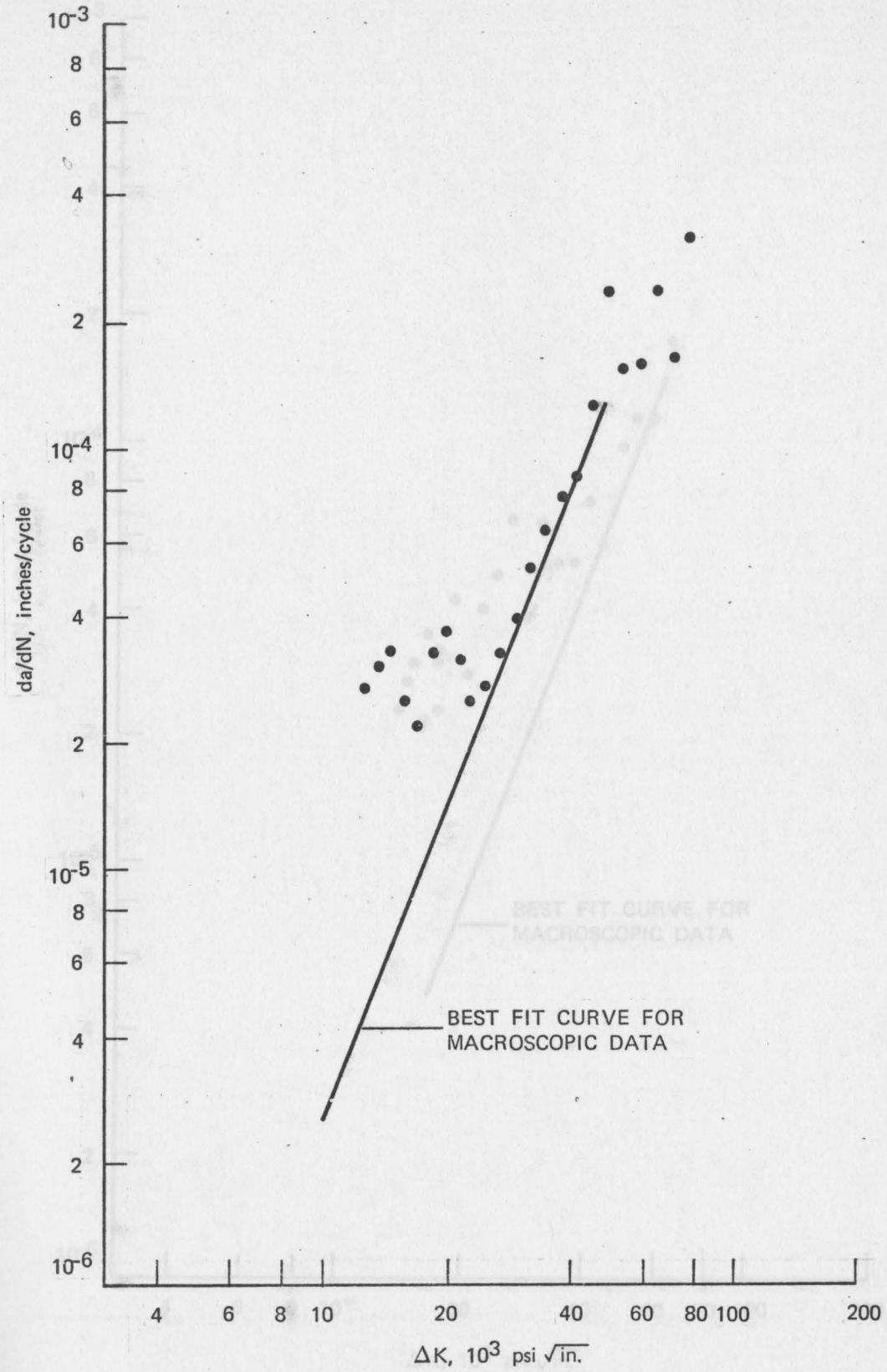

FIGURE 42 FATIGUE CRACK GROWTH DATA FROM STRIATION MEASUREMENTS FOR TITANIUM SPECIMEN PTF-6 (GRAIN SIZE 35.4 μ)

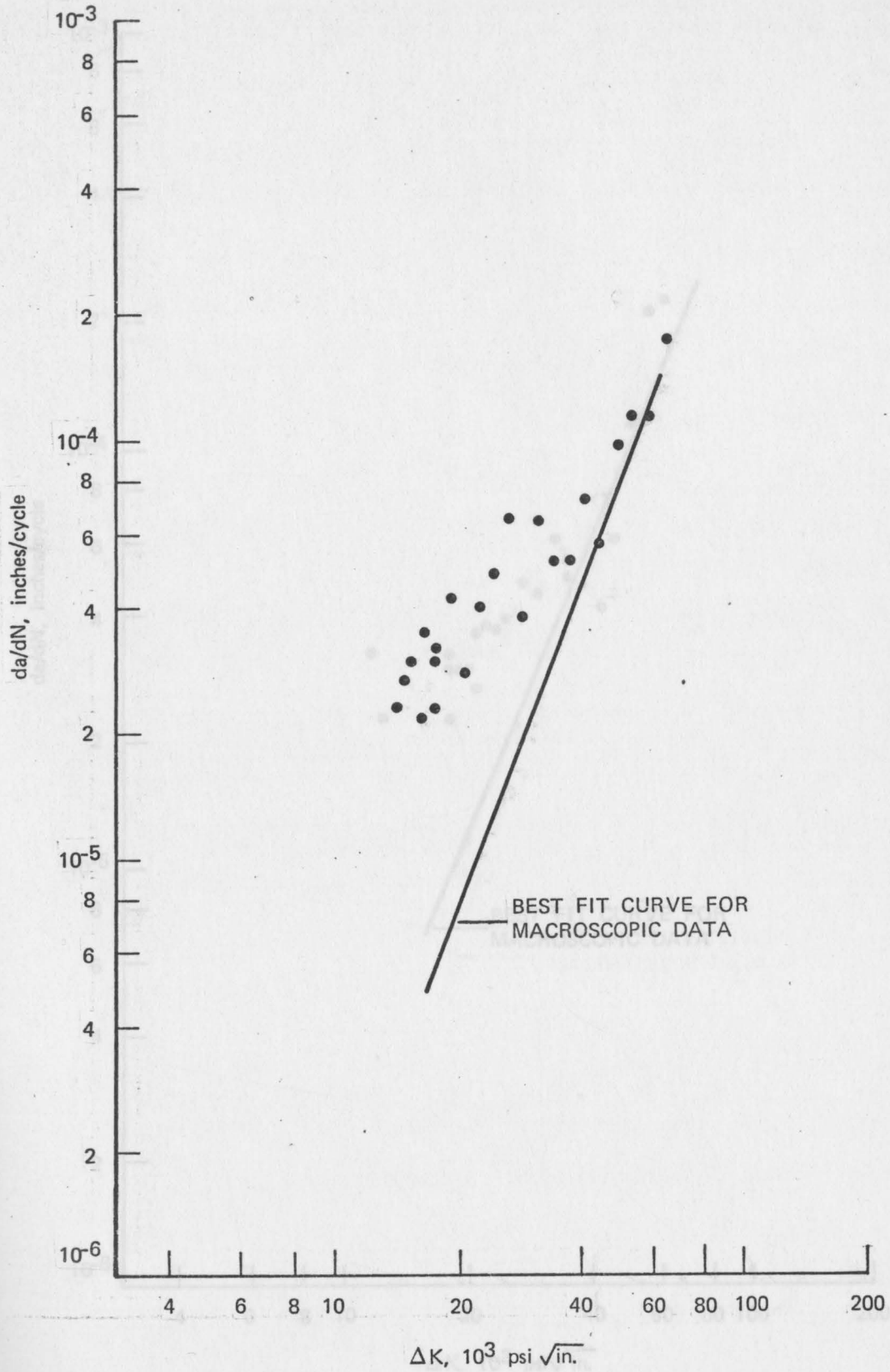

FIGURE 43 FATIGUE CRACK GROWTH DATA FROM STRIATION MEASUREMENTS FOR TITANIUM-8 Al SPECIMEN ATF-2 (GRAIN SIZE 29.4 μ)

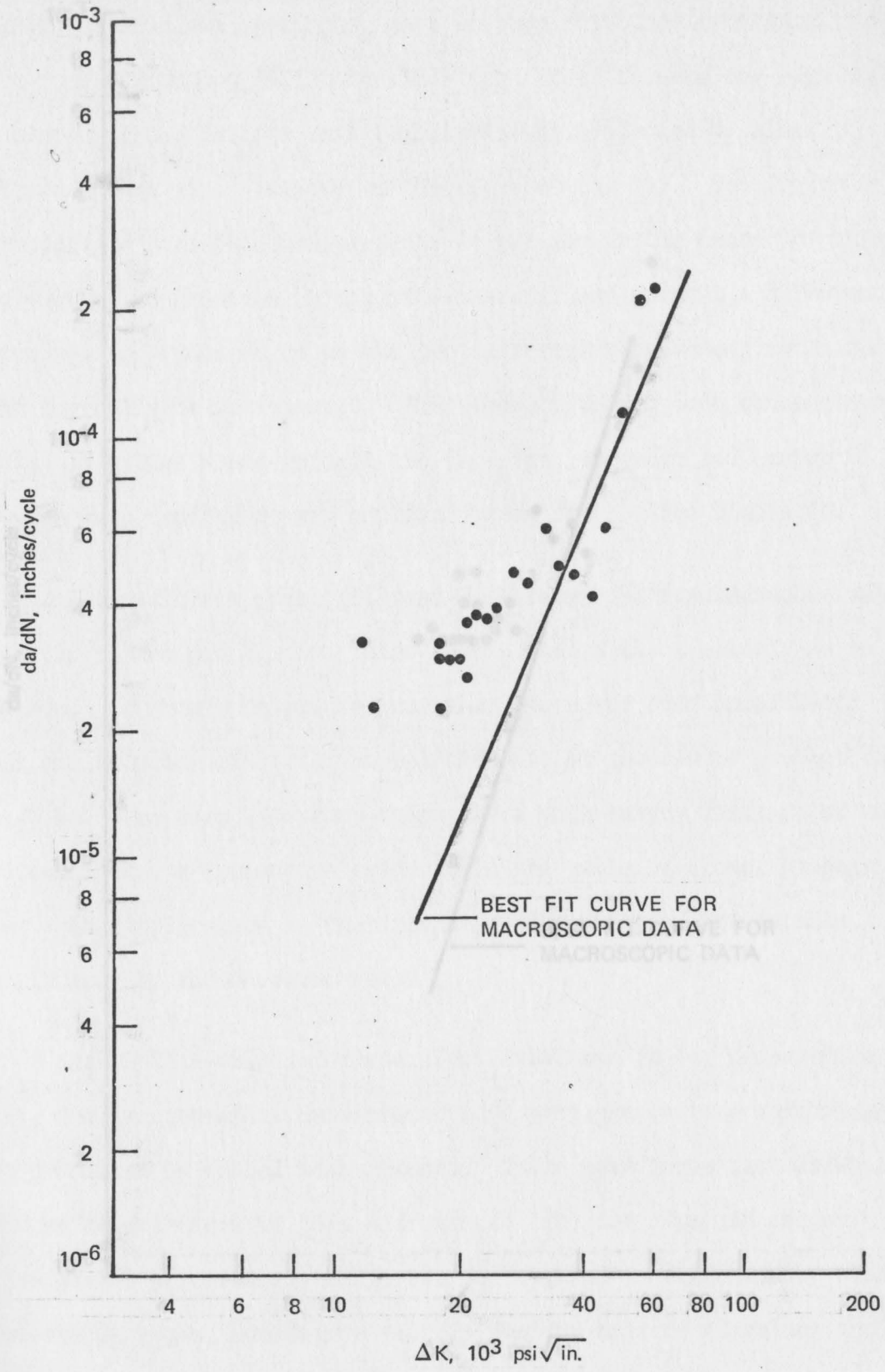

FIGURE 44 FATIGUE CRACK GROWTH DATA FROM STRIATION MEASUREMENTS FOR TITANIUM-8 Al SPECIMEN ATF-6 (GRAIN SIZE 60.1 μ)

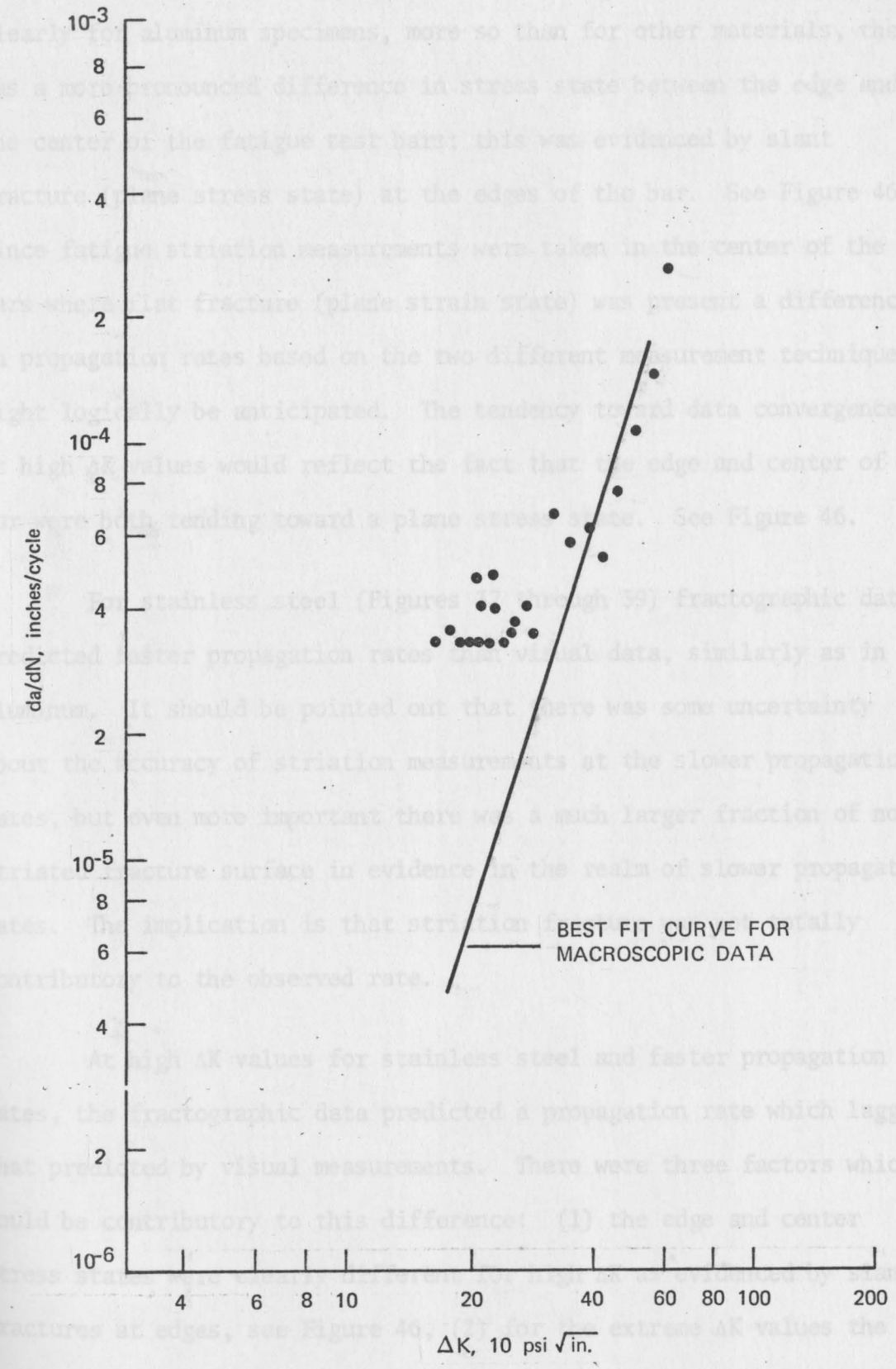

FIGURE 45 FATIGUE CRACK GROWTH DATA FROM STRIATION MEASUREMENTS FOR TITANIUM-8 Al SPECIMEN ATF-4 (GRAIN SIZE 137.5 μ)

Clearly for aluminum specimens, more so than for other materials, there was a more pronounced difference in stress state between the edge and the center of the fatigue test bars; this was evidenced by slant fracture (plane stress state) at the edges of the bar. See Figure 46. Since fatigue striation measurements were taken in the center of the bars where flat fracture (plane strain state) was present a difference in propagation rates based on the two different measurement techniques might logically be anticipated. The tendency toward data convergence at high ΔK values would reflect the fact that the edge and center of the bar were both tending toward a plane stress state. See Figure 46.

For stainless steel (Figures 37 through 39) fractographic data predicted faster propagation rates than visual data, similarly as in aluminum. It should be pointed out that there was some uncertainty about the accuracy of striation measurements at the slower propagation rates, but even more important there was a much larger fraction of non-striated fracture surface in evidence in the realm of slower propagation rates. The implication is that striation fracture was not totally contributory to the observed rate.

At high ΔK values for stainless steel and faster propagation rates, the fractographic data predicted a propagation rate which lagged that predicted by visual measurements. There were three factors which could be contributory to this difference: (1) the edge and center stress states were clearly different for high ΔK as evidenced by slant fractures at edges, see Figure 46, (2) for the extreme ΔK values the calibration length of the fatigue bar had been exceeded so there was some uncertainty as to the exact ΔK value, and (3) mixed mechanism

Figure 46. Optical Photomacrographs Showing Fatigue Fracture Surface Characteristics of Aluminum, Stainless Steel, Titanium, and Titanium-8% Aluminum.

Magnification 4.5X

fracture was evident in the center of the bar, i.e., dimpling and striation formation, implying that striation fracture was not totally responsible for the observed crack propagation rate.

For titanium rather good agreement between visual and fractographic crack propagation data was observed (Figures 40 through 42). These fractures were quite flat in a macroscopic sense (see Figure 46) and clearly under the influence of a plane strain state throughout the test length. Fractographic data did indicate faster crack propagation rates for lower ΔK values, but in this region there was substantial non-striated fracture so the contribution of striation fracture to determining the net crack propagation rate would be uncertain.

For titanium-8% aluminum (Figures 43 through 45) the agreement between visual and fractographic crack propagation data was fair, with best agreement for higher ΔK values. As for the titanium specimens the entire propagation appeared to proceed under a state of plane strain, i.e., flat fracture (see Figure 46). For lower ΔK values the fractographic data predicted faster propagation rates than the visual data. For these same lower ΔK values the propagation mechanism consisted of mixed non-striation cracking and striation fracture; therefore, as for previous data it appeared that the non-striation fracture is rate-limiting with respect to the net crack front. While higher rates may be indicated locally for propagation by the striation mechanism, the net propagation rate appears to be limited, at low levels of ΔK, by the rate associated with non-striation fracture. This postulate seems logical when one considers that substantially more non-striation fracture occurred at the lower ΔK levels.

Crack Propagation Data Analysis

Some authors[20, 21] have attempted to analyze the effects of microstructure, particularly grain size, on crack propagation rate through a direct comparison at constant stress intensity levels. IT IS OUR THESIS THAT THE USUAL METHODS OF ANALYSIS EMPLOYED IN THESE OTHER STUDIES HAVE NEGLECTED A CRITICAL ASPECT OF THE FATIGUE PROCESS--THE EFFECT OF STRESS STATE. Therefore, we have undertaken to evaluate the effects of grain size on crack propagation rate at levels of stress intensity corresponding to equivalent stress states by taking into account additionally the effects of specimen size and the monotonic yield stress of the material.

It was pointed out (in the Introduction) that the specimen thickness and material yield strength influences the stress state at the tip of a fatigue crack. It is evident that in the aluminum and stainless steel fatigue test specimens, various mixtures of plane strain (flat fracture) and plane stress (slant fracture) were present (see Figure 46). The test specimens of the titanium materials exhibited plane strain fatigue fractures. Since the fatigue fracture mode appears to be influenced by stress state[17], it is imperative that analysis of fatigue crack growth data be conducted for a constant stress state, thus encompassing the influence yield strength. Since this analysis of cyclic crack growth data involves the calculation of the plastic zone size in terms of the monotonic yield stress σ_Y, this approach may be criticized on the basis that yield strength may change under cyclic loading conditions in which higher straining rates and cyclic hardening or softening effects may exist.

The basis of our analysis hinges upon the thesis that a true comparison of crack propagation rates may be made only under constant conditions of stress state and that the stress state can be described by a constant ratio of fatigue crack plastic zone size to specimen thickness, i.e.,

$$\frac{r_p}{B} = \text{a constant, } C'$$

where r_p = plastic zone size

B = specimen thickness

Since

$$r_p = \frac{1}{12\pi}\left(\frac{K_{max}}{\sigma_Y}\right)^2$$

it follows that $K_{max} = \sigma_Y \sqrt{12\pi r_p}$

and substituting $r_p = BC'$

it is found that $K_{max} = \sigma_Y \sqrt{12\pi BC'}$

Then since for an R ratio near 0 (zero to tension loading),

$$K_{max} = \Delta K$$

$$\Delta K = \sigma_Y \sqrt{12\pi BC'}$$

This equation may then be used to calculate the stress intensity range consistent with a constant r_p/B ratio, i.e., a constant stress state.

Values of ΔK were calculated according to the preceding procedure for each fatigue specimen and the corresponding crack growth rates were determined from the power law for each material condition. Results for several r_p/B ratios are compiled in Table 8.

Constant r_p/B ratios were selected such that the crack propagation data for each material could be encompassed. It was determined that the entire set of data for all materials could be embraced by the ratio $r_p/B = 0.5$. Thus, it was possible to (a) compare all of the material conditions for constant stress state, as well as (b) examine the stress state sensitivity of crack propagation rates to grain size for each material. The crack propagation rates corresponding to constant stress state defined as $r_p/B = C'$ are plotted as a function of material grain size (Hall-Petch function) in Figures 47 and 48 for the FCC materials (aluminum and stainless steel) and HCP materials (titanium and titanium-8% aluminum), respectively.

In these plots the basic results of this work are illustrated.

Aluminum

As the stress state, defined by r_p/B was increased, i.e., as plastic zone size was increased relative to specimen thickness, there was a very slight systematic increase in crack propagation rate (see Figure 47). There was, however, no change in crack propagation rate as a function of grain size for any stress state examined.

Stainless Steel

An increase in stress state resulted in a substantial increase in crack propagation rate (see Figure 47). Further, the rate of propagation increased consistently with decreasing grain size. The rate of change of propagation rate increased systematically with increased level of stress state. Thus, it is seen that crack propagation rate is

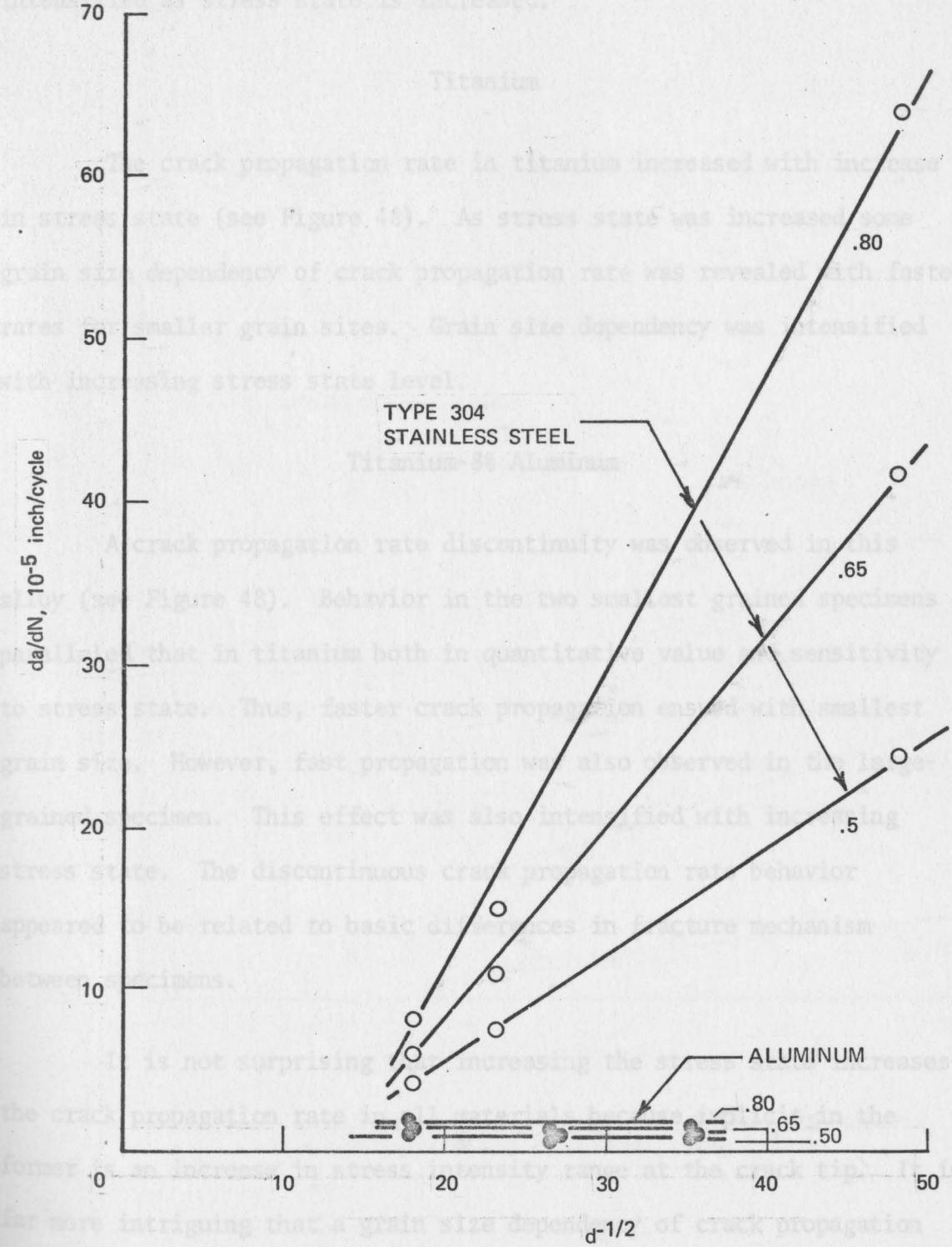

FIGURE 47 INFLUENCE OF GRAIN SIZE ON FATIGUE CRACK GROWTH IN FCC METALS FOR CONSTANT STRESS STATE

dependent upon grain size in stainless steel, and this dependency is intensified as stress state is increased.

Titanium

The crack propagation rate in titanium increased with increase in stress state (see Figure 48). As stress state was increased some grain size dependency of crack propagation rate was revealed with faster rates for smaller grain sizes. Grain size dependency was intensified with increasing stress state level.

Titanium-8% Aluminum

A crack propagation rate discontinuity was observed in this alloy (see Figure 48). Behavior in the two smallest grained specimens paralleled that in titanium both in quantitative value and sensitivity to stress state. Thus, faster crack propagation ensued with smallest grain size. However, fast propagation was also observed in the large-grained specimen. This effect was also intensified with increasing stress state. The discontinuous crack propagation rate behavior appeared to be related to basic differences in fracture mechanism between specimens.

It is not surprising that increasing the stress state increases the crack propagation rate in all materials because implicit in the former is an increase in stress intensity range at the crack tip. It is far more intriguing that a grain size dependency of crack propagation rate, when exhibited (stainless steel, titanium, titanium-8% aluminum),

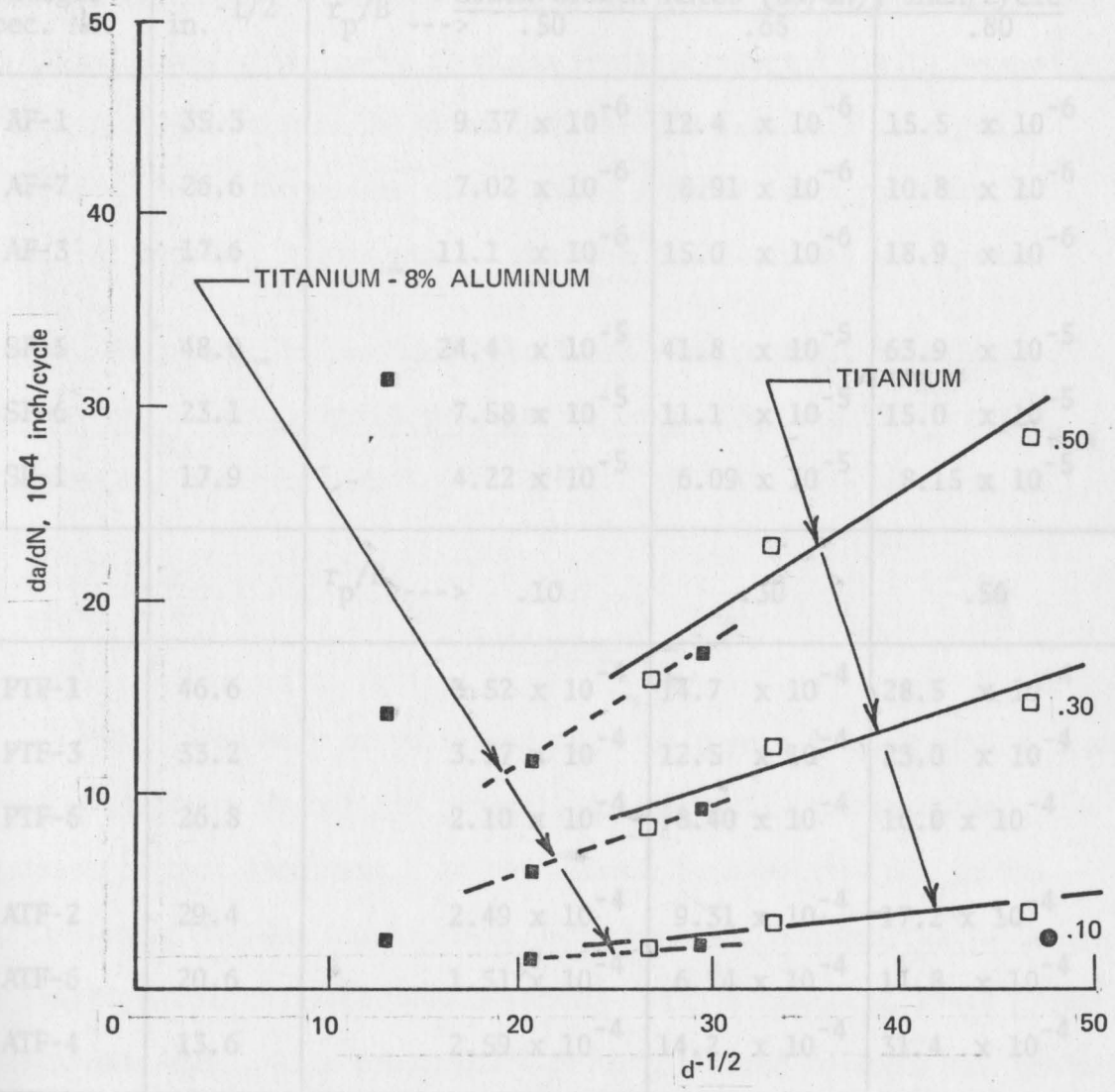

FIGURE 48 INFLUENCE OF GRAIN SIZE ON FATIGUE CRACK GROWTH IN HCP METALS FOR CONSTANT STRESS STATE

TABLE 8

CRACK GROWTH RATES AT CONSTANT STRESS STATES

Fatigue Spec. No.	$d^{-1/2}$ in. $^{-1/2}$	r_p/B --->	Crack Growth Rates (da/dN), inch/cycle .50	.65	.80
AF-1	35.3		9.37×10^{-6}	12.4×10^{-6}	15.5×10^{-6}
AF-7	26.6		7.02×10^{-6}	8.91×10^{-6}	10.8×10^{-6}
AF-3	17.6		11.1×10^{-6}	15.0×10^{-6}	18.9×10^{-6}
SF-5	48.0		24.4×10^{-5}	41.8×10^{-5}	63.9×10^{-5}
SF-6	23.1		7.58×10^{-5}	11.1×10^{-5}	15.0×10^{-5}
SF-1	17.9		4.22×10^{-5}	6.09×10^{-5}	8.15×10^{-5}
		r_p/B --->	.10	.30	.50
PTF-1	46.6		3.52×10^{-4}	14.7×10^{-4}	28.5×10^{-4}
PTF-3	33.2		3.37×10^{-4}	12.5×10^{-4}	23.0×10^{-4}
PTF-6	26.8		2.10×10^{-4}	8.40×10^{-4}	16.0×10^{-4}
ATF-2	29.4		2.49×10^{-4}	9.31×10^{-4}	17.2×10^{-4}
ATF-6	20.6		1.51×10^{-4}	6.14×10^{-4}	11.8×10^{-4}
ATF-4	13.6		2.59×10^{-4}	14.2×10^{-4}	31.4×10^{-4}

was intensified with increasing level of stress state. The trend of grain size dependency is increasingly more evident at higher r_p/B ratios.

In Figures 47 and 48 it will also be noted that a comparison of crack propagation characteristics of all materials may be made at $r_p/B = 0.5$. In this comparison it is observed that aluminum exhibited the lowest crack propagation rate, with a faster rate for stainless steel (accelerating with decreasing grain size), and much faster rates in titanium and titanium-8% aluminum (both accelerating with decreasing grain size). It should be noted that the HCP materials as a group exhibited one to two orders of magnitude greater crack propagation rates, at constant stress state, than the FCC materials as a group.

The reader is reminded that these results apply to effects of grain size on fatigue crack propagation rate. The results do not apply to the separate question of effects of grain size on total fatigue life.

Fractography

The large body of published research papers dealing with fatigue crack propagation do not, in general, include full fractographic analyses of test specimens. As has already been pointed out in the discussion of fatigue crack growth data, we have observed that a change in fractographic character was associated with a change in crack propagation character. This preliminary result is cited to focus the reader's attention on the value of fractographic characterization. In fact, it will be seen in the fractographic results which follow, that we have found evidence of structure-sensitive fracture at low levels of stress intensity in the materials investigated in this study which other investigators have only recently discovered, i.e., in the time period since

the inception of this work. Inckle, et al, have reported this phenomenon in FCC[19] and BCC[39] materials and Robinson and Beevers in HCP titanium[40].

Fractography Analysis

Aluminum

Aluminum fatigue specimens exhibited considerable fracture surface microrelief, with tearing in the direction of macroscopic crack propagation, for lower stress intensity ranges. This resulted in a terraced topology due to a somewhat structure-sensitive fracture mechanism. A typical example of this feature is shown in Figure 49; note that the process is wholly transgranular and there is no evidence of any grain boundary influence on the fatigue fracture process. For intermediate ΔK values (above 5000 psi $\sqrt{in.}$) the propagation mechanism tended to change to a classical stage II striation pattern (Figure 49). The point of transition to principally striation fracture has been indicated in the da/dN-ΔK plots of Figures 20 through 22. At high ΔK values the fatigue propagation changed from stage II "plane strain" to "plane stress" as evidenced by rotation of the fracture plane to some angle with respect to the stress axis. In conjunction with this the fracture surface markings changed from striations to "dimples" (see Figure 49) the latter evidence of substantial plastic deformation. Figures 50 through 52 document the fracture surface character for each of the grain size conditions over the range of stress intensities applied in the fatigue tests. Figures 20 through 22 indicate the ΔK

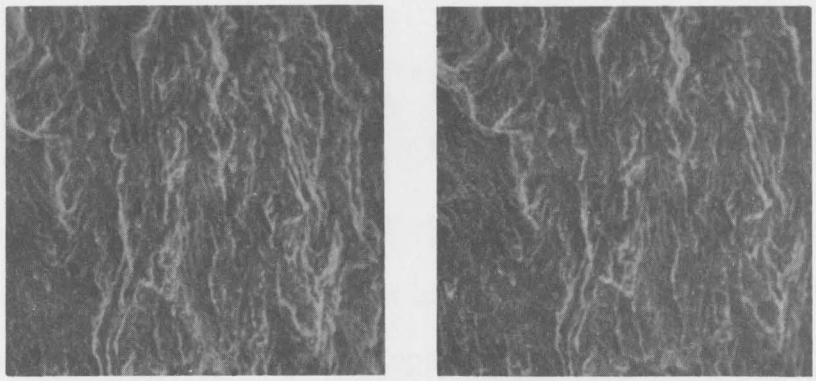

"Terraced" Fracture
Low ΔK

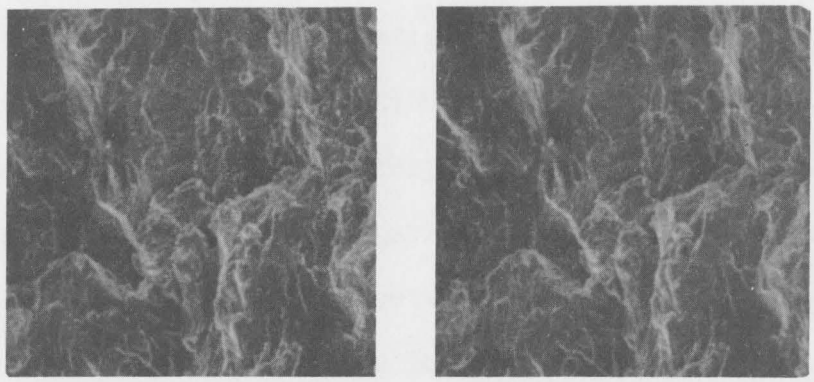

Striated Fracture
Intermediate ΔK

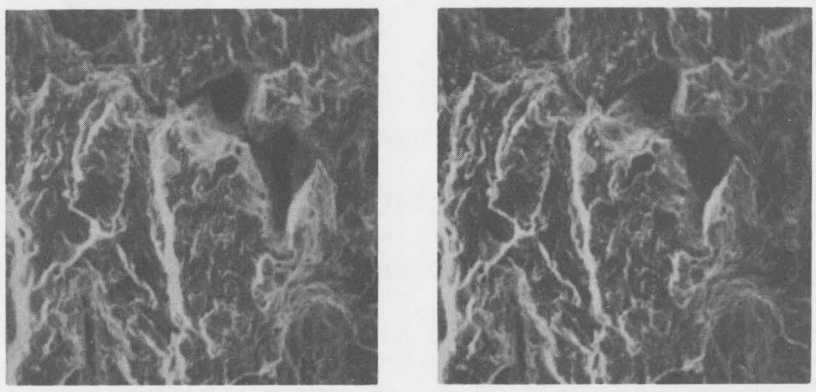

Dimpled Rupture
High ΔK

Figure 49. Scanning Electron Microscope Fractographs (Stereo-Pairs) at 100X Showing Major Fracture Surface Features as a Function of ΔK Exhibited in Aluminum Fatigue Test Specimens.

values at which these fractographs were taken. The reader should note the slight increase in fatigue striation spacing for increasing ΔK values.

The micropropagation rates of fatigue cracks in the aluminum specimens were determined by measuring fatigue striation spacings where that was possible. It should be kept in mind that these results apply to local propagation rates and should therefore not necessarily correlate with macroscopic growth rates. Figures 34 through 36 in the previous section of Microscopic Fatigue Crack Growth show micropropagation rate data derived from striation spacing measurements. Note that these data show considerable scatter; this should be anticipated since the data reflect very local propagation conditions. There was no clear trend in the pattern of variance between crack propagation rates as a function of stress intensity range for different grain sizes. Thus, the interpretation of these micropropagation data is that they represent a single band of scatter for three materials which exhibit similar behavior.

Aluminum is known to exhibit the wavy slip mode, reflecting easy cross slip, due to its high stacking fault energy. Examination of the microplastic deformation character, as reflected in the geometry of striation surfaces, shows virtually identical characteristics at constant stress state for the three grain size conditions. See Figure 53. Note that these ductile striations are relatively short, shallow, and irregularly formed. Most importantly, striation spacing

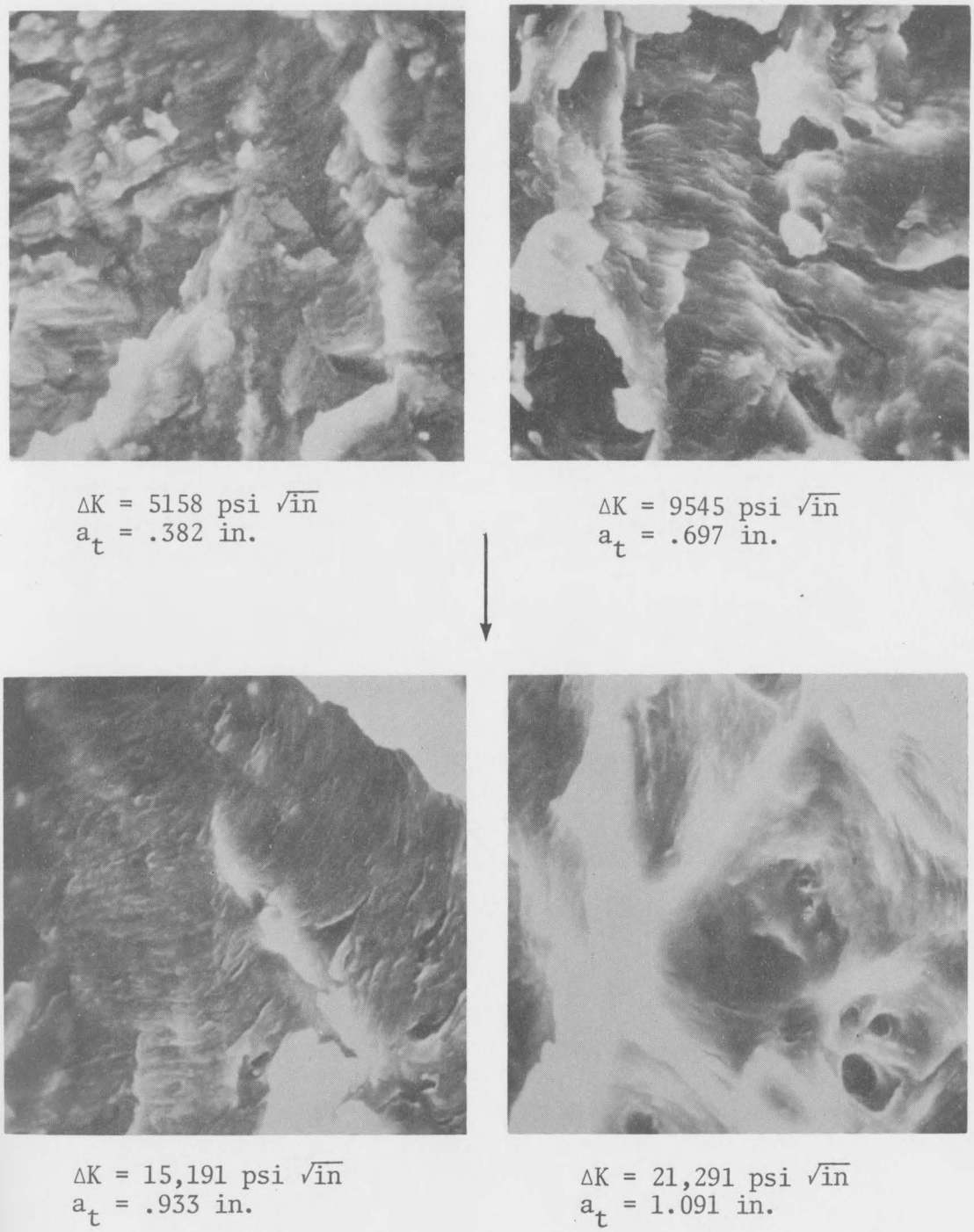

Figure 50. Scanning Electron Microscope Fractographs at 1000X Showing Fracture Surface Features at Different Stress Intensity Factor Levels for Aluminum Fatigue Specimen AF-1 (Grain Size 20.4μm).

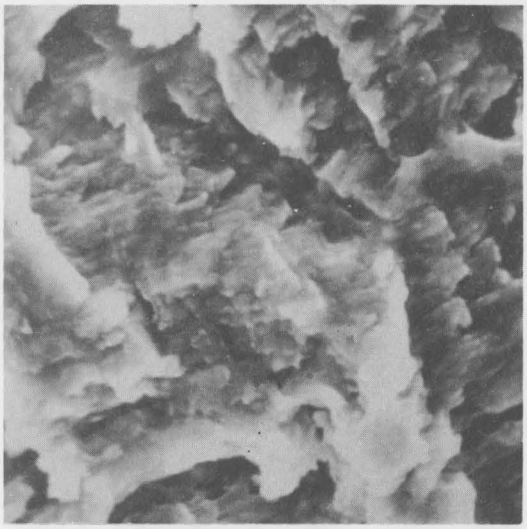

$\Delta K = 2875$ psi $\sqrt{in}$
$a_t = .375$ in.

$\Delta K = 4594$ psi $\sqrt{in}$
$a_t = .611$ in.

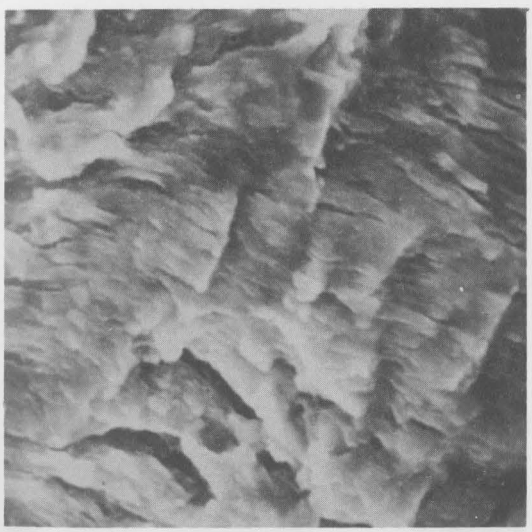

$\Delta K = 7225$ psi $\sqrt{in}$
$a_t = .848$ in.

$\Delta K = 11{,}860$ psi $\sqrt{in}$
$a_t = 1.084$ in.

Figure 51. Scanning Electron Microscope Fractographs at 1000X Showing Fracture Surface Features at Different Stress Intensity Factor Levels for Aluminum Fatigue Specimen AF-7 (Grain Size 36.0μm).

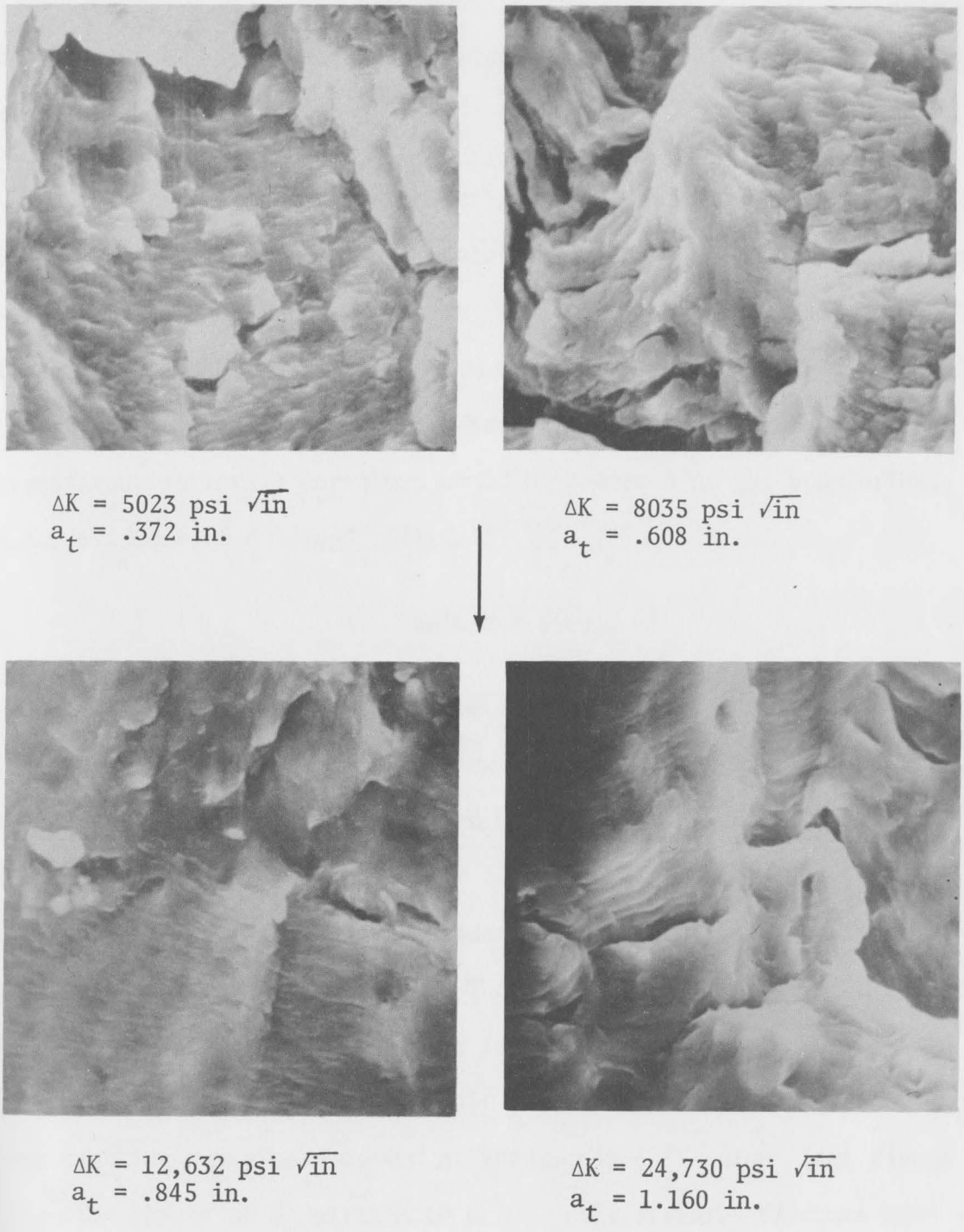

Figure 52. Scanning Electron Microscope Fractographs at 1000X Showing Fracture Surface Features at Different Stress Intensity Factor Levels for Aluminum Fatigue Specimen AF-3 (Grain Size 81.8μm).

is the same for all three specimens. This observation supports a conclusion that this micropropagation data for aluminum is independent of grain size.

Examination of the interaction of striations and boundaries, or the edges of ledges on which striations formed, showed that striations were relatively unaffected by such "barriers" (see Figure 54). This is to say that boundaries did not seem to exert much influence on crack propagation in aluminum. If they had, it would be expected that significant striation curvature would be observed at the boundaries, i.e., evidence of a "drag" effect.

Stainless Steel

Stainless steel fatigue specimens exhibited a most pronounced structure-sensitive fracture for low ΔK values (see Figure 55). Similar results have recently been reported by Birkbeck, et al[19]. This fracture type consisted of shallow faceted surface morphology, with distinct delineation of grain boundaries, although the fracture mechanism was entirely transgranular. The faceting has been attributed to slip band cracking[19]. At higher levels of ΔK (above 20,000 psi $\sqrt{\text{in.}}$) fracture tended to change to classic striated flat fracture; some secondary cracking was also observed at intermediate ΔK values (see Figure 55). The points of transition to principally striated fracture have been indicated in the da/dN-ΔK plots (Figures 23 through 25). For highest values of ΔK, crack plane rotation to a plane stress configuration occurred with concomitant dimpled rupture becoming the predominant fracture mode. Refer to Figure 55. Dimpling originating from round

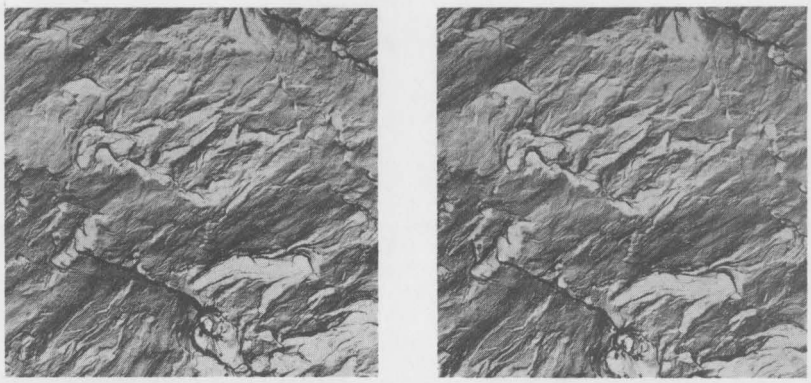

Grain Size 20.4μm

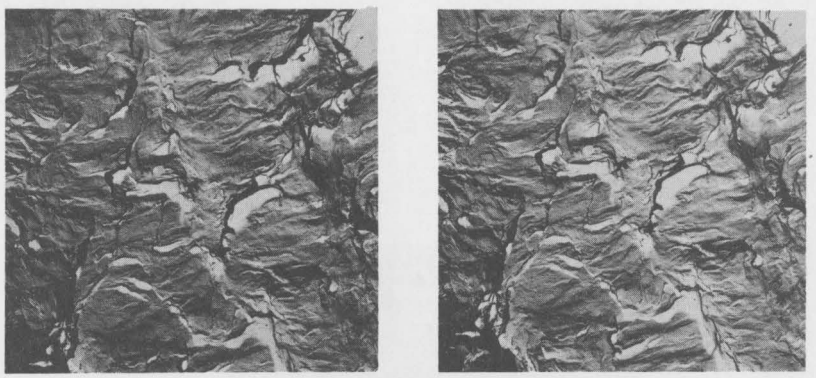

Grain Size 36.0μm

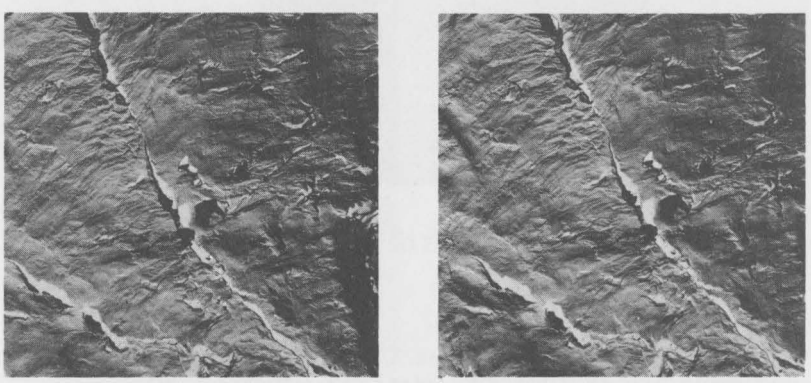

Grain Size 81.8μm

Figure 53. Transmission Electron Microscope Fractographs (Stereo-Pairs) at 5000X Showing Surface Topology of Fatigue Striations Formed in Aluminum Specimens for a Constant Stress State $r_p/B = 0.5$.

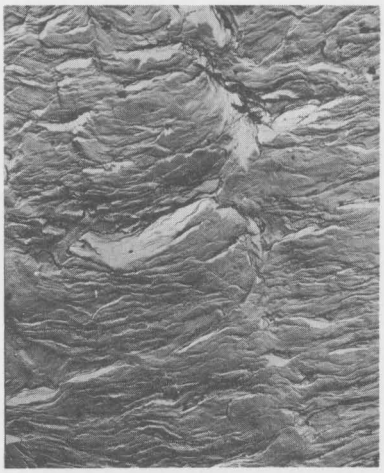

Grain Size 20.4μm

Grain Size 36.0μm

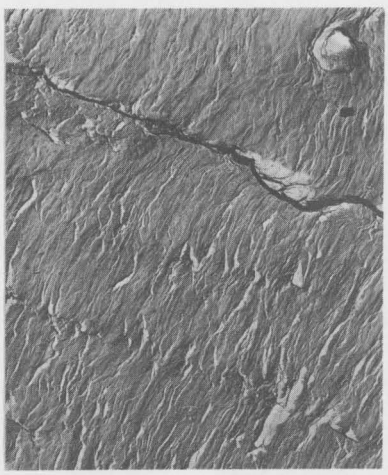

Grain Size 81.8μm

Figure 54. Transmission Electron Microscope Fractographs at 5000X Showing Fatigue Striations in Aluminum Specimens for a Constant Propagation Rate of 10^{-5} inch per cycle.

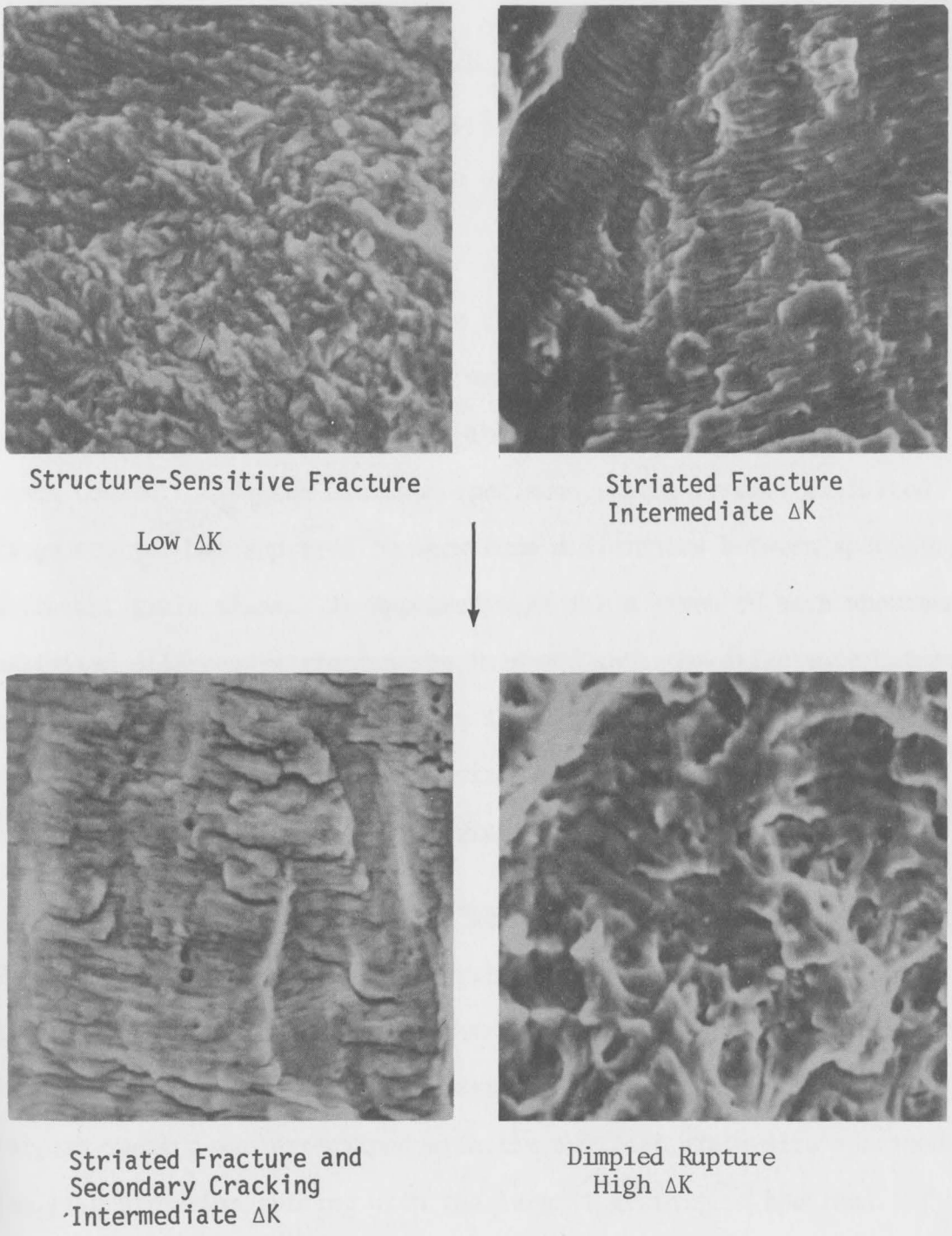

Figure 55. Scanning Electron Microscope Fractographs at 1000X Showing Major Fracture Surface Features Exhibited in Stainless Steel Fatigue Test Specimens.

inclusion particles was prominent. Figures 56 through 58 document the fracture surface character for each of the grain size conditions over the range of stress intensities applied in the fatigue tests. The reader should note the increase in striation spacing with an increase in ΔK levels.

The microcrack propagation characteristics of stainless steel as determined from fatigue striation measurements are summarized in the plots of Figures 37 through 39 in the section on Microscopic Fatigue Crack Growth. Like the aluminum specimens, these results exhibited large scatter but appeared to show some differences between specimens of different grain sizes. It appeared that for a given ΔK each specimen exhibited different striation spacings and that the difference between them became greater for increasing ΔK. The fastest propagation rate was suggested for the smallest grain size specimen, with lower rates for the intermediate and the largest grain size specimens.

For conditions of similar stress state ($r_p/B = 0.5$) the stainless steel samples of different grain size exhibited substantial differences in fracture surface character (see Figure 59). There were large differences in fatigue striation spacing with the trend that largest spacing was associated with the smallest grain size specimen and smallest striation spacing with the largest grain size specimen. These results tend to support a conclusion that there is a relationship between grain size and fatigue crack propagation rate in stainless steel.

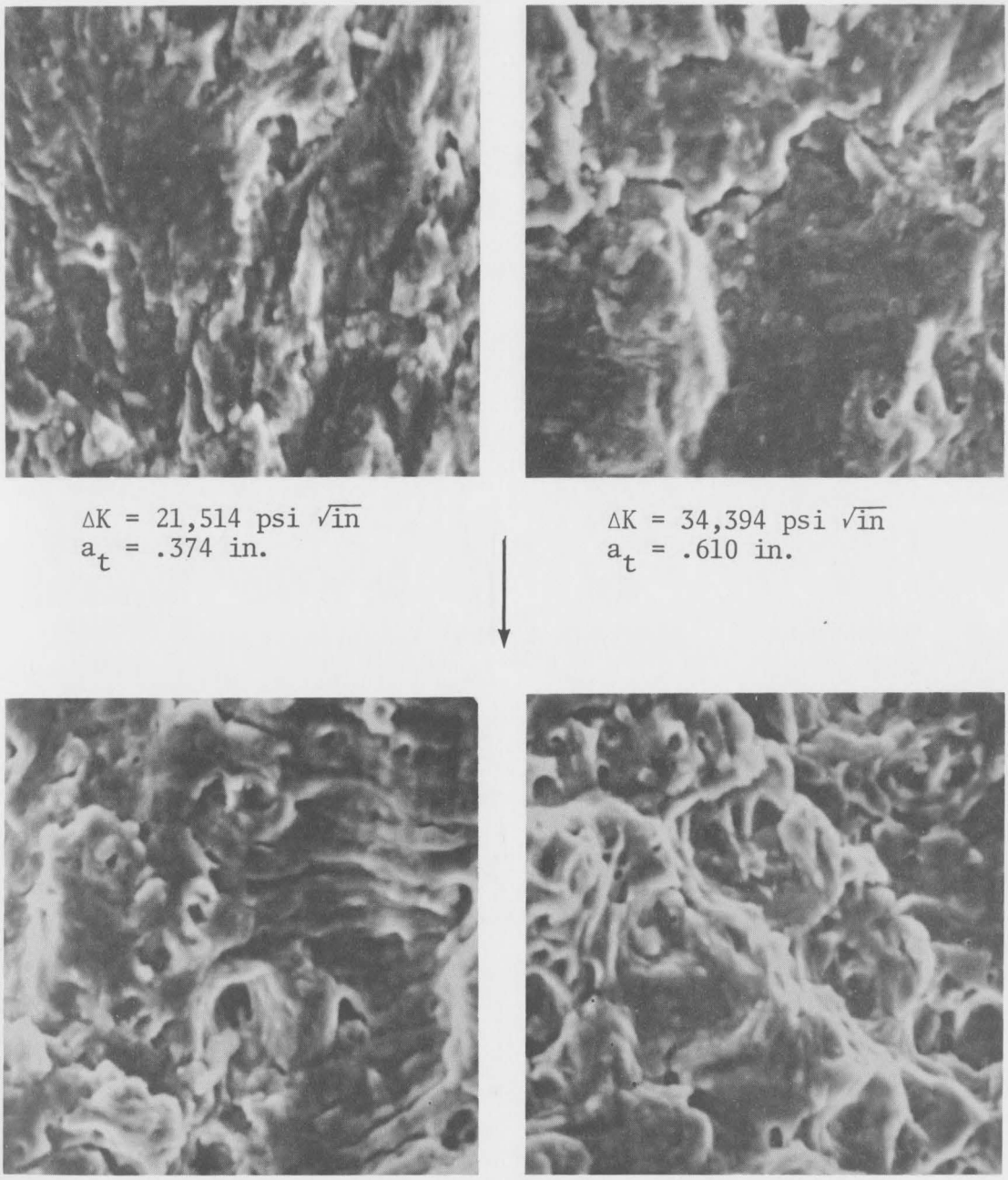

ΔK = 21,514 psi $\sqrt{in}$
a_t = .374 in.

ΔK = 34,394 psi $\sqrt{in}$
a_t = .610 in.

ΔK = 63,408 psi $\sqrt{in}$
a_t = .925 in.

ΔK = 105,944 psi $\sqrt{in}$
a_t = 1.162 in.

Figure 56. Scanning Electron Microscope Fractographs at 1000X Showing Fracture Surface Features at Different Stress Intensity Factor Levels for Stainless Steel Fatigue Specimen SF-5 (Grain Size 11.0μm).

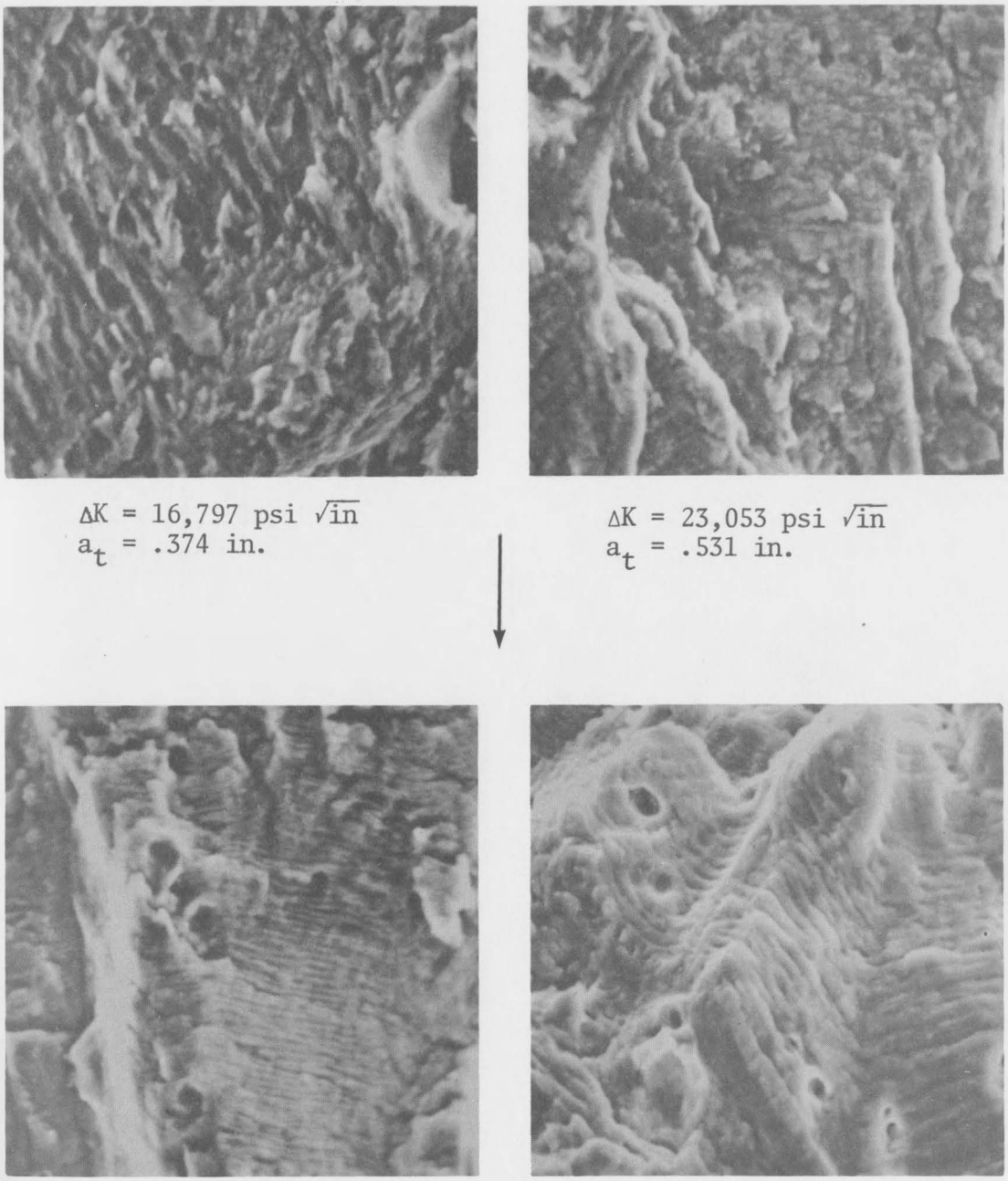

Figure 57. Scanning Electron Microscope Fractographs at 1000X Showing Fracture Surface Features at Different Stress Intensity Factor Levels for Stainless Steel Fatigue Specimen SF-6 (Grain Size 47.7μm).

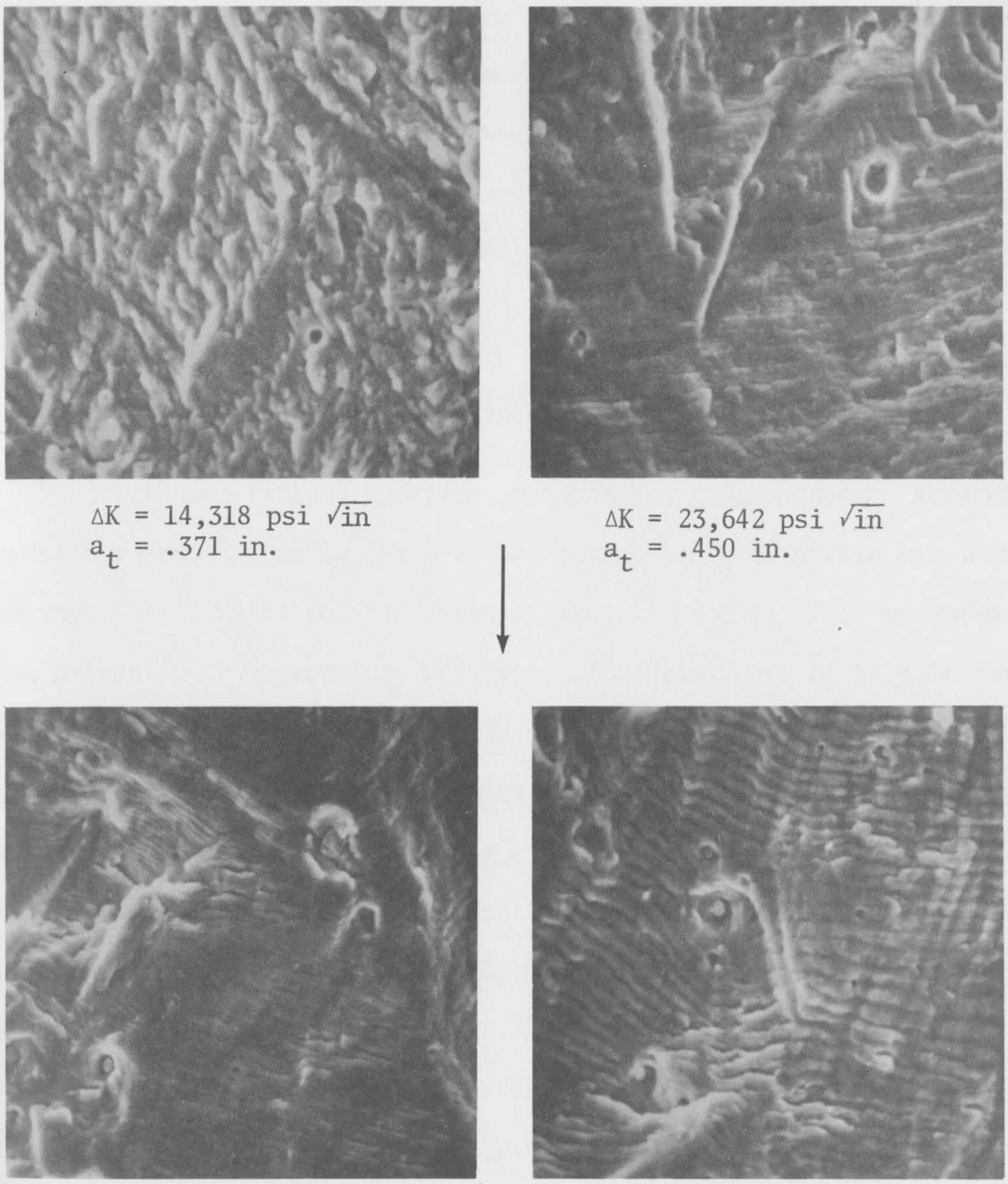

ΔK = 14,318 psi $\sqrt{in}$
a_t = .371 in.

ΔK = 23,642 psi $\sqrt{in}$
a_t = .450 in.

ΔK = 45,967 psi $\sqrt{in}$
a_t = .686 in.

ΔK = 75,715 psi $\sqrt{in}$
a_t = .844 in.

Figure 58. Scanning Electron Microscope Fractographs at 1000X Showing Fracture Surface Features at Different Stress Intensity Factor Levels for Stainless Steel Fatigue Specimen SF-1 (Grain Size 79.6μm).

Close examinations to ascertain the extent of interactions between fatigue striations and boundaries in the three stainless steel fatigue specimens (Figure 60) showed very little tendency toward interaction. Thus, we do not have direct topological confirmation that grain boundaries in themselves control the propagation rate in stainless steel.

Titanium

Titanium fatigue specimens exhibited a grain boundary structure-sensitive fracture mechanism over the entire range of stress intensity factors (ΔK) studied for all grain sizes (Figure 61). This mechanism was primarily transgranular, but grain boundaries were clearly delineated as the crack changed direction slightly at boundaries as it propagated through successive grains. This aspect of the mechanism did not appear to change substantially with increasing level of ΔK (see Figure 61). Another structure-sensitive aspect of fatigue fracture in titanium was exhibited at ΔK levels below 18,000 psi $\sqrt{\text{in.}}$ where faceting, i.e., slip band cracking occurred (see Figures 63 and 64). As ΔK increased (above 18,000 psi $\sqrt{\text{in.}}$) fatigue striations became more clearly discernible and fatigue striation spacing (microcrack propagation rate) increased. The points of transition to principally striated fracture have been indicated in the da/dN-ΔK plots (Figures 26 through 28). Striations were regular in geometry at all levels of ΔK. Figures 62 through 64 document the fracture character for each of the grain size conditions over the range of stress intensities applied in the fatigue tests. The reader will note a marked increase in fatigue striation with an increase in ΔK range.

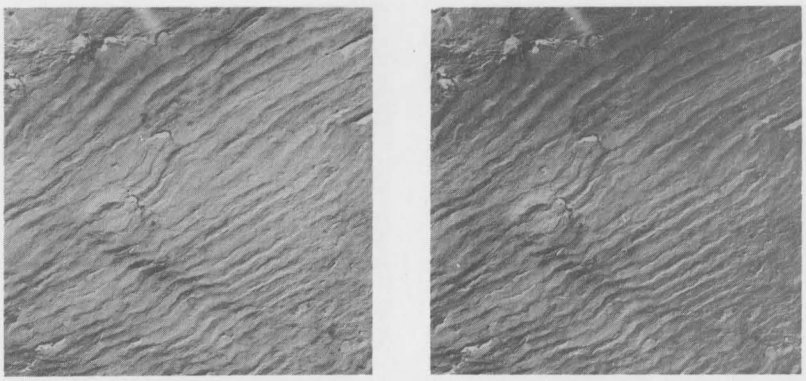

Grain Size 11.0μm

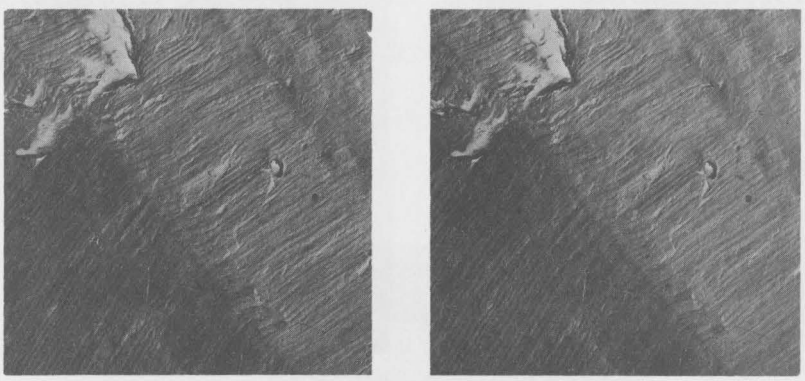

Grain Size 47.7μm

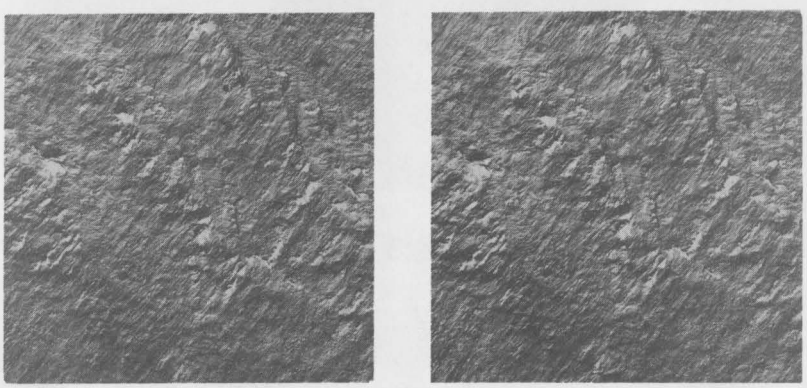

Grain Size 79.6μm

Figure 59. Transmission Electron Microscope Fractographs (Stero-Pairs) at 5000X Showing Surface Topology of Fatigue Striations Formed in Stainless Steel Specimens for a Constant Stress State $r_p/B = 0.5$.

Grain Size 11.0μm

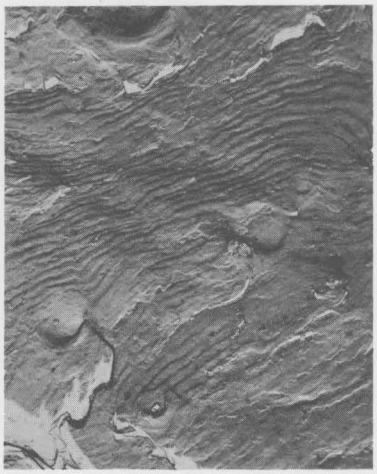

Grain Size 47.7μm

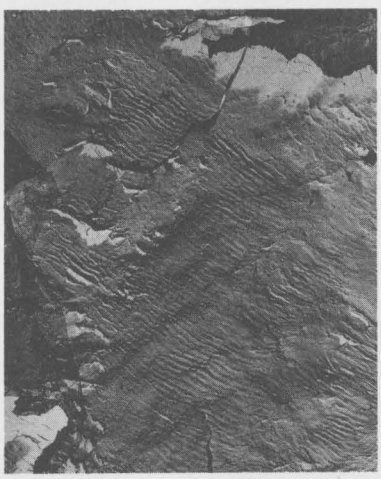

Grain Size 79.6μm

Figure 60. Transmission Electron Microscope Fractographs at 5000X Showing Fatigue Striations in Stainless Steel Specimens for a Constant Propagation Rate of 10^{-5} inch per cycle.

Grain Size 11.0μm

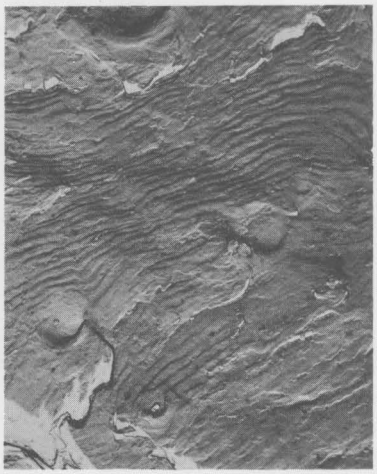

Grain Size 47.7μm

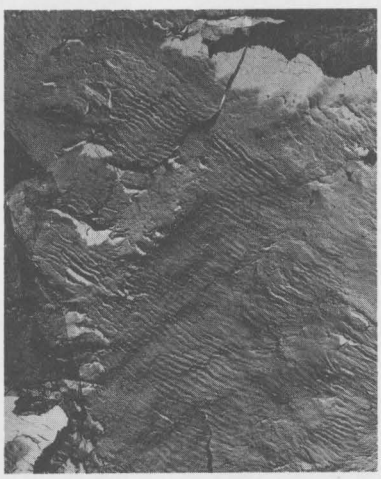

Grain Size 79.6μm

Figure 60. Transmission Electron Microscope Fractographs at 5000X Showing Fatigue Striations in Stainless Steel Specimens for a Constant Propagation Rate of 10^{-5} inch per cycle.

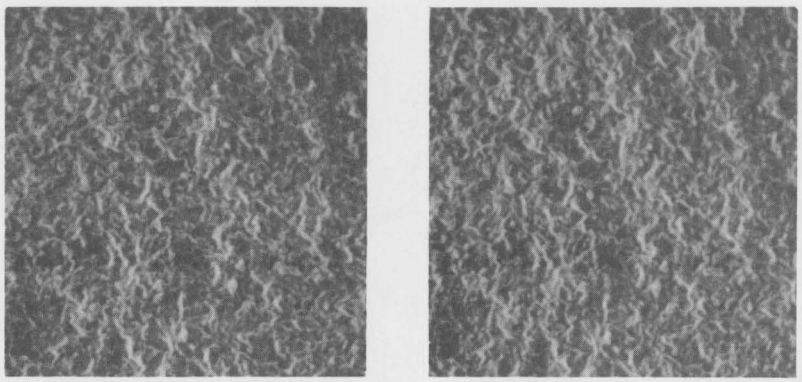

Grain Size 11.7μm

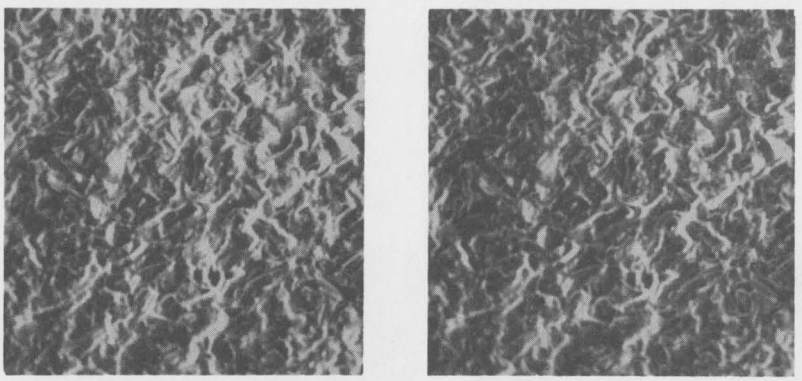

Grain Size 23.1μm

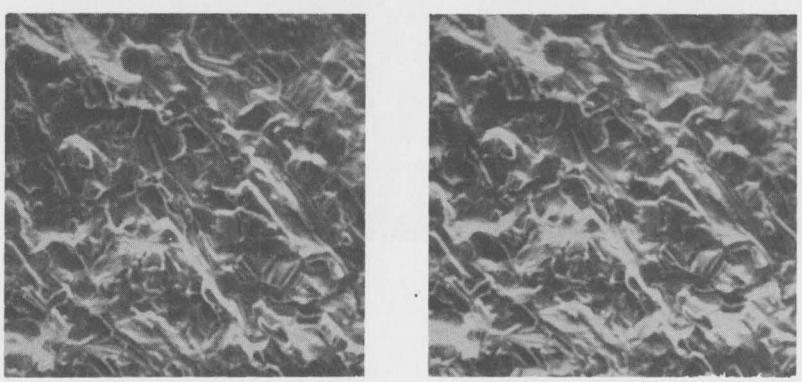

Grain Size 35.4μm

Figure 61. Scanning Electron Microscope Fractographs (Stereo-Pairs) at 100X Showing Major Fracture Surface Features as a Function of Grain Size Exhibited in Titanium Fatigue Test Specimens.

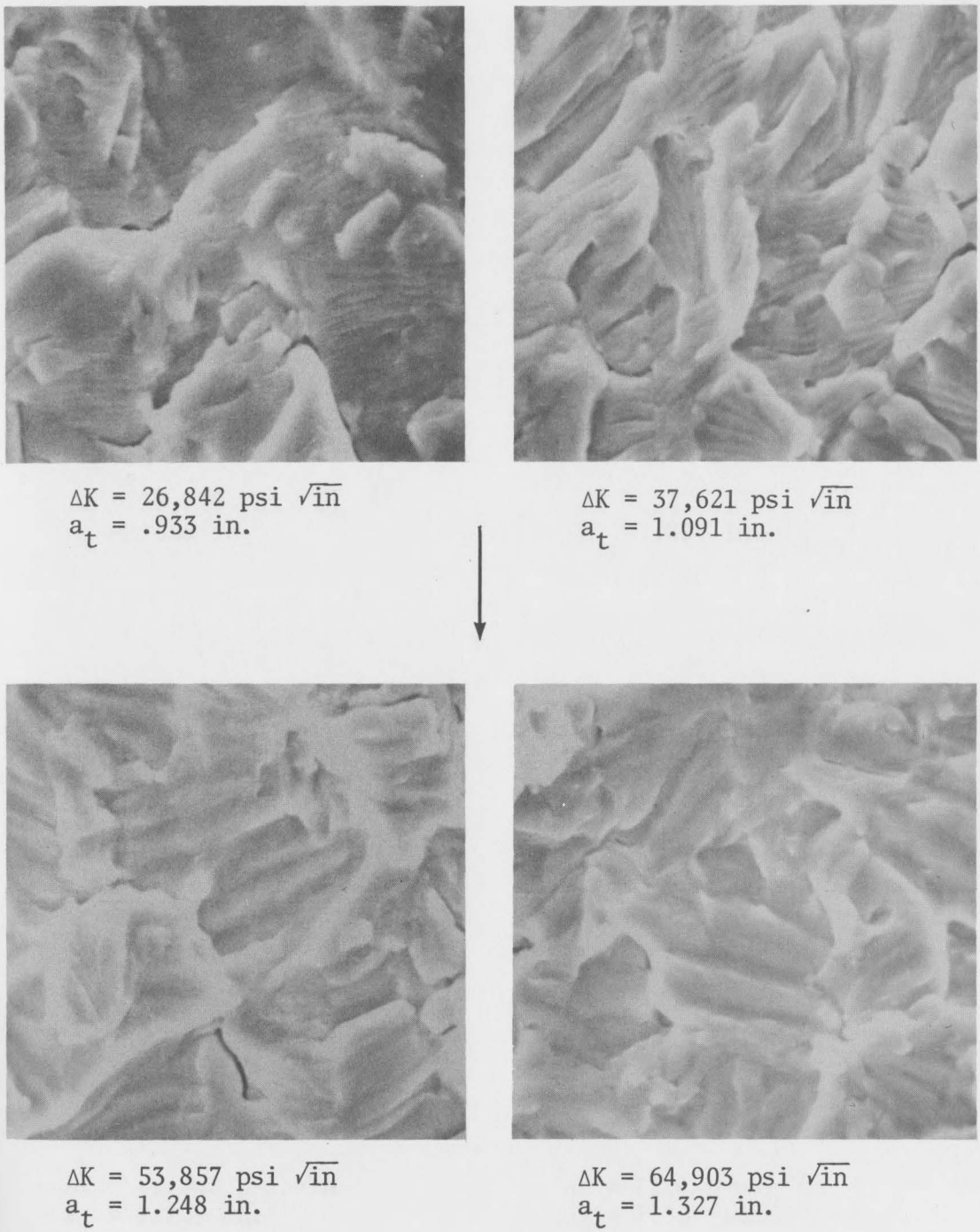

ΔK = 26,842 psi $\sqrt{in}$
a_t = .933 in.

ΔK = 37,621 psi $\sqrt{in}$
a_t = 1.091 in.

ΔK = 53,857 psi $\sqrt{in}$
a_t = 1.248 in.

ΔK = 64,903 psi $\sqrt{in}$
a_t = 1.327 in.

Figure 62. Scanning Electron Microscope Fractographs at 1000X Showing Fracture Surface Features at Different Stress Intensity Factor Levels for Titanium Fatigue Specimen PTF-1 (Grain Size 11.7μm).

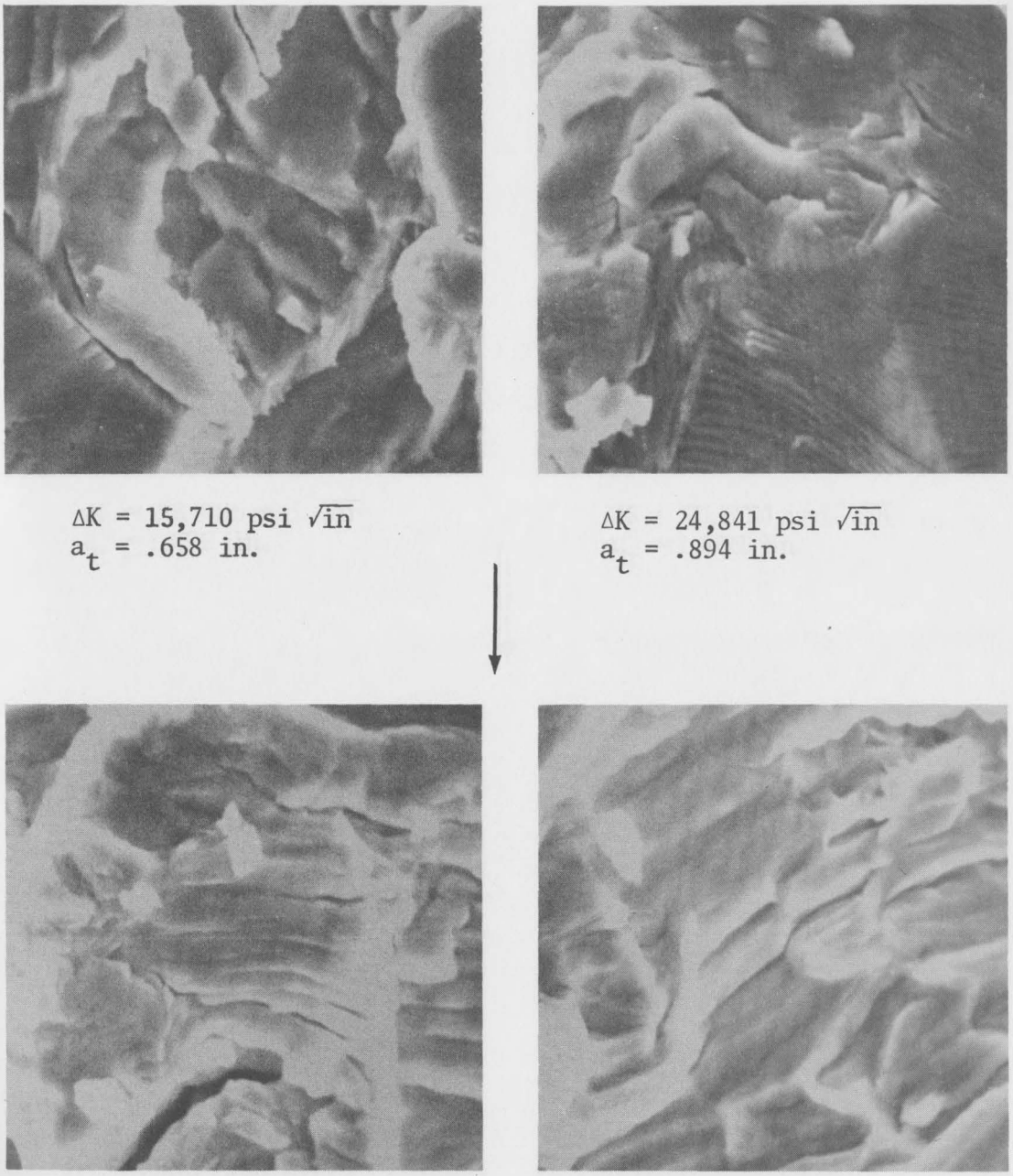

ΔK = 15,710 psi $\sqrt{in}$
a_t = .658 in.

ΔK = 24,841 psi $\sqrt{in}$
a_t = .894 in.

ΔK = 49,340 psi $\sqrt{in}$
a_t = 1.209 in.

ΔK = 71,499 psi $\sqrt{in}$
a_t = 1.367 in.

Figure 63. Scanning Electron Microscope Fractographs at 1000X Showing Fracture Surface Features at Different Stress Intensity Factor Levels for Titanium Fatigue Specimen PTF-3 (Grain Size 23.1μm).

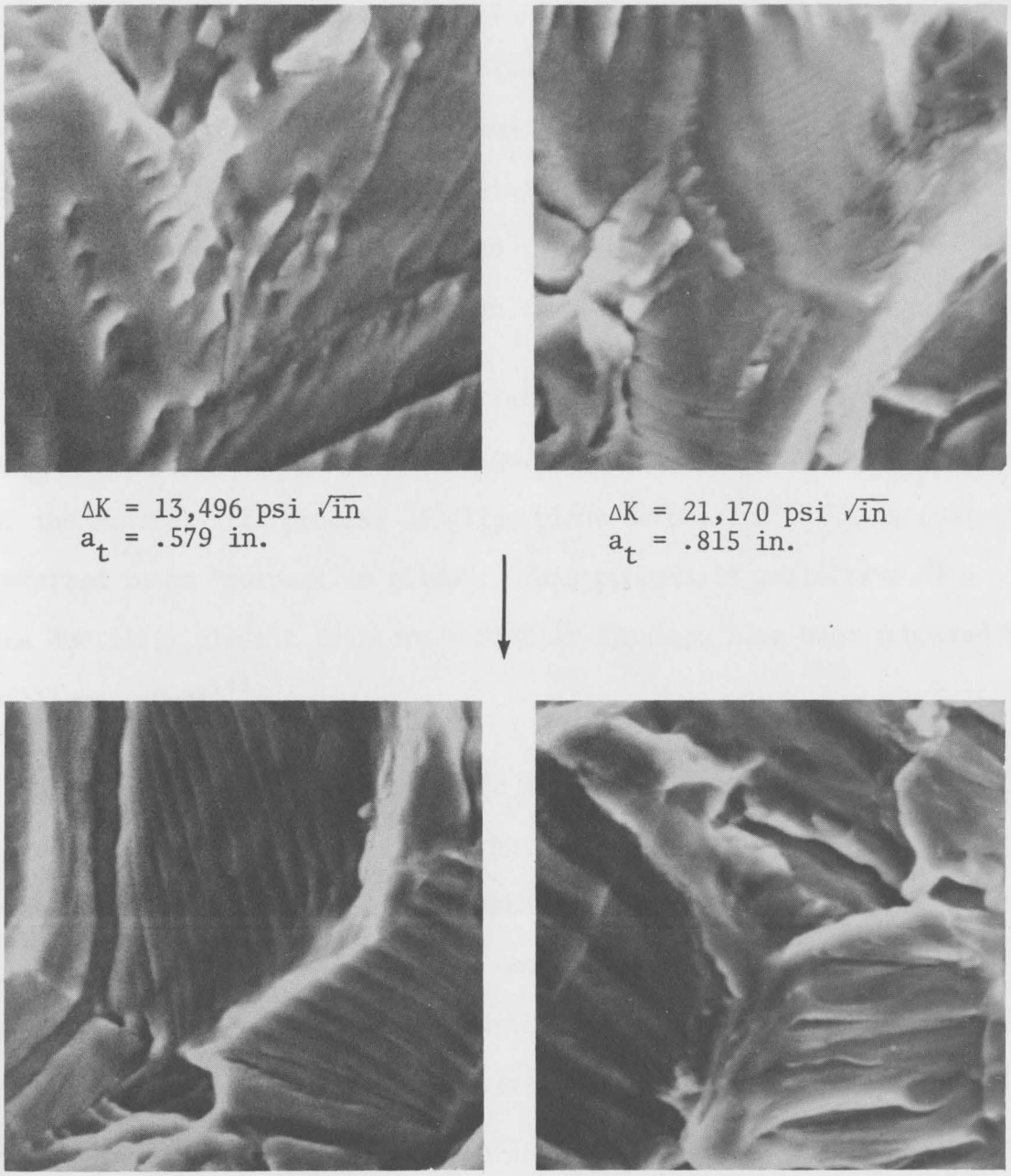

ΔK = 13,496 psi $\sqrt{in}$
a_t = .579 in.

ΔK = 21,170 psi $\sqrt{in}$
a_t = .815 in.

ΔK = 41,086 psi $\sqrt{in}$
a_t = 1.130 in.

ΔK = 59,130 psi $\sqrt{in}$
a_t = 1.288 in.

Figure 64. Scanning Electron Microscope Fractographs at 1000X Showing Fracture Surface Features at Different Stress Intensity Factor Levels for Titanium Fatigue Specimen PTF-6 (Grain Size 35.4μm).

All fractures observed in titanium were of the stage II "plane strain" type. Little plastic deformation was observed in macroscopic examination of the fracture specimens. This more brittle behavior contrasted to the aluminum and stainless steel behavior, where for both of the latter, substantial specimen thinning and prominent "plane stress" fractures occurred for high ΔK conditions.

Examination of fatigue striations in titanium samples, at high magnification as illustrated in Figure 65, showed that they had formed by the microplastic process of glide plane decohesion which is commonly referred to as "serpentine glide". This process is reflective of a low ductility plastic fracture. Similar findings have been reported by Williams, et al[41].

At constant stress state ($r_p/B = 0.5$) for the different grain size specimens (Figure 65) shows that fatigue striation spacing, or microcrack propagation rate was essentially the same for the two largest grain size specimens and somewhat smaller (faster rate) for the small grain size specimen. The mechanistic details of microplastic formation of striations in these specimens were identical. Within the scope of our work, these results suggest that grain size has a slight influence on crack propagation rate in titanium. However, the range in grain sizes of the titanium materials was somewhat small.

For conditions of similar crack propagation rate ($\sim 10^{-5}$ inch per cycle) it was observed that fatigue striations tended to interact slightly with grain boundaries in titanium (see Figure 66). This effect was small, manifested as slight striation curvature in the vicinity of

Grain Size 11.7μm

Grain Size 23.1μm

Grain Size 35.4μm

Figure 65. Transmission Electron Microscope Fractographs (Stereo-Pairs) at 5000X Showing Surface Topology of Fatigue Striations Formed in Ti Specimens for a Constant Stress State $r_p/B = 0.5$

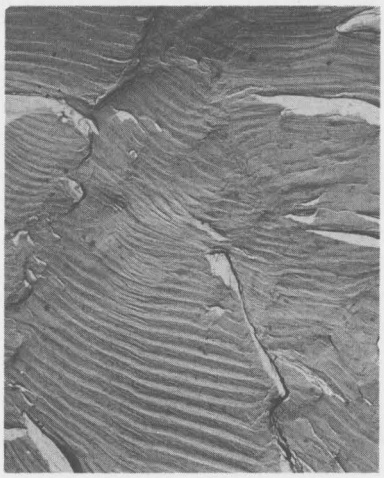

Grain Size 11.7μm

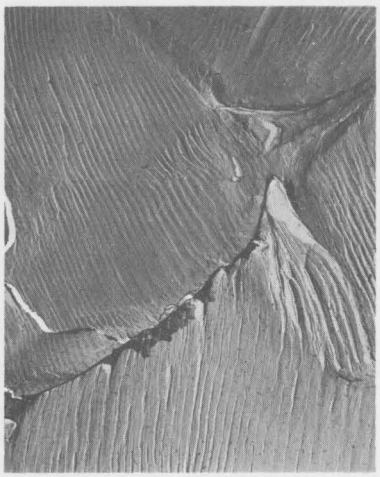

Grain Size 23.1μm

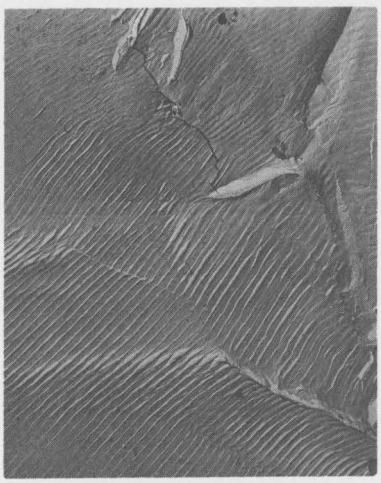

Grain Size 35.4μm

Figure 66. Transmission Electron Microscope Fractographs at 5000X Showing Fatigue Striations in Titanium Specimens for a Constant Propagation Rate of 10^{-5} inch per cycle.

boundaries. This is believed to represent a small retarding influence on propagation due to grain boundary interaction. The effect seemed to be present to the same degree in all specimens. Since the effect is so short range it might be expected to be a second order and therefore probably undetectable on a macroscopic scale.

Microcrack propagation rates, as a function of stress intensity factor range, were determined for the three titanium specimens of different grain sizes by measurement of fatigue striation spacings. These results are plotted in Figures 40 through 42 in the section on Microscopic Fatigue Crack Growth. A comparison of these data suggest an increased propagation rate with decreased grain size, with comparable rates for the two larger grain size specimens.

Titanium-8% Aluminum Alloy

The titanium alloy exhibited both differences and similarities in fatigue fracture character as compared to the unalloyed titanium material. The titanium alloy also exhibited a grain boundary structure-sensitive fracture that was prominent at all levels of stress intensity factor range (ΔK). For low ΔK values, fracture surfaces exhibited a structure-sensitive prestriation fracture with slip plane cracking oriented approximately in the direction of macroscopic crack advance; this resulting in an angular faceted fracture surface (Figure 67). Grain boundaries were prominently marked because the crack changed direction upon advancing through successive grains. With increasing ΔK, (above 18,000 psi $\sqrt{\text{in.}}$) flat striated fracture surfaces became more prominent (Figure 67). These areas were delineated by grain boundaries,

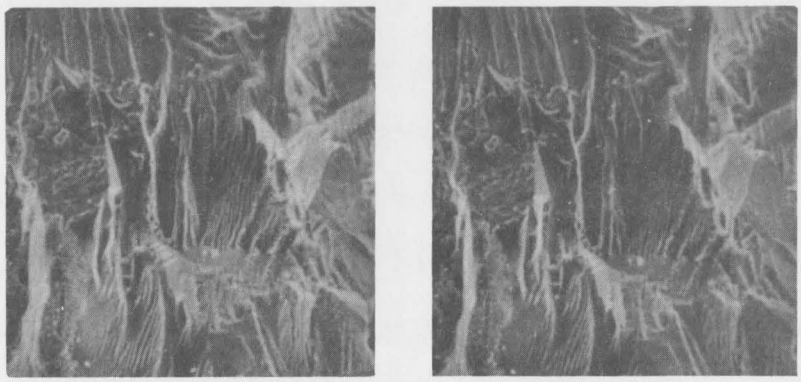

Structure - Sensitive Fracture
Low ΔK

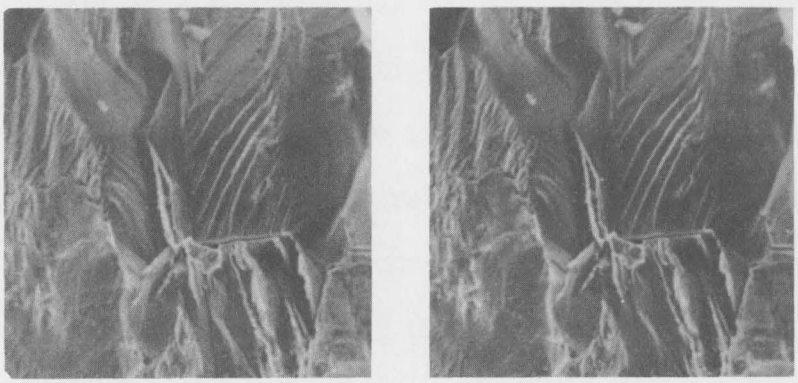

Mixed Structure - Sensitive and Striated Fracture.
Intermediate ΔK

Striated Fracture (Note Grain Structure Sensitivity).
High ΔK

Figure 67. Scanning Electron Microscope Fractographs (Stereo-Pairs) at 100X Showing Major Fracture Surface Features as a Function of ΔK Exhibited in Titanium-8 Aluminum Fatigue Test Specimens.

i.e., subject to the same grain boundary sensitivity effect as the faceted fracture. This is due to the crack path changing direction upon passage from one grain to another. Thus, the transgranular propagation process marked grain boundary positions. The points of transition to principally striated fracture have been indicated in the da/dN-ΔK plots (Figures 29 through 31). At high ΔK values fatigue fracture was almost exclusively flat and striated (Figure 67), with striation spacing increasing with increasing ΔK. Grain boundary structure sensitivity was still evident at the highest ΔK values. Figure 68 illustrates the influence of grain size on fatigue fracture surface texture. Here it should be noted that the large grain size specimen exhibited a most pronounced brittle slip band cracking (cleavage), particularly at low ΔK. Figures 69 through 71 document the fracture character for each of the grain size conditions over the range of stress intensities applied in the fatigue tests. The reader should note the increase in fatigue striation spacing with increasing ΔK.

Ti-8% Al exhibited marked similarities to titanium in propagation character observed in the striated regions of the fatigue fracture surface. Striations were formed by a serpentine glide process as illustrated in Figure 72. For constant stress state ($r_p/B = 0.5$) striation spacings were similar, and in fact were similar to those in pure titanium for the same stress state. This result suggests that since the microplastic deformation character of Ti and Ti-8% Al are virtually the same they do not differ substantially in crack propagation character. This is seen to be the case by comparison of the microcrack propagation

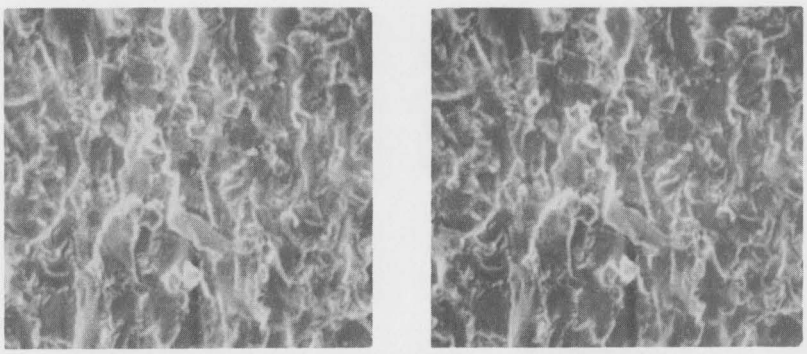

Grain Size 29.4μm

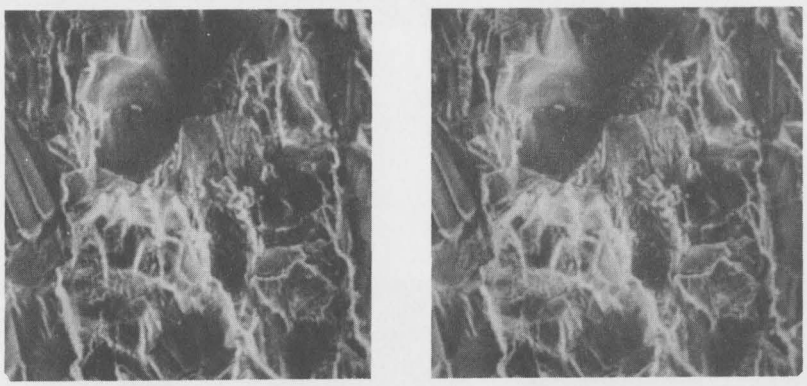

Grain Size 60.1μm

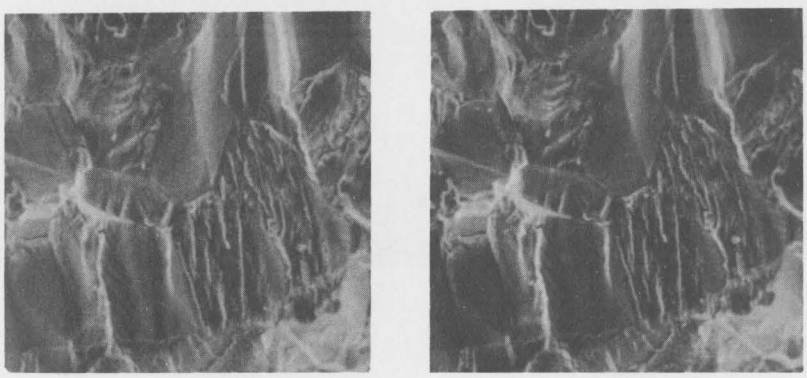

Grain Size 137.5μm

Figure 68. Scanning Electron Microscope Fractographs (Stereo-Pairs) at 100X Showing Major Fracture Surface Features as a Function of Grain Size Exhibited in Titanium-8 Aluminum Fatigue Test Specimens.

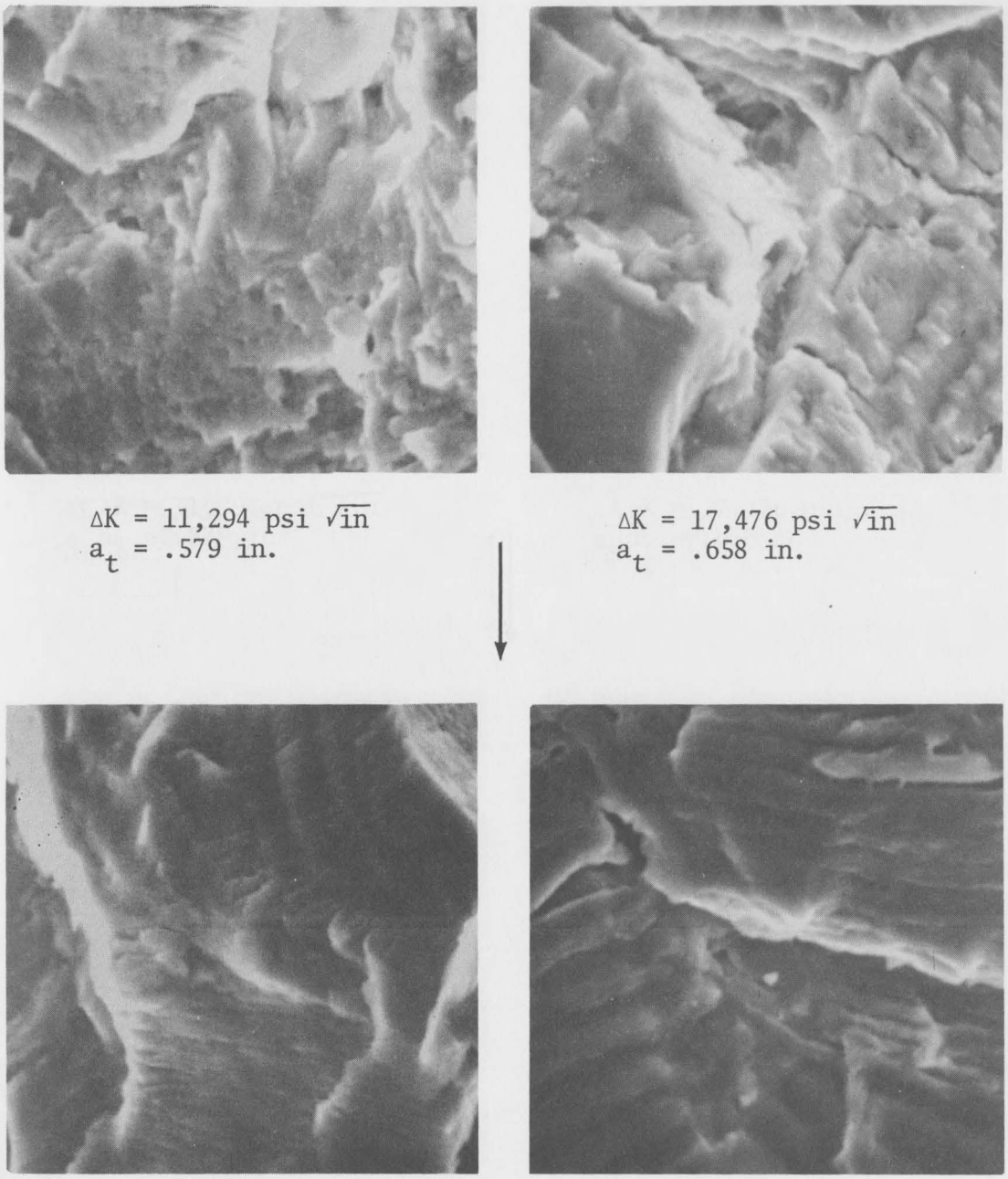

ΔK = 11,294 psi $\sqrt{in}$
a_t = .579 in.

ΔK = 17,476 psi $\sqrt{in}$
a_t = .658 in.

ΔK = 34,386 psi $\sqrt{in}$
a_t = 1.130 in.

ΔK = 59,654 psi $\sqrt{in}$
a_t = 1.367 in.

Figure 69. Scanning Electron Microscope Fractographs at 1000X Showing Fracture Surface Features at Different Stress Intensity Factor Levels for Titanium-8 Aluminum Fatigue Specimen ATF-6 (Grain Size 29.4μm).

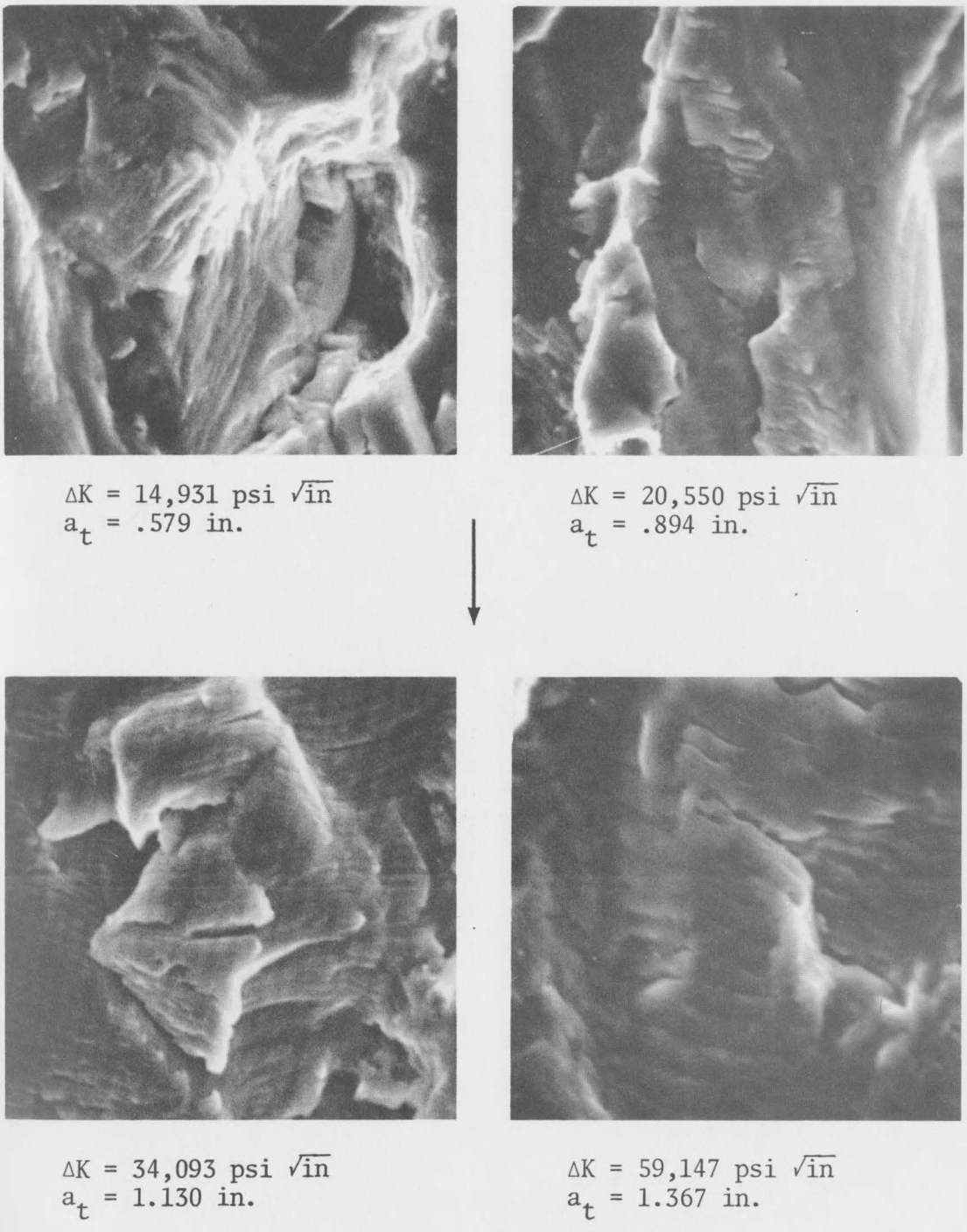

Figure 70. Scanning Electron Microscope Fractographs at 1000X Showing Fracture Surface Features at Different Stress Intensity Factor Levels for Titanium-8 Aluminum Fatigue Specimen ATF-2 (Grain Size 60.1μm).

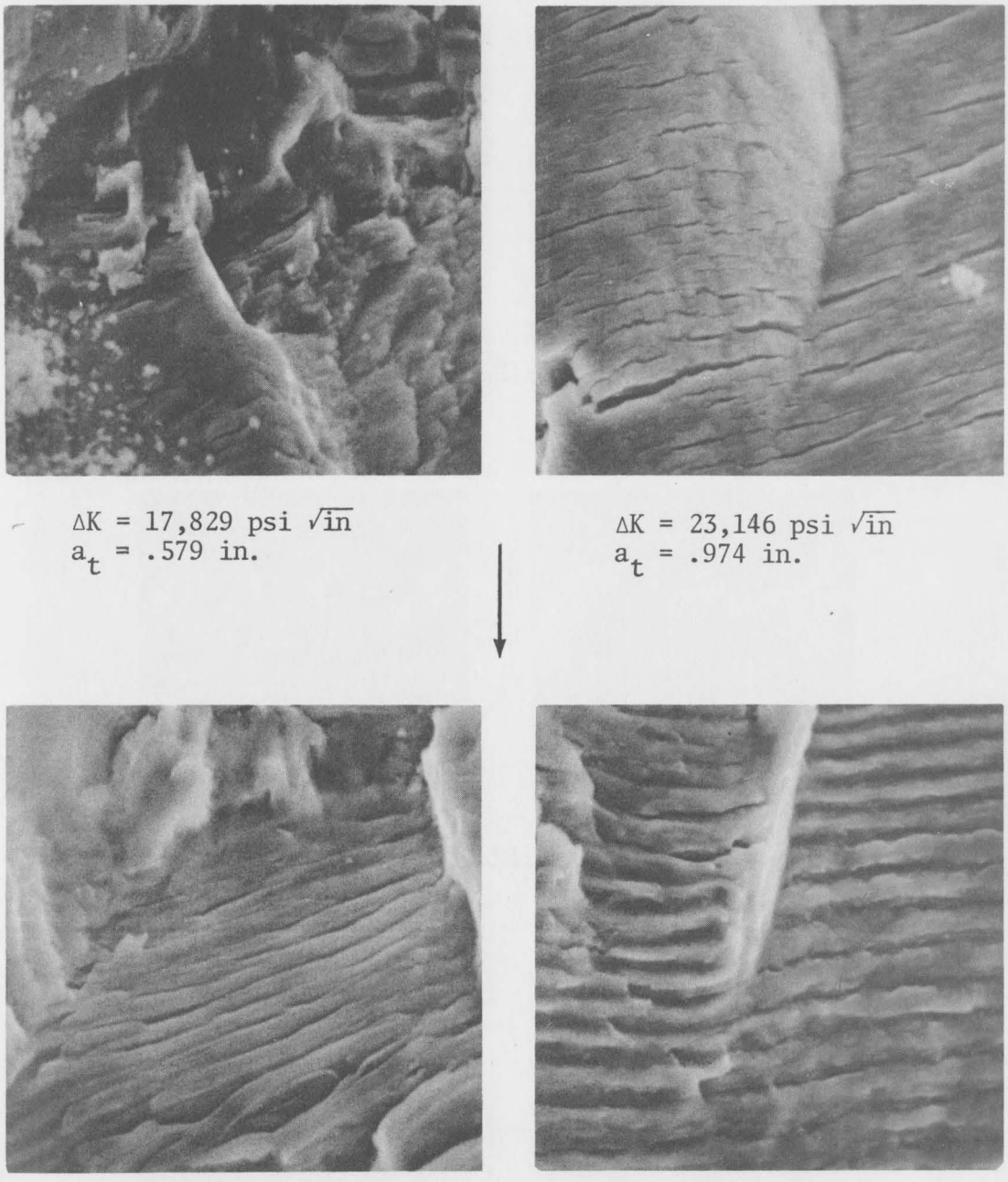

ΔK = 17,829 psi $\sqrt{in}$
a_t = .579 in.

ΔK = 23,146 psi $\sqrt{in}$
a_t = .974 in.

ΔK = 38,991 psi $\sqrt{in}$
a_t = 1.209 in.

ΔK = 56,502 psi $\sqrt{in}$
a_t = 1.367 in.

Figure 71. Scanning Electron Microscope Fractographs at 1000X Showing Fracture Surface Features at Different Stress Intensity Factor Levels for Titanium-8 Aluminum Fatigue Specimen ATF-4 (Grain Size 137.5μm).

Grain Size 29.4μm

Grain Size 60.1μm

Grain Size 137.5μm

Figure 72. Transmission Electron Microscope Fractographs (Stereo-Pairs) at 5000X Showing Surface Topology of Fatigue Striations Formed in Ti-8Al Specimens for a Constant Stress State $r_p/B = 0.5$.

data for the two materials, i.e., Figures 40 through 42 for Ti versus Figures 43 through 45 for Ti-8% Al.

Comparison of the Ti-8% Al results to Ti results shows a data overlap which suggests that the crack propagation characteristics of the two materials are the same. Fractographic results on the scale of striation spacings support this analysis, although the mechanistic details of crack propagation at lower ΔK values appear different for pure Ti versus Ti-8% Al. This does not seem to influence propagation rate between the two materials.

Ti-8% Al fatigue striations exhibited some curvature as they interacted with grain boundaries, as did striations in Ti material (Figure 73). This effect was small and was considered also to be a second order effect insofar as it influences crack propagation.

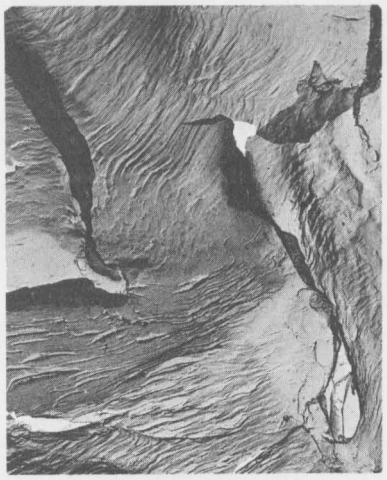

Grain Size 29.4μm

Grain Size 60.1μm

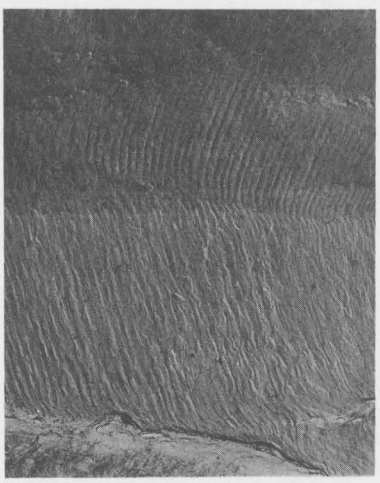

Grain Size 137.5μm

Figure 73. Transmission Electron Microscope Fractographs at 5000X Showing Fatigue Striations in Ti-8Al Specimens for a Constant Propagation Rate of 10^{-5} inch per cycle.

CHAPTER IV

DISCUSSION

Stress State, Grain Size, and Fatigue Crack Propagation Rate

The influence of grain size on fatigue crack growth in FCC and HCP metals is illustrated in Figures 47 and 48. The crack growth data were analyzed on the basis of constant state of stress since other investigators have indicated that specimen thickness and flow stress influence fatigue crack growth. We have arbitrarily defined the state of stress at the crack tip by the ratio of plastic zone size (r_p) for cyclic loading to the specimen thickness (B). Low values of r_p/B approach plane strain conditions (flat fracture with little or no lateral contraction; while high values of this ratio approach plane stress conditions (slanted fracture with noticeable or gross lateral contraction).

For the FCC crystal system, aluminum exhibits no significant dependence of fatigue crack growth on grain size over the range of grain sizes investigated (8×10^{-4} to 32×10^{-4} inches). In addition, crack growth rates in aluminum do not seem to be influenced by the state of stress within the range of r_p/B ratios of 0.30 to 0.80. The Type 304 austenitic stainless steel, however, shows a significant dependence of crack growth rate on grain size (in the range of 4.3×10^{-4} to 31.3×10^{-4} inches). This dependency appears quite linear when grain size is plotted as $d^{-1/2}$, and therefore relates to the theories of

Hall and Petch on the relationship of grain size and mechanical properties. The stainless steel, moreover, exhibited a greater sensitivity or degree of dependency at higher r_p/B ratios or in other words, as the state of stress tends toward plane stress. The sensitivity of crack growth rate dependency on grain size is taken here as the slope of the da/dN-$d^{-1/2}$ linear curves. This dependency may be equally interpreted as being greater as the plastic zone size grows in relation to the specimen thickness. An overall comparison of the crack growth rates of aluminum (a high stacking fault energy material) and the stainless steel (a low stacking fault energy material) indicates aluminum has lower crack growth rates and no grain size or stress state sensitivity. It is clear that when fatigue crack growth data is analyzed on the basis of constant stress state, low stacking fault energy may be associated with a growth rate dependency on grain size.

The materials from the HCP crystal system (titanium and titanium-8% aluminum) illustrate some similar tendencies. The fatigue crack growth data for titanium illustrated a mild grain size dependency which became more sensitive at higher r_p/B ratios. The two smaller grain size conditions of titanium-8% aluminum illustrated similar dependencies. In fact, the data for these materials overlap and agree very well. The largest grain size conditions of the Ti-8% Al group did not follow this trend. The crack growth rates for this condition were greater than that which might be predicted by the linear growth rate grain size curve. In fact, these growth rates were greater than any of the Ti-8% Al materials. We believe the reason for this discrepancy lies in the relationship of plastic zone size and grain size.

The plastic zone developed around the tip of the fatigue crack during fatigue loading may be smaller at the beginning of a test than the grain size, particularly for the large grain conditions. This plastic zone will then grow in size during a constant load fatigue test, and at the end of the test may be several times larger than the grain size. Inckle, et al, have noted a structure-sensitive crack growth mechanism[19] for carbon steel, austenitic stainless steels, and titanium. This structure-sensitive mechanism changes into a striation formation mechanism at a point which was suggested to occur when the plastic zone size became equal to the grain size. We have noted a similar crack growth mechanism which appears to be sensitive to or related to the grain size of the material. Rearranging the relationship for the cyclic plastic zone size

$$r_p = \frac{1}{12\pi}\left(\frac{\Delta K}{\sigma_{YS}}\right)$$

to read

$$\Delta K = \sigma_{YS}\sqrt{12\pi r_p}$$

we can determine the value of ΔK at which the plastic zone size is equal to the grain size, d. Then,

$$\Delta K = \sigma_{YS}\sqrt{12\pi d}$$

This value of ΔK was calculated for each material condition and is identified in Figures 20 through 31 by a vertical arrow. All of the crack growth data for the aluminum and stainless steel specimens and

almost all of the data for the titanium specimens occurred at ΔK levels greater than that at which r_p equals d. Increasingly greater amounts of the crack growth data for the Ti-8% Al specimens occurred above ΔK levels at which $r_p = d$. During almost all of the fatigue test for the largest grain size Ti-8% Al specimen (Figure 31), the plastic zone size was smaller than the grain size. Examination of the fatigue crack growth power law constants (Table 7) reveals the exponent, m, (slope of the power law curve) to be greatest for the largest grain size specimen. In fact, the value of m increases as more of the Ti-8% Al crack growth data occurs below the level of ΔK where $r_p = d$. This indicates that the structure-sensitive crack growth mechanism becomes more dominant as r_p approaches the grain size, and when r_p is less than the grain size higher crack growth rates occur than would be predicted by the crack growth power law. These observations were made entirely within the framework of a constant stress state.

The sensitivity of crack growth rate to grain size (taken as the slope of the da/dN-$d^{-1/2}$ curves) for the materials discussed here can be examined by plotting sensitivity against the r_p/B ratio as in Figure 74. This figure shows aluminum has virtually no sensitivity of crack growth rate to state of stress (r_p/B ratio), stainless steel has a moderate sensitivity, and titanium and some of the Ti-8% Al material has a strong sensitivity. The strong sensitivity of the titanium materials as compared to the stainless steel may simply be a manifestation of the order of magnitude higher crack growth rates of the HCP materials.

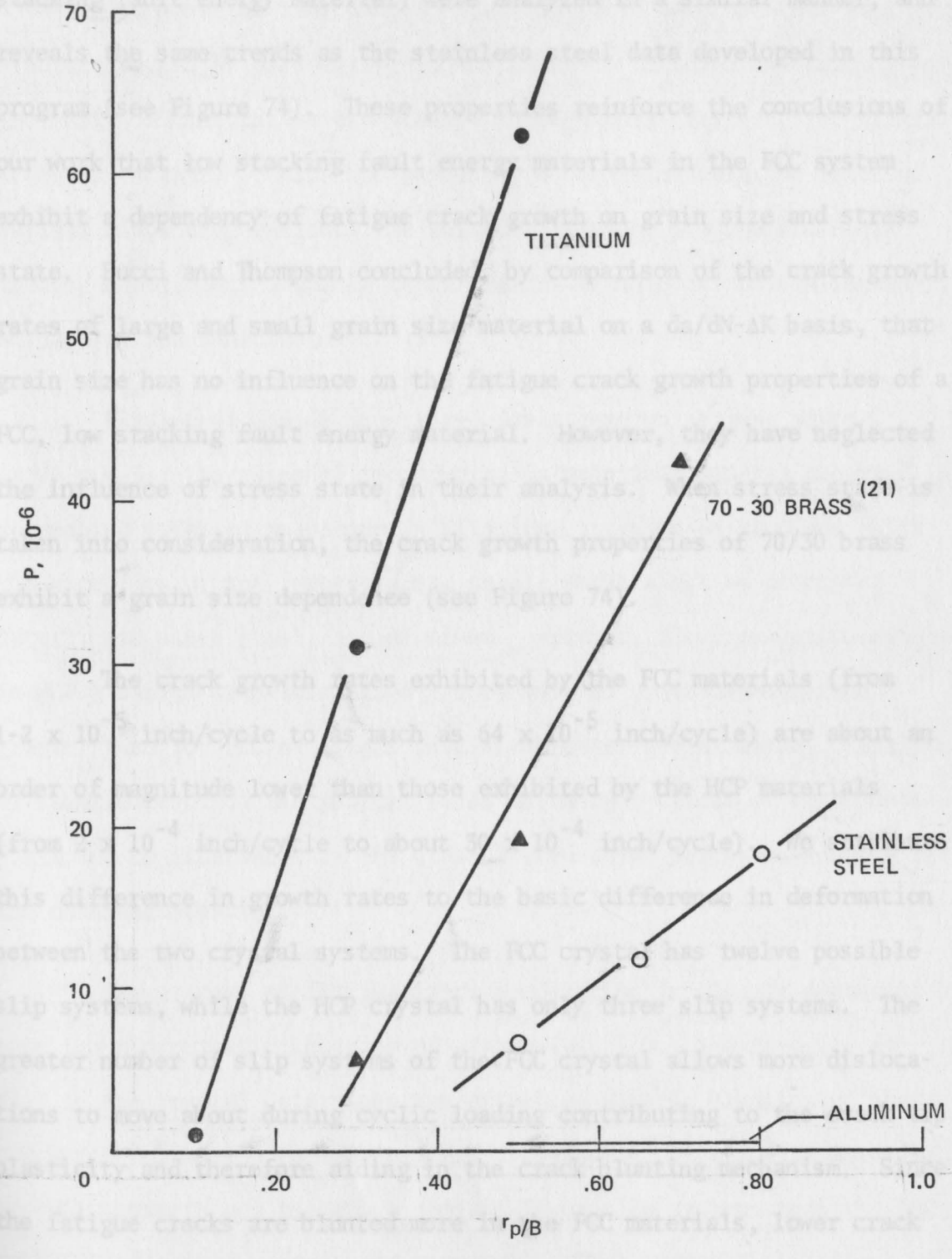

FIGURE 74 INFLUENCE OF STRESS STATE ($r_{p/B}$) ON CRACK GROWTH RATE SENSITIVITY (P)

Recent fatigue crack growth data for 70/30 brass[21] (a low stacking fault energy material) were analyzed in a similar manner, and reveals the same trends as the stainless steel data developed in this program (see Figure 74). These properties reinforce the conclusions of our work that low stacking fault energy materials in the FCC system exhibit a dependency of fatigue crack growth on grain size and stress state. Bucci and Thompson concluded, by comparison of the crack growth rates of large and small grain size material on a da/dN-ΔK basis, that grain size has no influence on the fatigue crack growth properties of a FCC, low stacking fault energy material. However, they have neglected the influence of stress state in their analysis. When stress state is taken into consideration, the crack growth properties of 70/30 brass exhibit a grain size dependence (see Figure 74).

The crack growth rates exhibited by the FCC materials (from 1-2 x 10^{-5} inch/cycle to as much as 64 x 10^{-5} inch/cycle) are about an order of magnitude lower than those exhibited by the HCP materials (from 2 x 10^{-4} inch/cycle to about 30 x 10^{-4} inch/cycle). We attribute this difference in growth rates to the basic difference in deformation between the two crystal systems. The FCC crystal has twelve possible slip systems, while the HCP crystal has only three slip systems. The greater number of slip systems of the FCC crystal allows more dislocations to move about during cyclic loading contributing to the crack tip plasticity and therefore aiding in the crack blunting mechanism. Since the fatigue cracks are blunted more in the FCC materials, lower crack growth rates occur.

Substructure and Crack Growth

Owing to the fact that fatigue test data were obtained employing fracture mechanics procedures, it was possible to normalize results on the basis of constant stress state. Through normalization, for similar states of stress, it was thus possible to determine relative rates of fatigue crack propagation. The relative rates of propagation could thereby be attributed solely to influences of material crystallography, structure, and substructure.

Figures 47 and 48 show that, for a constant stress state ($r_p/B = 0.5$), the rates of propagation in materials studied occurred in decreasing order of magnitude in titanium, titanium-8% aluminum (with the exception of the large-grained sample which shall be discussed later), stainless steel, and aluminum. Further, the propagation rates in HCP titanium materials, as a group, were an order of magnitude greater than for FCC materials (stainless steel and aluminum). Analyses of substructures of the plastic zones of fatigue cracks of these materials and consideration of the crystal structures suggested reasons for the observed behavior.

The process of fatigue crack propagation is clearly dependent upon the microplastic behavior of a material, i.e., the capacity for slip in the crystal determines the extent of plastic blunting of the crack tip during the fatigue process. Consider that titanium materials are HCP crystals and therefore contain fewer slip systems than the FCC materials (stainless steel and aluminum). Thus, HCP materials must be expected to offer less capacity for slip needed to blunt propagating

fatigue cracks. Accordingly, one should expect higher fatigue crack propagation rates in HCP materials compared to FCC materials for similar stress states. This anticipated behavior is in fact manifested in the order-of-magnitude difference in rates observed between HCP and FCC materials.

Aside from the consideration of propagation rates through crystals, there is the consideration of propagation between crystals. Obviously, extension of cracks from one HCP grain of a polycrystalline aggregate to another is more difficult than the analogous process in the FCC system due to limited slip systems. This difficulty was manifest in the fractographic condition which we have termed grain structure sensitivity. This was a general characteristic of HCP materials for the full spectrum of stress intensities studied. It was noted that abrupt changes in fatigue crack propagation direction were experienced in HCP materials upon their crossing of grain boundaries. This resulted in the demarcation of grain boundaries on the fracture surface of the transgranular fractures.

The only deviation from what appeared to be systematic fatigue crack propagation behavior in HCP materials occurred for the large-grained Ti-8% Al specimen. Fractographic examinations, however, revealed that this specimen experienced a marked structure-sensitivity manifest as intense slip band cracking whereas smaller grained specimens did not. Thus, accelerated propagation in the large-grained specimen were attributed to a basic difference in fracture mechanism. It will be shown later that the operation of this mechanism is

apparently related to critically small plastic zone sizes with respect to grain size in the HCP material.

In general, within crystal systems the differences in crack propagation rates which were observed appeared to relate to the particular substructures or dislocation arrangements formed in the plastic zones of fatigue cracks. There are alternative ways of viewing the influence of these substructural differences. One view is that the substructures provide potential slip dislocations that eventually participate in the plastic blunting process. Certain substructure geometries or distributions may be more efficient than others in the blunting process. The other view is that the substructures provide preferential paths for crack propagation. Certain substructure distributions may lead to rapid propagation. In either event the substructures which form in the plastic zones are attributable to the amount of deformation and precise chemical constitution of the particular crystals and to the basic crystal property which chemistry predetermines, i.e., stacking fault energy. This in turn determines the slip or microdeformation character of the crystal. Differences in substructure were observed in all materials studied.

Our results indicated that substructure actually acts in a dual sense with respect to fatigue crack propagation. For low ΔK values there were in some materials tendencies for the crack to follow substructural paths. For higher ΔK values, indications were that substructure was more active in crack blunting processes rather than in providing preferential crack paths.

FCC System

Stainless steel exhibited higher fatigue crack propagation rates than aluminum for similar stress state. Plastic zone substructures for these materials were radically different. Stainless steel exhibited planar substructure with pronounced slip band formations and dislocations situated primarily in the slip bands. On the other hand, aluminum exhibited cellular dislocation configurations of nonplanar dislocations and no evidence of slip band formation.

Stainless steel exhibited structure-sensitive fracture at low levels of stress intensity which we have identified as slip band cracking. Comparison of fractographic evidence and substructural evidence shows good agreement between the spacing of "slip band" crack indications and intensified substructural slip bands. Thus, it is concluded that crack propagation in stainless steel is influenced largely by localized plastic deformation on slip bands.

Although a structure-sensitive cracking was observed in aluminum at lower stress intensities, it clearly was not restricted to slip bands. The plastic zone substructure of aluminum consisted of small cellular arrays of dislocations in a relatively uniform distribution. Thus, by comparison to stainless steel, it may be concluded that aluminum should experience more uniform microplastic deformation by processes where dislocations may cross slip and not remain localized on slip bands.

By virtue of the more localized or restricted nature of slip in stainless steel compared to aluminum, it is postulated that stainless

steel has less inherent ability to blunt fatigue cracks than aluminum. Therefore, crack propagation rates in stainless steel would be expected to be greater than in aluminum, as has been observed.

HCP System

Both titanium materials exhibited similar crack propagation rates for constant stress state. Titanium-8% aluminum exhibited pronounced slip band development in its substructure and in this sense was similar to stainless steel. At low ΔK levels, it was observed that slip band cracking was prominent in Ti-8% Al and therefore, that cracking along these preferred paths in the microstructure had occurred. Examination of the slip bands revealed that dislocations within slip bands tended to interact in a manner suggestive of sessile character. In contrast to this, dislocations in the FCC stainless steel were arrayed more generally normal to the long axis of slip bands and appeared glissile in character. In view of this immobile dislocation character in the HCP material, it would be expected that fast crack propagation rates would be observed. Further, at high ΔK values where the crack path did not follow slip bands it would be expected that the sessile dislocations in slip bands would offer little capacity for crack blunting leading also to fast propagation of cracks.

Titanium also exhibited relatively stable appearing networks of dislocations in the plastic zone substructure, although in a more uniform distribution. Indications of subgrain divisions of anistropic or linear character were perceived on the basis of diffraction contrast variation in the thin foils, however, these were not slip bands. In fact, the

plastic zone substructure of titanium was judged to be free of persistent slip bands. The dislocation networks were continuous, extending through the regions of slight subcrystal misorientation. These networks were judged to be composed of highly sessile dislocations.

Although there were qualitative differences in the substructures observed in titanium materials, there apparently was little quantitative difference as our fatigue crack propagation data show and this is believed to be due to the immobile character of dislocations common to both. Titanium also exhibited a structure-sensitive crack propagation tendency at low ΔK values. This could be attributed to preferential cracking along the subgrain boundaries. At higher ΔK values the crack path was more stress sensitive than structure sensitive, as indicated fractographically. The substructure of grain interiors revealed that there was a little dislocation deterrent to crack propagation.

That titanium and titanium-8% aluminum exhibit limited microplastic character, as the substructural evidence of sessile dislocations suggest they should, is evidenced in the deformation topology of fatigue striations in these materials. Both materials exhibited "serpentine glide" fatigue striations which by comparison to the "stretched" fatigue striations of FCC materials were indicative of less microplasticity and therefore faster crack propagation rates in the HCP system.

Stress Intensity (ΔK) Level and Fatigue Fracture Mechanism

The apparent correlation between change in fracture mechanism and change in fatigue fracture character requires additional explanation.

It was observed in all materials that a structure-sensitive fracture mechanism was exhibited for lower values of ΔK and low crack propagation rates. This mechanism assumed morphological differences between materials but in all cases exhibited common characteristics of a general lack of striation fracture, rather than a predominance of microtopological relief features ("facets" in stainless steel, titanium, and titanium-8% aluminum) or tearing (aluminum) in the direction of macroscopic crack propagation. It may be said that this fracture mechanism is structure sensitive because the crack path is not necessarily normal to the stress axis (which is by definition stage II propagation). Furthermore, the "faceting" which was particularly pronounced in stainless steel and titanium-8% aluminum appeared to be the result of slip band or twin band cracking, clearly a structure-sensitive fracture mechanism.

Low propagation rate structure-sensitive fracture has recently been reported in stainless steels and titanium by independent investigators[19, 40]. In these investigations the structure-sensitive cracking has been referred to as stage IIa and the flat striation cracking mode as stage IIb. It seems that these notations have been adopted in deference to and without challenging the long held view that stage I cracking (structure sensitive along persistent slip bands) is short-lived and no more pervasive than several grain diameters. Our results suggest that structure-sensitive fracture is more like stage I cracking (structure sensitive) than stage II cracking (striation formation).

We suspect that there may be some relationship between fatigue crack tip plastic zone size and material grain size that determines

structure-sensitive fracture tendency. For example, consider that when the plastic zone is small (extending less than or only one or two grains ahead of the crack tip) constraint is high and a restricted number of slip systems are available. Under these circumstances it might be expected that specific planes would tend to fracture due to accumulation of strain energy ahead of the crack tip. It would also be expected that microplastic deformation might occur on such surfaces after the passage of the crack tip. Evidence to support these views was in fact observed in the structure-sensitive fractures. Our data indicated that the smaller the plastic zone was with respect to grain size, the more pronounced was the tendency toward structure-sensitive fracture.

Table 9 has been assembled to show relationships between material grain size, selected reversed loading plastic zone sizes, and approximate ΔK values for transition from stage IIa to total stage IIb fatigue crack propagation (see Figures 20 through 31). It should be noted that at the points of transition to total stage IIb propagation the ratio of plastic zone size to grain size ranged between 15.2 and 46.5 for aluminum, 6.9 and 64.2 for stainless steel, 1.7 and 3.2 for titanium and 0.2 and 0.7 for titanium-8% aluminum. In the realm of stage IIa propagation even smaller ratios existed. This evidence may be interpreted as indicative that stage IIa propagation is favored in FCC materials when plastic zone size is less than one to two orders of magnitude greater than grain size and in HCP materials when plastic zone size is of the order of grain size or less.

TABLE 9

RELATIONSHIPS BETWEEN GRAIN SIZE,
PLASTIC ZONE SIZE, AND ΔK LEVEL

Spec. No.	d, in.	σ_{YS} psi	Transition ΔK psi $\sqrt{in.}$	r_p at Trans. ΔK	r_p T/d	ΔK at which r_p = d
AF-7	8.03×10^{-4}	5,500	6,000	3.16×10^{-2}	39.4	957
AF-1	1.42×10^{-3}	5,700	9,000	6.61×10^{-2}	46.5	1,319
AF-3	3.22×10^{-3}	5,900	8,000	4.88×10^{-2}	15.2	2,056
SF-5	4.33×10^{-4}	34,200	35,000	2.78×10^{-2}	64.2	4,370
SF-6	1.88×10^{-3}	27,000	25,000	2.27×10^{-2}	12.1	7,188
SF-1	3.13×10^{-3}	25,500	23,000	2.16×10^{-2}	6.9	8,759
PTF-1	4.61×10^{-4}	80,600	19,000	1.47×10^{-3}	3.19	10,626
PTF-3	9.09×10^{-4}	75,100	24,000	2.71×10^{-3}	2.98	13,902
PTF-6	1.39×10^{-3}	73,200	22,000	2.40×10^{-3}	1.73	16,756
ATF-2	1.16×10^{-3}	102,900	18,000	8.12×10^{-4}	.70	21,518
ATF-6	2.37×10^{-3}	97,500	20,000	1.12×10^{-3}	.47	29,144
ATF-4	5.41×10^{-3}	93,300	19,000	1.10×10^{-3}	.20	42,135

As the plastic zone increases in size ahead of the crack tip, the degree of constraint would be reduced and the crack would propagate in a much larger predeformed zone. As this necessarily implies higher levels of straining, greater incidence of cross slip might be anticipated due to strain level alone independent of material stacking fault

energy, i.e., an assumption that sufficient strain energy is imparted to the material to exceed the limiting cross slip activation energy. As a result, fracture should be much less sensitive to structure (less crystallographic in nature) and more prone to flat stage II cracking by striation formation.

A separate and distinct type of structure-sensitivity fracture was observed in both titanium materials over the entire range of stress intensities studied. This phenomenon was a grain structure sensitivity that was indicated fractographically by distinct marking of grain boundary outlines. This occurred in spite of the fact that fracture was essentially all transgranular in nature. Fractographic study indicated that substantial change in direction of crack propagation occurred as the crack front proceeded from one grain to another; this was attributed to the difficulty of extending the microplastic deformation fatigue process from one grain to another in the HCP crystal (which has limited capacity for slip). By virtue of this marked reorientation of crack propagation direction between crystals, grain boundaries were delineated. It should be noted that the grain structure sensitivity was present in titanium materials for both stage IIa (structure-sensitive faceting) and stage IIb (striation formation) fracture mechanisms.

It was observed that all materials exhibited differences in propagation character which seemed to be associated with the transition from stage IIa to stage IIb propagation. The reader should note in Figures 20 through 31 that the data could be described by two linear power law curves--one applicable to low ΔK ranges and another applicable to high ΔK ranges. Note also that independent fractographic analysis

places points of transition to total stage IIb cracking approximately at the positions of transition which might be defined by two power law curves based on macroscopic fatigue crack propagation data.

It should be noted in Figures 20 through 31 that the macroscopic rate of propagation accelerates faster in the stage IIa region compared to the IIb region. This result may be interpreted as indicative that the processes of structure-sensitive cracking, i.e., along substructural paths, proceed at a faster rate than nonstructure-sensitive fracture. This result seems intuitively correct as one considers that structure-sensitive propagation is essentially a microcleavage fracture phenomenon.

Grain Size and Crack Growth

Stainless steel exhibited a decided trend indicating that grain size controlled fatigue crack propagation rate. Results indicated that propagation rate was faster for smaller grain size. Titanium and titanium-8% aluminum behaved similarly. Aluminum clearly did not give any indication that grain size influenced crack propagation rate.

Review of the literature has shown that stainless steel and titanium materials have the common feature of planar slip band formation whereas aluminum has a tendency toward wavy slip band formation. These differences in slip character are related to ease of cross slip in the material (easier in wavy slip band character materials) and therefore to stacking fault energy. Thus, the titanium materials and stainless steel constitute low stacking fault energy materials while aluminum represents a high stacking fault energy material. So our results indicate that

there is a connection between low stacking fault energy in a material and a grain size dependency on fatigue crack propagation rate.

If grain size controls fatigue crack propagation rate in a material, by what mechanism may we expect this control to be exerted? An obvious possibility is that grain boundaries exert some drag effect on the propagating crack; if this were an effective mechanism one would expect to observe slower rates of propagation for increasing quantity of grain boundary, i.e., for smaller grain sizes. In addition, one would expect to observe some fractographic evidence of retardation of the crack as it intersects grain boundaries. We have observed neither of these; we have observed accelerated crack propagation with decrease in grain size.

Another mechanism to consider is that grain boundaries act to induce accelerated crack propagation. If this were an effective mechanism, one would expect to observe a tendency for fatigue striations to exhibit broader spacing in the vicinity of grain boundaries for the case of transgranular crack mode; further it would be expected that smaller grain sizes, (i.e., more grain boundary area) would lead to faster rates of propagation. This mechanism does not seem particularly viable when one considers that the portion of the crack front moving through the interior of a given grain would provide a substantial and most likely a limiting "drag" on the propagating crack.

Grain boundaries could more likely contribute to accelerated crack propagation through an intergranular fracturing mode. For the case of a striation mechanism intergranular mode fatigue fracture it seems

reasonable to expect that the less frequently a discontinuity in the propagation path is encountered, e.g., if grain size is large, the faster the rate of crack propagation will be. An assumption implicit in this reasoning is that crack propagation will be impeded as a propagating crack changes direction from one grain face to another of a different orientation. Thus, one might expect slower rates of propagation for smaller grain sizes.

In the context of a fatigue crack blunting model one may view grain boundaries as composed of dislocation arrays, most likely in sessile configurations; grain boundaries as such should not be expected to provide substantial numbers of dislocations to be effective in blunting and thereby retarding a propagating fatigue crack. Thus, a reduced grain size could lead to a net acceleration of crack rate due to local accelerations upon crossing many boundaries. All of the preceding considerations relative to effects of grain boundaries, per se (as distinguished from grain size), on fatigue crack propagation characteristics are largely academic because little supportive evidence exists for such arguments.

Of greater importance than grain boundaries in the question of how does grain size exert an influence on fatigue crack propagation rate, is the matter of substructure within the grains. Since the largest fraction of the crack path is transgranular, the basic question that must be dealt with is what happens to a crack front as it proceeds through the grains of a polycrystal and how does the average size of the grains affect this process? In the first part of this section we have dealt with the relationship between substructure and the observed

differences in crack propagation rates in the four materials studied. We have considered differences in fracture path for low levels of ΔK versus high levels of ΔK and the applicability of the plastic blunting model to the latter.

Our findings indicate that there are two transgranular fracture processes which must be considered. One is the structure-sensitive crack path through substructural features and the other is the more stress-sensitive path associated with propagation by fatigue striation formation. It must be realized that even the latter cannot be totally structure insensitive, e.g., crack segments propagate through grains in a planar fashion, often change direction at grain boundaries, then propagate in a planar fashion through the next grain. According to the plastic blunting theory these planar segments are oriented at approximately 45° to a high density of slip planes; further, the constraints of stress state under which this fracture mechanism exists dictate that the crack plane deviate as little as possible from 90° to the stress axis.

It follows from the preceding that for planar transgranular crack propagation, as the grain size in a material is increased more net deviation from a path oriented 90° to the stress axis might occur. Thus, the observed macroscopic crack propagation rate would be expected to be lower, the larger the grain size. This rationalization is believed to apply to our data because we have in fact observed more devious fracture paths in the larger grained specimens of stainless steel, titanium, and titanium-8% aluminum. These are precisely those

substructural array. Therefore, one must conclude that substantial crack blunting is possible as a propagating crack encounters cell boundaries in aluminum. The cell boundaries should be expected to exert far more control on crack propagation than grain boundaries for reasons of (1) the small size and large quantity of cells and (2) the consideration that grain boundaries are ineffectual crack propagation barriers. The conclusions which emerges from consideration of aluminum plastic zone substructures is that the cellular substructure must be a limiting factor so crack propagation rate may logically be totally independent of grain size.

Stainless steel, titanium, and titanium-8% aluminum have been observed to exhibit clear grain size dependent crack propagation rates. It should be recalled that these materials exhibit planar substructural features consisting of either slip band dislocations or planar sub-crystal boundaries (titanium). Let us first consider how a propagating fatigue crack might interact with this type of substructure. When a crack tip encounters the slip band or sub-boundary it may undergo blunting by a process of sliding off along the band, or may extend by cracking through the band. In the latter instance, which our observations suggest is the case at lower stress intensities, it is clear that for larger crystals extensive crack deviation would be possible, i.e., large surface areas could form due to substantial crack deviation resulting in relatively slow crack propagation. On the other hand, for small crystals, a propagating crack would enter a new crystal and continue propagating before substantial deviation could occur within a

given crystal. Under the circumstances described, one would expect to observe fast propagation rates in small-grained materials with planar substructures.

It does not seem possible for the process of intersection of a propagating fatigue crack with a slip band or sub-boundary to provide a means of controlling crack propagation rate. For a constant substructure pattern there would be no variable factor unless it were the grain boundaries themselves. In such a situation the controlling factor could be some acceleration as the crack proceeds through grain boundaries (it has been argued previously that grain boundaries consist of sessile dislocations, implying little crack blunting tendency). If such were true, accelerated rates of propagation would be consistent with small grain size; the magnitude of this effect would not be expected to be large.

The fact that fractographic study has revealed substantial topological differences between large (most relief) and small-grained stainless steel, titanium, and titanium-8% aluminum fatigue specimens would tend to support a theory that grain structure rather than substructure ultimately controls crack propagation in these materials. It seems that planar substructures cannot provide efficient deterrents to crack propagation. Accordingly, the principal role of planar substructure is viewed as that of providing crack nucleation sites within grains of the material. However, it was observed at low ΔK levels that extensive crack propagation through planar substructure may occur. For higher ΔK levels it is seen that planar crack extension occurs through the grains. In the latter case it seems that crack planes become

aligned with singular crystallographic directions which may be extensions of cracks initiating along substructural paths.

In simplified terms, it seems that crack propagation at relatively high ΔK levels in low stacking fault energy materials proceeds grain by grain in essentially planar fashion and does not deviate substantially from a plane until entering a new grain. A given crack propagation plane might be expected to depend upon availability of initiation sites and constraints of stress state, but to represent most likely the extension of a crystallographic slip plane. It would be anticipated that cracking would initiate at grain boundaries along slip planes, then continue propagating parallel to these crystallographic directions.

For different grain sizes, different degrees of potential crack deviation with respect to a normal to the stress axis would be possible. The likelihood of substantial crack deviation would be reduced as the grain size of the material was reduced. The net effect of reduced grain size would be to increase macroscopic crack propagation rate in the materials with planar substructure.

The influence of grain size on fatigue crack growth in low stacking fault energy materials as illustrated in Figures 47 and 48 may be discussed from two mechanics-oriented points of view. One approach is to consider the energy contributing to the cracking process, and the other is to consider the relationship of slip band orientation and planes of greatest stress. These two approaches will be considered separately.

An Energy Approach

The energy approach to influence of grain size on fatigue crack growth has some basis in the original ideas concerning fracture of solids. The earliest explanations of fractures by Griffith[42] stated that when a crack in a body under a rising tensile stress grew, a certain amount of energy was released. This energy later came to be known as G, the energy release rate which is now related to stress intensity factor, K. During fracture when the released energy became equal to that energy necessary to promote fracture, crack extension became unstable and failure occurred. Moreover, it was felt in these early times that there was a significant relationship between the amount of fracture surface created during crack extension and the energy required to extend the crack.

These basic ideas may be brought to bear in the area of fatigue crack growth. Our examinations of the fatigue fracture surfaces of the stainless steel, titanium, and titanium-8% aluminum revealed a grain size influence on the general surface texture. The large grain materials exhibited a much rougher fracture surface than the fine grain material. In a qualitative sense, this indicates cracks in large grain material have more surface area (A) than those in small grain material for a given macroscopic distance along the general crack path. A given macroscopic distance is chosen as a basis of comparison since it is over this distance that macroscopic growth rates are measured.

During the fatigue crack growth test, a given amount of energy is supplied to the specimen (by the test machine), although not all of this energy enters into the cracking process. By considering that

amount of energy which causes the fatigue crack to grow and the new surface area created by the advancing fatigue crack, we may form a ratio of energy necessary for cracking, E, to newly created surface area, A, and call it the Energy-Area ratio.

$$\text{EA Ratio} = E/A$$

Furthermore, it is reasonable to assume that for any value of the EA ratio, a characteristic constant crack growth rate will occur. This idea follows out of the early fracture theories wherein crack growth instability was predicted to occur at characteristic critical values of released energy. The EA ratio for a given crack growth rate would probably vary in magnitude for different materials. If the EA ratio were increased in some manner, higher crack growth rates would probably occur, since more energy per unit surface area is being supplied. How then may we change the magnitude of the EA ratio? One way is to increase or decrease E, and the resultant growth rate would be higher or lower. If the amount of newly created surface area were changed, the EA ratio would change as the mathematics predicts. The fractographic evidence indicates that the larger grain material exhibits rougher fracture surfaces, or the surface area of the crack within a given macroscopic distance is greater for the large than for the small grain material.

When the fatigue crack growth data is analyzed and examined for a constant state of stress (constant r_p/B), the energy put into the specimen is kept constant and therefore the energy contributing to the cracking process is constant. The relationship between stress intensity

factor K during fatigue and energy is:

$$K^2 = EG$$

where E is the elastic modulus of the material, and G is the energy release rate during crack extension (either by fatigue or monotonic loading). This relationship provides the qualitative link necessary to discuss the energy input during the fatigue cracking process.

Since crack growth rates are analyzed in this work for a constant state of stress or a constant input of energy, we can observe that if the surface area of the crack extension is increased, the EA ratio becomes smaller and the crack growth rate should probably decrease. Our experimental data shown in Figures 47 and 48 substantiate these trends in that for constant stress state, the fine grain material (less fracture surface area) exhibits higher crack growth rates. These conclusions apply only to low stacking fault energy materials containing planar slip bands in their deformed substructures.

A Slip Band Orientation Approach

Another approach to the influence of grain size on fatigue crack growth for low stacking fault energy materials is to consider when the tensile stress component (σ_Y) is greatest and what relationship this has to the orientation of slip bands with respect to the crack plane. The Appendix contains expressions for various stress components at a point near the tip of a stress fatigue crack. The tensile component σ_Y is the greatest of the three (σ_X, σ_Y, and τ_{XY}) and is most influential in loading or stressing the crack. If we choose constant values for K or

K_{max} in fatigue loading and for r in the expression for σ_Y:

$$\sigma_Y = \frac{K}{\sqrt{2\pi r}} \cos\frac{\theta}{2}\left[1 + \sin\frac{\theta}{2}\sin\frac{3\theta}{2}\right]$$

and evaluate σ_Y for various values of θ, from 0 to 90^o, we find σ_Y reaches a maximum at 60^o. Therefore, the major stress in crack extension is greatest on a plane 60^o from the plane of the crack. We have determined that fatigue cracking in these materials tends to proceed along slip bands formed in the substructure and extend across individual grains. If these slip bands or planes are oriented parallel to the plane of greatest σ_Y, crack growth rates would be higher through that particular grain. If the slip planes in a grain are not oriented near the maximum σ_Y plane, the cracking force would tend to be lower and therefore crack growth rates would be lower through that grain.

We now examine the probability of slip planes being oriented parallel to (or nearly so) to the maximum σ_Y plane in large and small grain materials. Because of the heat treatments used to achieve the range of grain sizes for the various materials, we assume the orientation of slip planes to be random throughout the microstructure. It was noted previously that the microstructures of the materials were equiaxed. Within a given macroscopic distance on a plane perpendicular to the loading axis, the small grain material will have more grains than the large grain material. Because of the random orientation of slip planes, it is probably that a greater number of slip planes will be parallel (or nearly so) to the plane of greatest σ_Y for the fine grain material. Within a given number of grains of any size the number of favorably oriented slip planes should be equal. However, since we are

measuring crack lengths and crack growth rates over a given macroscopic distance, we have to consider the number of favorably oriented planes within that distance.

The slip band orientation approach then predicts faster crack growth rates in a fine grain material since it is probable that more slip planes will be favorably oriented. This prediction is borne out by the experimental data in Figures 47 and 48.

In addition to considering the effects of grain size on crack propagation rate we must consider the relative effects of stress state. Comparisons have been made between grain size conditions exhibiting both stage IIa and IIb crack propagation. It should be noted in Figures 47 and 48 that irrespective of the mechanistic differences in crack propagation there appears to be an internal consistency in all the data (with the exception of titanium-8% aluminum which has been discussed).

The effect of increasing stress state was to produce a slight systematic increase in propagation rate with no grain size dependency in the high stacking fault energy material (aluminum). On the other hand, in the low stacking fault energy materials (all others), propagation rate enhancement with increase in stress state was observed. The latter effect is believed to be the result of high stress state forcing the crack path to approach a normal to the stress axis. It is clear that many crack initiation sites, along substructure paths, are available within a grain. However, with increasing stress state it is to be expected that there would be more tendency for initiation on paths as

closely aligned to a normal to the stress axis as possible. Accordingly, less crack deviation and higher macroscopic crack propagation rates should be expected.

CHAPTER V

SUMMARY

This investigation elucidated the effects of variable grain size on the rates of fatigue crack propagation in aluminum, stainless steel, titanium, and titanium-8% aluminum. Aluminum and stainless steel of the FCC crystal structure, represented high and low stacking fault energy materials, respectively. Both titanium and titanium-8% aluminum, of the HCP crystal structure, represent relatively low stacking fault energy materials. Fatigue crack propagation characteristics were analyzed, using fracture mechanics principles, as a function of grain size, stacking fault energy, and crystal system.

Similar grain sizes were prepared in all materials for the study. The microstructures produced were essentially equiaxed and single phase with only minor inclusion or secondary phase content.

Transmission electron microscopy was employed to study the plastic zone substructure of fatigue cracks. In this analysis it was demonstrated that aluminum contained nonplanar cellular dislocation substructure that was reflective of a high stacking fault energy material. Stainless steel, titanium and titanium-8% aluminum on the other hand, contained planar dislocation configurations that were reflective of materials with low stacking fault energies.

Complete tensile data were obtained for each material condition in anticipation of grain size influences on material yield stress. The

yield stress data were in fact necessary for the fatigue crack propagation analysis.

The tensile results followed the classical trend of the Hall-Petch relationship, i.e., higher strengths for smaller grain sizes, for all materials studied, except aluminum. Aluminum exhibited a weak reverse trend. The findings were consistent with those of McEvily and Johnston, that for increasing difficulty of cross slip in the material, the slope of the yield stress grain size curves increased.

An attempt was made to correlate strain hardening character and microplastic fatigue crack propagation character in the materials studied. There was an indication that relative plasticity within crystal systems may be indicated by strain hardening exponent value, but that this parameter is not useful in contrasts made between HCP and FCC systems.

Fatigue crack propagation data were observed to follow the classical power relationship of Paris, i.e., propagation rate = $C\ (\Delta K)^m$. Most material conditions seemed to obey two different crack propagation power laws over different stress intensity factor (ΔK) ranges. The trend displayed was one of a fast rate of change of fatigue crack propagation rate over a low ΔK range changing to a slower rate over a higher ΔK range.

Most data, and incidentally those exhibiting least scatter, were encompassed in the higher ΔK range; power law equations were developed analytically for each of these sets of data for use in other analytic procedures. It was observed that the power law equation exponent was a

reasonably good indicator of relative crack propagation tendencies within each crystal system.

Fracture mechanisms varied with stress intensity levels in all materials. In aluminum, a terraced mechanism resulted at low ΔK, followed by striation formation at intermediate ΔK, then microvoid coalescence at highest ΔK. Stainless steel exhibited structure-sensitive slip band fracture at low ΔK followed by striation formation at intermediate ΔK, and microvoid coalescence at highest ΔK. Both titanium and titanium-8% aluminum exhibited structure-sensitive fracture at low ΔK followed by striation formation at intermediate and highest ΔK. Titanium-8% aluminum exhibited microcleavage at lowest ΔK. Both titanium materials exhibited grain structure sensitivity fatigue fracture over the entire range of ΔK examined.

Thus, the fractographic evidence confirms that the materials exhibit dual fatigue crack propagation character in different ΔK ranges. This takes the form of a microstructure sensitive fracture over the lower ΔK ranges followed by a predominating classical fatigue striation fracture mechanism over the higher ΔK ranges. Breaks in the linear crack propagation power law curves were observed to correspond well to points of transition from substantial structure sensitive to striation fracture.

Relative microplastic character of the materials was reflected qualitatively in the topology of fatigue striations. Aluminum and stainless steel exhibited more plastic striation character ("stretched surfaces") than titanium and titanium-8% aluminum ("serpentine glide").

Over certain ΔK ranges for all materials, substantial disagreement between macroscopic and microscopic (fatigue striation spacing) fatigue crack propagation rate data was observed. Greatest deviation occurred at lower ΔK where dual fracture mechanisms were operative. Best agreement was observed at higher ΔK in all materials and in general in the HCP materials. The differential was attributed primarily to differences in stress state between edge (macroscopic rate) and center (microscopic rate) of fatigue specimens. The FCC materials were tested under mixed stress states, whereas HCP materials were tested under essentially plane strain only.

In previous investigations of this type, attempts have been made to analyze effects of grain size on fatigue crack propagation rate through direct comparisons at constant stress intensity levels. In this investigation, an improved analysis was attempted under equivalent stress states by taking into account the effects of specimen size and material yield stress.

The principal findings of this investigation are thus summarized as follows:

Aluminum

There was no change in crack propagation rate as a function of grain size for any stress state examined. With intensified stress state there was only a slight systematic increase in crack propagation rate.

Stainless Steel

Crack propagation rate was dependent upon grain size in stainless steel, with faster rates for smaller grain sizes. An increase in stress state resulted in a substantial increase in crack propagation rate and a greater sensitivity of propagation rate to grain size.

Titanium

As stress state was increased, some grain size dependency of crack propagation rate was revealed, with faster rates for smaller grain sizes. Grain size dependency was intensified with increasing stress state level.

Titanium-8% Aluminum

Smaller grained conditions of this alloy exhibited behavior virtually the same as that observed in titanium. However, a behavioral discontinuity was discovered in the large-grained condition of this alloy. The large-grained sample exhibited fastest crack propagation rates; however, this occurred in association with a predominating cleavage fracture mechanism, differing in that regard from the others.

In the preceding, it was apparent that the HCP materials as a group exhibited one to two orders of magnitude greater crack propagation rates, at constant stress state, than the FCC materials as a group. Aluminum exhibited the lowest crack propagation rate, with a faster rate for stainless steel, and much faster rates in titanium and titanium-8% aluminum (all of the latter three rates accelerating with decreasing material grain size).

The results indicate that a grain size dependency of fatigue crack propagation rate is probably associated with low stacking fault energy and therefore a planar substructure in a material. This was observed to be the case in stainless steel, titanium and titanium-8% aluminum. Aluminum on the other hand exhibits nonplanar substructure (high stacking fault energy), and does not exhibit a grain size dependent fatigue crack propagation rate. The high density of nonplanar (cellular) dislocation substructure in aluminum is believed to contribute a substantial deterrent to fatigue crack propagation. The small unit size of cellular substructure is believed to preempt any grain size influence on crack propagation rate.

The grain size dependency observed in low stacking fault energy materials indicated faster rates in finer-grained materials for the same stress state. Fast propagation in fine-grained materials was attributed to less deviation of the crack path as compared to coarse-grained materials. It is believed that the planar substructures were relatively ineffectual barriers to fatigue crack propagation (as compared to the nonplanar substructure of aluminum) thereby permitting crack deviations on the order of grain size to result from planar transgranular crack propagation. When substantial deviation of the crack occurred, as in large-grained specimens, the resolved rate of propagation (macroscopic rate) was reduced.

An order of magnitude difference in propagation rates was observed between FCC and HCP materials. This is attributed to the characteristic differences in plasticity of the two crystal structures.

Fractographic evidence of less plastic character of HCP fatigue striations supported this interpretation.

All but one material condition was tested under circumstances where fatigue crack plastic zone size was equal to or larger than grain size. It was concluded that structure-sensitive crack growth mechanisms become more dominant as plastic zone size approaches grain size. With increasing ratio of plastic zone size to grain size it appeared that striation fracture was fostered.

The fast propagation rate observed in large-grained titanium-8% aluminum resulted when plastic zone size was much less than grain size. It is believed that this critical ratio of plastic zone size to grain size fostered the observed fast-rate cleavage fracture mechanism. Aside from this one material condition, an internal consistency in crack propagation rate behavior was observed.

As stress intensity was increased, an intensification of the differences in fatigue crack propagation rates between grain size conditions in low stacking fault energy materials was observed, i.e., differences between conditions became greater at higher ΔK levels. This effect very clearly demonstrated the grain size dependency of fatigue crack propagation rates in the low stacking fault energy materials.

In addition to the results of this work, the constant stress state analysis was applied to other materials reported in the literature for which comparable crack propagation data were available. A crack propagation rate grain size dependency was thus demonstrated in 70/30 brass. A consistent trend in relationship between level of stacking

fault energy of FCC material and sensitivity of the grain size crack propagation rate dependency was found. Indications were that grain size dependency is more sensitive with reduction in stacking fault energy and this is true in diverse FCC materials.

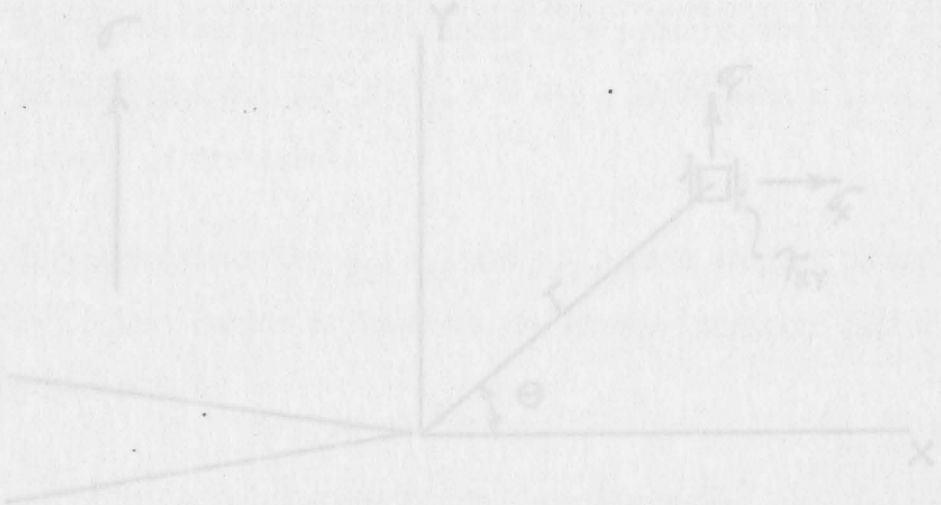

APPENDIX A

Fracture Mechanics Stress Intensity Factor

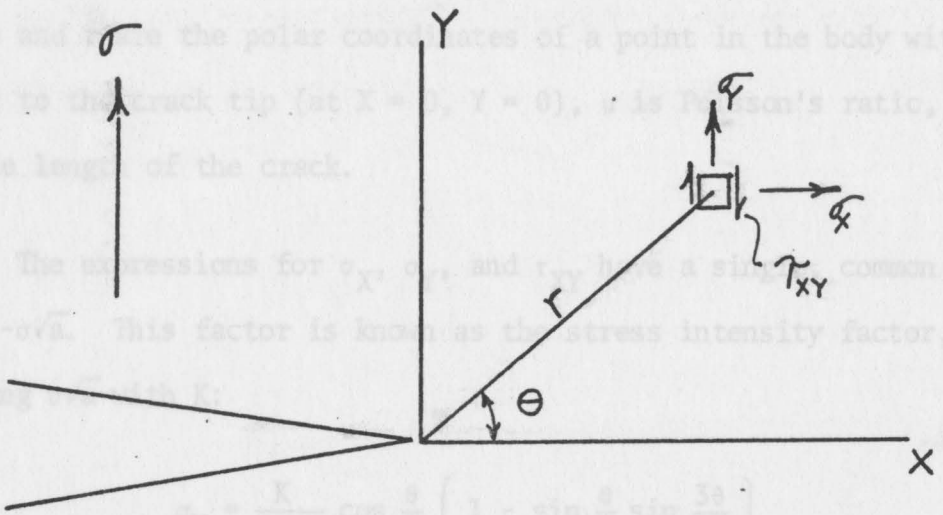

The stress field around a sharp crack in a structure or test specimen under a tensile stress, σ, can be described in terms of the stresses σ_X, σ_Y, σ_Z, τ_{XY}, τ_{XZ}, τ_{YZ} by the following expressions[(a)]:

$$\sigma_X = \frac{\sigma\sqrt{a}}{\sqrt{2\pi r}} \cos\frac{\theta}{2}\left(1 - \sin\frac{\theta}{2}\sin\frac{3\theta}{2}\right)$$

$$\sigma_Y = \frac{\sigma\sqrt{a}}{\sqrt{2\pi r}} \cos\frac{\theta}{2}\left(1 + \sin\frac{\theta}{2}\sin\frac{3\theta}{2}\right)$$

(a) G. R. Irwin, "Analysis of Stresses and Strains Near the End of a Crack." Journal of Applied Mechanics. Vol. 24, 1957, p. 361.

$$\sigma_Z = \mu (\sigma_X + \sigma_Y)$$

$$\tau_{XY} = \frac{\sigma\sqrt{a}}{\sqrt{2\pi r}} \sin\frac{\theta}{2} \cos\frac{\theta}{2} \cos\frac{3\theta}{2}$$

$$\tau_{XZ} = \tau_{YZ} = 0$$

where θ and r are the polar coordinates of a point in the body with respect to the crack tip (at X = 0, Y = 0), μ is Poisson's ratio, and a is the length of the crack.

The expressions for σ_X, σ_Y, and τ_{XY} have a single, common factor--$\sigma\sqrt{a}$. This factor is known as the stress intensity factor, K. Replacing $\sigma\sqrt{a}$ with K:

$$\sigma_X = \frac{K}{\sqrt{2\pi r}} \cos\frac{\theta}{2} \left(1 - \sin\frac{\theta}{2} \sin\frac{3\theta}{2} \right)$$

$$\sigma_Y = \frac{K}{\sqrt{2\pi r}} \cos\frac{\theta}{2} \left(1 + \sin\frac{\theta}{2} \sin\frac{3\theta}{2} \right)$$

$$\tau_{XY} = \frac{K}{\sqrt{2\pi r}} \sin\frac{\theta}{2} \cos\frac{\theta}{2} \cos\frac{3\theta}{2}$$

Therefore, the stress intensity factor K is a single parameter description of the stress field near a sharp crack in a loaded body. This single factor is very useful in describing a material's response to loading when a sharp crack is present in the materials.

The stress intensity factor, K, is dependent on structural or specimen geometry, load, and crack length. The unit dimensions of K are psi$\sqrt{\text{in.}}$ or ksi$\sqrt{\text{in.}}$ coming from the equivalency of K = $\sigma\sqrt{a}$.

APPENDIX B

Fatigue Crack Growth Data

TABLE B-1

FATIGUE CRACK GROWTH DATA

Material: Aluminum Specimen No. AF-1

Grain Size: 8.42×10^{-4} in. B = .201 in. W = 2.00 in. a_o = .303 in.

Fatigue Load, lb.	Life, 1000 Cycles	a, in.	da/dN, in./cycle	ΔK, psi $\sqrt{in.}$	Fatigue Load, lb.	Life, 1000 Cycles	a, in.	da/dN, in./cycle	ΔK, psi $\sqrt{in.}$
1400	80	.316	--	--	1400	215	.628	5.40×10^{-6}	8,171
1400	813	.330	1.08×10^{-5}	4,525	1400	220	.656	5.60×10^{-6}	8,606
1400	86	.333	6.38×10^{-7}	4,614	1400	223	.673	5.67×10^{-6}	8,979
1400	90	.338	1.25×10^{-6}	4,656	1400	226	.703	1.00×10^{-5}	9,387
1400	95	.340	4.00×10^{-7}	4,694	1400	229	.721	6.00×10^{-6}	9,823
1400	100	.346	1.20×10^{-6}	4,736	1400	232	.745	8.00×10^{-6}	10,223
1400	105	.350	8.00×10^{-7}	4,790	1400	235	.779	1.13×10^{-5}	10,807
1400	115	.364	1.40×10^{-6}	4,887	1400	238	.798	6.33×10^{-6}	11,374
1400	125	.379	1.50×10^{-6}	5,044	1400	241	.834	1.20×10^{-5}	12,000
1400	135	.392	1.30×10^{-6}	5,199	1400	244	.876	1.40×10^{-5}	12,960
1400	145	.412	2.00×10^{-6}	5,384	1400	247	.921	1.50×10^{-5}	14,144
1400	155	.429	1.70×10^{-6}	5,596	1400	248	.948	2.70×10^{-5}	15,225
1400	165	.447	1.80×10^{-6}	5,801	1400	249	.967	1.90×10^{-5}	15,970
1400	175	.470	2.30×10^{-6}	6,046	1400	250	.979	1.20×10^{-5}	16,497
1400	185	.500	3.00×10^{-6}	6,373	1400	251	1.013	3.40×10^{-5}	17,319

TABLE B-1 (cont'd)

Fatigue Load, lb.	Life, 1000 Cycles	a, in.	da/dN, in./cycle	ΔK, psi $\sqrt{in.}$	Fatigue Load, lb.	Life, 1000 Cycles	a, in.	da/dN, in./cycle	ΔK, psi $\sqrt{in.}$
1400	190	.516	3.20×10^{-6}	6,667	1400	252	1.052	3.90×10^{-5}	18,729
1400	195	.534	3.60×10^{-6}	6,890	1400	253	1.089	3.70×10^{-5}	20,348
1400	200	.556	4.40×10^{-6}	7,161	1400	254	1.120	3.10×10^{-5}	21,940
1400	205	.578	4.40×10^{-6}	7,468	1400	255	1.171	5.10×10^{-5}	24,058
1400	210	.601	4.60×10^{-6}	7,794	1400	256	1.268	9.70×10^{-5}	28,509

TABLE B-2

FATIGUE CRACK GROWTH DATA

Material: Aluminum Specimen No. AF-7

Grain Size: 12.95×10^{-4} in. B = .203 in. W = 2.00 in. a_o = .296 in.

Fatigue Load, lb.	Life, 1000 Cycles	a, in.	da/dN, in./cycle	ΔK, psi $\sqrt{in.}$	Fatigue Load, lb.	Life, 1000 Cycles	a, in.	da/dN, in./cycle	ΔK, psi $\sqrt{in.}$
800	470	.330	--	--	800	965	.684	2.60×10^{-6}	5,018
800	520	.339	1.80×10^{-7}	2,629	800	980	.710	1.73×10^{-6}	5,402
800	554	.355	4.70×10^{-7}	2,704	800	990	.726	1.66×10^{-6}	5,622
800	579	.359	1.61×10^{-7}	2,765	800	1000	.742	1.60×10^{-6}	5,795
800	609	.374	5.00×10^{-7}	2,823	800	1010	.777	3.50×10^{-6}	6,085
800	639	.378	1.33×10^{-7}	2,882	800	1020	.799	2.20×10^{-6}	6,429
1000	652	.385	5.36×10^{-7}	3,646	800	1030	.839	4.00×10^{-6}	6,829
1000	672	.386	5.00×10^{-8}	3,677	800	1035	.852	2.60×10^{-6}	7,196
1000	702	.403	5.67×10^{-7}	3,748	800	1040	.864	2.40×10^{-6}	7,376
1000	722	.417	7.00×10^{-7}	3,872	800	1045	.879	3.00×10^{-6}	7,578
1000	742	.428	5.50×10^{-7}	3,974	800	1050	.891	2.40×10^{-6}	7,787
1000	762	.444	8.00×10^{-7}	4,086	800	1055	.920	5.80×10^{-6}	8,117
1000	782	.465	1.05×10^{-6}	4,242	800	1060	.940	4.00×10^{-6}	8,535
1000	802	.477	6.00×10^{-7}	4,384	800	1065	.960	4.00×10^{-6}	8,896
1000	822	.507	1.50×10^{-6}	4,570	800	1070	.979	3.80×10^{-6}	9,266

TABLE B-2 (cont'd)

Fatigue Load, lb.	Life, 1000 Cycles	a, in.	da/dN, in./cycle	ΔK, psi $\sqrt{in.}$	Fatigue Load, lb.	Life, 1000 Cycles	a, in.	da/dN, in./cycle	ΔK, psi $\sqrt{in.}$
1000	832	.519	1.20×10^{-6}	4,761	800	1075	.997	3.60×10^{-6}	9,634
1000	842	.535	1.60×10^{-6}	4,891	800	1080	1.027	6.00×10^{-6}	10,140
1000	852	.560	2.50×10^{-6}	5,089	800	1085	1.059	6.40×10^{-6}	10,841
800	882	.578	6.00×10^{-7}	4,241	800	1090	1.075	3.20×10^{-6}	11,425
800	912	.601	7.67×10^{-7}	4,410	800	1095	1.175	2.00×10^{-5}	12,997
800	933	.628	1.28×10^{-6}	4,623	800	1100	1.258	1.66×10^{-5}	16,018
800	945	.632	3.33×10^{-7}	4,760	800	1105	1.332	1.48×10^{-5}	19,248

TABLE B-3

FATIGUE CRACK GROWTH DATA

Material: Aluminum — Specimen No. AF-3

Grain Size: 32.80×10^{-4} in. — B = .202 in. — W = 2.00 in. — a_o = .293 in.

Fatigue Load, lb.	Life, 1000 Cycles	a, in.	da/dN, in./cycle	ΔK, psi $\sqrt{in.}$	Fatigue Load, lb.	Life, 1000 Cycles	a, in.	da/dN, in./cycle	ΔK, psi $\sqrt{in.}$
1200	160	.303	--	--	1400	195	.723	9.00×10^{-6}	9,728
1200	180	.310	3.90×10^{-7}	3,708	1400	198	.759	1.20×10^{-5}	10,329
1200	210	.311	3.39×10^{-8}	3,748	1400	201	.798	1.30×10^{-5}	11,100
1200	229.5	.346	1.79×10^{-6}	3,908	1400	204	.826	9.33×10^{-6}	11,847
1200	252	.352	2.67×10^{-7}	4,094	1400	205.5	.841	1.00×10^{-5}	12,358
1200	273	.366	6.67×10^{-7}	4,186	1400	207	.870	1.93×10^{-5}	12,908
(a) 1400	120	.436	--	--	1400	208.5	.904	2.27×10^{-5}	13,750
1400	130	.440	4.00×10^{-7}	5,772	1400	210	.925	1.40×10^{-5}	14,540
1400	150	.520	4.00×10^{-6}	6,279	1400	211	.949	2.40×10^{-5}	15,228
1400	160	.547	2.70×10^{-6}	6,969	1400	212	.970	2.10×10^{-5}	15,957
1400	170	.590	4.30×10^{-6}	7,452	1400	213	1.016	4.60×10^{-5}	17,124
1400	175	.614	4.80×10^{-6}	7,941	1400	214	1.026	1.00×10^{-5}	18,180
1400	180	.646	6.40×10^{-6}	8,372	1400	215	1.082	5.60×10^{-5}	19,528
1400	183	.652	2.00×10^{-6}	8,677	1400	216	1.120	3.80×10^{-5}	21,662

(a) Reset cycle counter

TABLE B-3 (cont'd)

Fatigue Load, lb.	Life, 1000 Cycles	a, in.	da/dN, in./cycle	ΔK, psi $\sqrt{in.}$	Fatigue Load, lb.	Life, 1000 Cycles	a, in.	da/dN, in./cycle	ΔK, psi $\sqrt{in.}$
1400	186	.662	3.33×10^{-6}	8,809	1400	217	1.160	4.00×10^{-5}	23,643
1400	189	.693	1.03×10^{-5}	9,157	1400	218	1.219	5.90×10^{-5}	26,469
1400	192	.696	1.00×10^{-6}	9,456					

TABLE B-4

FATIGUE CRACK GROWTH DATA

Material: Stainless Steel — Specimen No. SF-5

Grain Size: 2.04×10^{-4} in. B = .203 in. W = 2.00 in. a_o = .295 in.

Fatigue Load, lb.	Life, 1000 Cycles	a, in.	da/dN, in./cycle	ΔK, psi $\sqrt{in.}$	Fatigue Load, lb.	Life, 1000 Cycles	a, in.	da/dN, in./cycle	ΔK, psi $\sqrt{in.}$
6000	56	.314	--	--	6000	148	.673	2.40×10^{-5}	38,284
6000	76	.333	9.50×10^{-7}	19,223	6000	148.5	.685	2.40×10^{-5}	39,161
6000	86	.350	1.70×10^{-6}	20,031	6000	149	.698	2.60×10^{-5}	40,097
6000	93	.365	2.14×10^{-6}	20,760	6000	149.5	.713	3.00×10^{-5}	41,174
6000	98	.375	2.00×10^{-6}	21,337	6000	150	.728	3.00×10^{-5}	42,363
6000	103	.385	2.00×10^{-6}	21,804	6000	150.5	.747	3.80×10^{-5}	43,757
6000	108	.399	2.80×10^{-6}	22,371	6000	151	.761	2.80×10^{-5}	45,160
6000	113	.411	2.40×10^{-6}	22,993	6000	151.5	.775	2.80×10^{-5}	46,391
6000	118	.429	3.60×10^{-6}	23,723	6000	152	.790	3.00×10^{-5}	47,707
6000	123	.446	3.40×10^{-6}	24,590	6000	152.5	.807	3.40×10^{-5}	49,210
6000	126	.459	4.33×10^{-6}	25,349	6000	153	.832	3.20×10^{-5}	50,820
6000	129	.473	4.67×10^{-6}	26,044	6000	153.5	.846	4.60×10^{-5}	52,805
6000	132	.489	5.33×10^{-6}	26,832	6000	154	.870	4.80×10^{-5}	55,324
6000	135	.506	5.67×10^{-6}	27,717	6000	154.5	.901	6.20×10^{-5}	58,460
6000	137	.525	9.50×10^{-6}	28,706	6000	154.8	.937	1.20×10^{-4}	62,580

TABLE B-4 (cont'd)

Fatigue Load, lb.	Life, 1000 Cycles	a, in.	da/dN, in./cycle	ΔK, psi $\sqrt{in.}$	Fatigue Load, lb.	Life, 1000 Cycles	a, in.	da/dN, in./cycle	ΔK, psi $\sqrt{in.}$
6000	139	.452	8.50×10^{-6}	29,722	6000	155.1	.984	1.57×10^{-4}	68,194
6000	141	.563	1.05×10^{-5}	30,825	6000	155.2	1.002	1.80×10^{-4}	73,027
6000	142	.574	1.10×10^{-5}	31,781	6000	155.3	1.021	1.90×10^{-4}	75,966
6000	143	.587	1.30×10^{-5}	32,514	6000	155.4	1.043	2.20×10^{-4}	79,392
6000	144	.601	1.40×10^{-5}	33,357	6000	155.5	1.064	2.00×10^{-4}	82,287
6000	145	.615	1.40×10^{-5}	34,252	6000	155.6	1.095	3.40×10^{-4}	89,450
6000	146	.632	1.70×10^{-5}	35,269	6000	155.7	1.137	2.90×10^{-4}	96,930
6000	147	.651	1.90×10^{-5}	36,486	6000	155.8	1.169	4.80×10^{-4}	104,792
6000	147.5	.661	2.00×10^{-5}	37,498	6000	155.9	1.234	6.40×10^{-4}	120,556

TABLE B-5

FATIGUE CRACK GROWTH DATA

Material: Stainless Steel — Specimen No. SF-6

Grain Size: 33.60×10^{-4} in. B = .260 in. W = 2.00 in. a_o = .295 in.

Fatigue Load, lb.	Life, 1000 Cycles	a, in.	da/dN, in./cycle	ΔK, psi $\sqrt{in.}$	Fatigue Load, lb.	Life, 1000 Cycles	a, in.	da/dN, in./cycle	ΔK, psi $\sqrt{in.}$
6000	280	.327	--	--					
6000	290	.329	2.00×10^{-7}	14.8					
6000	310	.347	9.00×10^{-7}	15.2					
6000	330	.353	3.00×10^{-7}	15.6					
6000	350	.376	1.15×10^{-6}	16.1					
6000	365	.389	8.67×10^{-7}	16.7					
6000	380	.399	6.67×10^{-7}	17.1					
6000	395	.413	9.33×10^{-7}	17.6					
6000	405	.424	1.10×10^{-6}	18.0					
6000	415	.429	5.00×10^{-7}	18.3					
6000	425	.439	1.00×10^{-6}	18.6					
6000	435	.452	1.30×10^{-6}	19.1					
6000	445	.473	2.10×10^{-6}	19.7					
6000	453	.491	2.25×10^{-6}	20.5					
6000	458	.497	1.20×10^{-6}	21.0					

TABLE B-6

FATIGUE CRACK GROWTH DATA

Material: Stainless Steel — Specimen No. SF-1

Grain Size: 42.12×10^{-4} in. — B = .200 in. — W = 1.40 in. — a_o = .292 in.

Fatigue Load, lb.	Life, 1000 Cycles	a, in.	da/dN, in./cycle	ΔK, psi $\sqrt{in.}$	Fatigue Load, lb.	Life, 1000 Cycles	a, in.	da/dN, in./cycle	ΔK, psi $\sqrt{in.}$
2400	0	.338	--	--	3200	109	.545	7.50×10^{-6}	30,000
2400	4	.349	2.75×10^{-6}	13,300	3200	110	.561	1.60×10^{-5}	31,300
2400	8	.350	2.50×10^{-7}	13,500	3200	111	.574	1.30×10^{-5}	32,600
2400	12	.351	2.50×10^{-7}	13,500	3200	112	.587	1.30×10^{-5}	33,800
2400	16	.352	2.50×10^{-7}	13,600	3200	113	.607	2.00×10^{-5}	35,400
2400	26	.353	1.00×10^{-7}	13,600	3200	114	.628	2.10×10^{-5}	37,600
2400	36	.359	6.00×10^{-7}	13,700	3200	115	.651	2.30×10^{-5}	40,000
2400	48	.359	0×10^{-7}	13,800	3200	115.5	.661	2.00×10^{-5}	42,000
2400	63	.363	1.48×10^{-7}	13,900	3200	116	.676	3.00×10^{-5}	43,600
3200	71	.386	3.12×10^{-6}	19,200	3200	116.5	.687	2.20×10^{-5}	45,300
3200	76	.400	2.80×10^{-6}	20,300	3200	117	.710	4.60×10^{-5}	47,700
3200	80	.410	2.50×10^{-6}	21,000	3200	117.5	.736	5.20×10^{-5}	51,500
3200	84	.419	2.25×10^{-6}	21,500	3200	118	.761	5.00×10^{-5}	55,700
3200	88	.433	3.50×10^{-6}	22,200	3200	118.5	.782	4.20×10^{-5}	59,900

TABLE B-6 (cont'd)

Fatigue Load, lb.	Life, 1000 Cycles	a, in.	da/dN, in./cycle	ΔK, psi $\sqrt{in.}$	Fatigue Load, lb.	Life, 1000 Cycles	a, in.	da/dN, in./cycle	ΔK, psi $\sqrt{in.}$
3200	92	.442	2.25×10^{-6}	22,900	3200	119	.809	5.40×10^{-5}	64,700
3200	96	.460	4.50×10^{-6}	23,700	3200	119.5	.842	6.60×10^{-5}	71,300
3200	100	.487	5.50×10^{-6}	25,000	3200	120	.864	4.40×10^{-5}	78,100
3200	103	.501	6.33×10^{-6}	26,500	3200	120.5	.907	7.60×10^{-5}	86,300
3200	105	.515	7.00×10^{-6}	27,900	3200	121	.936	6.80×10^{-5}	97,400
3200	107	.530	7.50×10^{-6}	28,800					

TABLE B-7

FATIGUE CRACK GROWTH DATA

Material: Unalloyed Titanium — Specimen No. PTF-1

Grain Size: 4.06×10^{-4} in. — B = .162 in. — W = 2.00 in. — a_o = .500 in.

Fatigue Load, lb.	Life, 1000 Cycles	a, in.	da/dN, in./cycle	ΔK, psi $\sqrt{in.}$	Fatigue Load, lb.	Life, 1000 Cycles	a, in.	da/dN, in./cycle	ΔK, psi $\sqrt{in.}$
2000	22.2	.780	--	--	2000	32.4	1.112	1.00×10^{-4}	38,553
2000	24	.781	5.55×10^{-7}	19,789	2000	32.6	1.135	1.15×10^{-4}	40,453
2000	28	.888	2.68×10^{-5}	21,989	2000	32.8	1.161	1.30×10^{-4}	42,754
2000	29	.905	1.70×10^{-5}	24,891	2000	33.0	1.194	1.65×10^{-4}	45,727
2000	29.5	.937	6.40×10^{-5}	26,166	2000	33.2	1.235	2.05×10^{-4}	49,795
2000	30	.957	4.00×10^{-5}	27,609	2000	33.4	1.292	2.85×10^{-4}	55,820
2000	30.2	.964	3.50×10^{-5}	28,397	2000	33.5	1.331	3.90×10^{-4}	62,504
2000	30.4	.975	5.50×10^{-5}	28,937	2000	33.6	1.382	5.10×10^{-4}	69,552
2000	30.6	.984	4.50×10^{-5}	29,553					
2000	30.8	.993	4.50×10^{-5}	30,120					
2000	31.0	1.006	6.50×10^{-5}	30,832					
2000	31.2	1.016	5.00×10^{-5}	31,599					
2000	31.4	1.027	5.50×10^{-5}	32,319					
2000	31.6	1.040	6.50×10^{-5}	33,167					

TABLE B-7 (cont'd)

Fatigue Load, lb.	Life, 1000 Cycles	a, in.	da/dN, in./cycle	ΔK, psi $\sqrt{in.}$	Fatigue Load, lb.	Life, 1000 Cycles	a, in.	da/dN, in./cycle	ΔK, psi $\sqrt{in.}$
2000	31.8	1.057	8.50×10^{-5}	34,265					
2000	32.0	1.074	8.50×10^{-5}	35,563					
2000	32.2	1.092	9.00×10^{-5}	36,961					

TABLE B-8

FATIGUE CRACK GROWTH DATA

Material: Unalloyed Titanium — Specimen No. PTF-3

Grain Size: 7.44×10^{-4} in. — B = .162 in. — W = 2.00 in. — a_o = .500 in.

Fatigue Load, lb.	Life, 1000 Cycles	a, in.	da/dN, in./cycle	ΔK, psi $\sqrt{in.}$	Fatigue Load, lb.	Life, 1000 Cycles	a, in.	da/dN, in./cycle	ΔK, psi $\sqrt{in.}$
2000	24	.606	--	--	2000	41.5	.873	2.00×10^{-5}	23,574
2000	26	.615	4.50×10^{-6}	14,374	2000	42	.893	4.00×10^{-5}	24,300
2000	28	.638	1.15×10^{-5}	14,815	2000	42.5	.913	4.00×10^{-5}	25,299
2000	29	.646	8.00×10^{-6}	15,254	2000	43	.934	4.20×10^{-5}	26,382
2000	30	.658	1.20×10^{-5}	15,545	2000	43.5	.952	3.60×10^{-5}	27,462
2000	31	.662	4.00×10^{-6}	15,781	2000	44	.977	5.00×10^{-5}	28,724
2000	32	.682	2.00×10^{-5}	16,142	2000	44.5	1.005	5.60×10^{-5}	30,374
2000	33	.696	1.40×10^{-5}	16,669	2000	45	1.046	8.20×10^{-5}	32,700
2000	34	.708	1.20×10^{-5}	17,084	2000	45.2	1.062	8.00×10^{-5}	34,786
2000	35	.713	5.00×10^{-6}	17,362	2000	45.4	1.078	8.00×10^{-5}	36,027
2000	36	.737	2.40×10^{-5}	17,847	2000	45.6	1.085	3.50×10^{-5}	36,952
2000	37	.758	2.10×10^{-5}	18,630	2000	45.8	1.109	1.20×10^{-4}	38,244
2000	38	.780	2.20×10^{-5}	19,414	2000	46.2	1.166	1.42×10^{-4}	41,878
2000	39	.800	2.00×10^{-5}	20,218	2000	46.4	1.194	1.40×10^{-4}	46,132

TABLE B-8 (cont'd)

Fatigue Load, lb.	Life, 1000 Cycles	a, in.	da/dN, in./cycle	ΔK, psi $\sqrt{in.}$	Fatigue Load, lb.	Life, 1000 Cycles	a, in.	da/dN, in./cycle	ΔK, psi $\sqrt{in.}$
2000	40	.829	2.90×10^{-5}	21,207	2000	46.6	1.245	2.55×10^{-4}	50,531
2000	41	.863	3.40×10^{-5}	22,564	2000	46.7	1.282	3.70×10^{-4}	55,992
					2000	46.8	1.337	5.50×10^{-4}	62,401
					2000	46.9	1.448	1.11×10^{-3}	76,022

TABLE B-9

FATIGUE CRACK GROWTH DATA

Material: Unalloyed Titanium — Specimen No. PTF-6

Grain Size: 19.29×10^{-4} in. — B = .162 in. — W = 2.00 in. — a_o = .500 in.

Fatigue Load, lb.	Life, 1000 Cycles	a, in.	da/dN, in./cycle	ΔK, psi $\sqrt{in.}$	Fatigue Load, lb.	Life, 1000 Cycles	a, in.	da/dN, in./cycle	ΔK, psi $\sqrt{in.}$
2000	8	.508	--	--	2000	64.5	.892	2.80×10^{-5}	24,319
2000	10	.510	1.00×10^{-6}	11,803	2000	65	.903	2.20×10^{-5}	24,914
2000	12	.512	1.00×10^{-6}	11,849	2000	65.5	.917	2.80×10^{-5}	25,584
2000	18	.529	2.83×10^{-6}	12,070	2000	66	.930	2.60×10^{-5}	26,301
2000	23	.535	1.20×10^{-6}	12,341	2000	66.5	.951	4.20×10^{-5}	27,239
2000	28	.558	4.60×10^{-6}	12,689	2000	67	.966	3.00×10^{-5}	28,278
2000	33	.571	2.60×10^{-6}	13,133	2000	67.5	.990	4.80×10^{-5}	29,459
2000	38	.598	5.40×10^{-6}	13,642	2000	68	1.013	4.60×10^{-5}	30,964
2000	43	.636	7.60×10^{-6}	14,507	2000	68.3	1.030	5.67×10^{-5}	32,319
2000	46	.646	3.33×10^{-6}	15,179	2000	68.6	1.047	5.67×10^{-5}	33,528
2000	49	.665	6.33×10^{-6}	15,600	2000	68.9	1.065	6.00×10^{-5}	34,831
2000	52	.691	8.67×10^{-6}	16,276	2000	69.2	1.084	6.33×10^{-5}	36,274
2000	54	.715	1.20×10^{-5}	17,064	2000	69.5	1.106	7.33×10^{-5}	37,957
2000	56	.739	1.20×10^{-5}	17,860	2000	69.7	1.132	1.30×10^{-4}	40,047

TABLE B-9 (cont'd)

Fatigue Load, lb.	Life, 1000 Cycles	a, in.	da/dN, in./cycle	ΔK, psi $\sqrt{in.}$	Fatigue Load, lb.	Life, 1000 Cycles	a, in.	da/dN, in./cycle	ΔK, psi $\sqrt{in.}$
2000	57	.754	1.50×10^{-5}	18,537	2000	69.9	1.157	1.25×10^{-4}	42,416
2000	58	.767	1.30×10^{-5}	19,041	2000	70	1.171	1.40×10^{-4}	44,338
2000	59	.781	1.40×10^{-5}	19,542	2000	70.1	1.185	1.40×10^{-4}	45,780
2000	60	.800	1.90×10^{-5}	20,176	2000	70.2	1.207	2.20×10^{-4}	47,712
2000	61	.816	1.60×10^{-5}	20,875	2000	70.3	1.227	2.00×10^{-4}	50,085
2000	62	.831	1.50×10^{-5}	21,518	2000	70.4	1.256	2.90×10^{-4}	53,021
2000	63	.857	2.60×10^{-5}	22,406	2000	70.5	1.298	4.20×10^{-4}	57,618
2000	64	.878	2.10×10^{-5}	23,478	2000	70.6	1.392	9.40×10^{-4}	67,674

TABLE B-10

FATIGUE CRACK GROWTH DATA

Material: Ti-8% Al Specimen No. ATF-2

Grain Size: 9.53×10^{-4} in. B = .118 in. W = 2.00 in. a_o = .500 in.

Fatigue Load, lb.	Life, 1000 Cycles	a, in.	da/dN, in./cycle	ΔK, psi $\sqrt{in.}$	Fatigue Load, lb.	Life, 1000 Cycles	a, in.	da/dN, in./cycle	ΔK, psi $\sqrt{in.}$
2000	15	.504	--	--	1200	115	.814	7.00×10^{-6}	16,938
2000	20	.519	3.00×10^{-6}	16,404	1200	117	.830	8.00×10^{-6}	17,803
2000	25	.534	3.20×10^{-6}	16,903	1200	119	.846	8.00×10^{-6}	18,372
2000	30	.565	6.00×10^{-6}	17,667	1200	121	.872	1.30×10^{-5}	19,154
1600	35	.581	3.20×10^{-6}	14,768	1200	123	.901	1.45×10^{-5}	20,240
1600	40	.612	6.20×10^{-6}	15,441	1200	124	.916	1.50×10^{-5}	21,164
1600	43	.619	2.33×10^{-6}	16,005	1200	125	.927	1.10×10^{-5}	21,735
1600	46	.637	6.00×10^{-6}	16,387	1200	126	.953	2.60×10^{-5}	22,579
1600	49	.658	7.00×10^{-6}	17,001	1200	127	.963	1.00×10^{-5}	23,440
1200	52	.658	0	13,006	1200	128	.982	1.90×10^{-5}	24,164
1200	57	.665	1.40×10^{-6}	13,092	1200	129	1.006	2.40×10^{-5}	25,289
1200	62	.668	6.00×10^{-7}	13,216	1200	130	1.027	2.10×10^{-5}	26,532
1200	70	.682	1.75×10^{-6}	13,429	1200	131	1.056	2.90×10^{-5}	28,003
1200	75	.690	1.60×10^{-6}	13,711	1200	132	1.081	3.30×10^{-5}	29,967

TABLE B-10 (cont'd)

Fatigue Load, lb.	Life, 1000 Cycles	a, in.	da/dN, in./cycle	ΔK, psi $\sqrt{in.}$	Fatigue Load, lb.	Life, 1000 Cycles	a, in.	da/dN, in./cycle	ΔK, psi $\sqrt{in.}$
1200	80	.699	1.80×10^{-6}	13,934	1200	133	1.133	4.40×10^{-5}	32,640
1200	85	.706	1.40×10^{-6}	14,146	1200	134	1.180	4.70×10^{-5}	36,168
1200	90	.714	1.60×10^{-6}	14,349	1200	134.6	1.220	6.67×10^{-5}	39,958
1200	95	.721	1.40×10^{-6}	14,554	1200	135.5	1.293	8.11×10^{-5}	45,566
1200	100	.742	4.20×10^{-6}	14,947	1200	135.9	1.350	1.42×10^{-4}	53,108
1200	105	.754	2.40×10^{-6}	15,426	1200	136.2	1.404	1.80×10^{-4}	60,603
1200	110	.779	5.00×10^{-6}	15,983					

TABLE B-11

FATIGUE CRACK GROWTH DATA

Material: Ti-8% Al Specimen No. ATF-6

Grain Size: 19.30×10^{-4} in. B = .116 in. W = 2.00 in. a_o = .500 in.

Fatigue Load, lb.	Life, 1000 Cycles	a, in.	da/dN, in./cycle	ΔK, psi $\sqrt{in.}$	Fatigue Load, lb.	Life, 1000 Cycles	a, in.	da/dN, in./cycle	ΔK, psi $\sqrt{in.}$
2000	10	.512	--	--	1200	255	.799	4.40×10^{-6}	16,804
2000	15	.533	4.20×10^{-6}	16,906	1200	260	.809	2.00×10^{-6}	17,334
2000	18	.545	4.00×10^{-6}	17,447	1200	265	.826	3.40×10^{-6}	17,798
2000	21	.559	4.67×10^{-6}	17,887	1200	270	.843	3.40×10^{-6}	18,402
1600	24	.563	1.33×10^{-6}	14,558	1200	275	.867	4.80×10^{-6}	19,165
1600	27	.570	2.33×10^{-6}	14,711	1200	280	.907	8.00×10^{-6}	20,435
1600	30	.573	1.00×10^{-6}	14,852	1200	283	.935	9.33×10^{-6}	21,899
1200	35	.576	6.00×10^{-7}	11,203	1200	286	.971	1.20×10^{-5}	23,396
1200	40	.580	8.00×10^{-7}	11,277	1200	289	1.015	1.47×10^{-5}	25,450
1200	50	.585	5.00×10^{-7}	11,374	1200	290.5	1.035	1.33×10^{-5}	27,253
1200	60	.589	4.00×10^{-7}	11,472	1200	292	1.066	2.07×10^{-5}	28,802
1200	70	.595	6.00×10^{-7}	11,581	1200	293	1.086	2.00×10^{-5}	30,458
1200	80	.601	6.00×10^{-7}	11,713	1200	294	1.115	2.90×10^{-5}	32,158
1200	90	.605	4.00×10^{-7}	11,824	1200	294.5	1.124	1.80×10^{-5}	33,553

TABLE B-11 (cont'd)

Fatigue Load, lb.	Life, 1000 Cycles	a, in.	da/dN, in./cycle	ΔK, psi $\sqrt{in.}$	Fatigue Load, lb.	Life, 1000 Cycles	a, in.	da/dN, in./cycle	ΔK, psi $\sqrt{in.}$
1200	110	.615	5.00×10^{-7}	11,982	1200	295	1.135	2.20×10^{-5}	34,316
1200	130	.622	3.50×10^{-7}	12,176	1200	295.5	1.149	2.80×10^{-5}	35,298
1200	150	.627	2.50×10^{-7}	12,314	1200	296	1.165	3.20×10^{-5}	36,520
1200	170	.634	3.50×10^{-7}	12,454	1200	296.5	1.179	2.80×10^{-5}	37,791
1200	190	.639	2.50×10^{-7}	12,596	1200	297	1.200	4.20×10^{-5}	39,338
1600	195	.645	1.20×10^{-6}	16,970	1200	297.5	1.224	4.80×10^{-5}	41,434
1600	210	.649	2.67×10^{-7}	17,130	1200	298	1.251	5.40×10^{-5}	43,962
1600	220	.659	1.00×10^{-6}	17,358	1200	298.5	1.281	6.00×10^{-5}	46,991
1600	230	.676	1.70×10^{-6}	17,806	1200	299	1.334	1.06×10^{-4}	51,817
1600	240	.716	4.00×10^{-6}	18,791					
1600	245	.740	4.80×10^{-6}	19,967					
1600	250	.777	7.40×10^{-6}	21,166					

TABLE B-12

FATIGUE CRACK GROWTH DATA

Material: Ti-8% Al — Specimen No. ATF-4

Grain Size: 53.20×10^{-4} in. — B = .123 in. — W = 2.00 in. — a_o = .500 in.

Fatigue Load, lb.	Life, 1000 Cycles	a, in.	da/dN, in./cycle	ΔK, psi $\sqrt{in.}$	Fatigue Load, lb.	Life, 1000 Cycles	a, in.	da/dN, in./cycle	ΔK, psi $\sqrt{in.}$
2000	15	.504	--	--	1200	160	.898	3.60×10^{-6}	19,433
2000	18	.508	1.33×10^{-6}	15,503	1200	165	.912	2.80×10^{-6}	20,074
2000	28	.532	2.40×10^{-6}	15,930	1200	170	.941	5.80×10^{-6}	20,977
2000	33	.539	1.40×10^{-6}	16,414	1200	173	.955	4.67×10^{-6}	21,931
2000	38	.543	8.00×10^{-7}	16,589	1200	176	.982	9.00×10^{-6}	22,890
2000	43	.546	6.00×10^{-7}	16,700	1200	179	1.022	1.33×10^{-5}	24,571
2000	53	.565	1.90×10^{-6}	17,056	1200	180.5	1.047	1.67×10^{-5}	26,348
2000	63	.573	8.00×10^{-7}	17,500	1200	181.5	1.058	1.10×10^{-5}	27,399
2000	73	.583	1.00×10^{-6}	17,802	1200	182.5	1.075	1.70×10^{-5}	28,252
2000	83	.592	9.00×10^{-7}	18,126	1200	183.5	1.099	2.40×10^{-5}	29,559
2000	93	.624	3.20×10^{-6}	18,843	1200	184.5	1.125	2.60×10^{-5}	31,250
2000	103	.647	2.30×10^{-6}	19,847	1200	185	1.143	3.60×10^{-5}	32,834
2000	113	.668	2.10×10^{-6}	20,687	1200	185.5	1.156	2.60×10^{-5}	34,006
2000	120	.718	7.14×10^{-6}	22,121	1200	186	1.177	4.20×10^{-5}	35,347

TABLE B-12 (cont'd)

Fatigue Load, lb.	Life, 1000 Cycles	a, in.	da/dN, in./cycle	ΔK, psi $\sqrt{in.}$	Fatigue Load, lb.	Life, 1000 Cycles	a, in.	da/dN, in./cycle	ΔK, psi $\sqrt{in.}$
2000	123	.773	1.83×10^{-5}	24,443	1200	186.5	1.196	3.80×10^{-5}	37,003
2000	124	.783	1.00×10^{-5}	26,018	1200	186.8	1.210	4.67×10^{-5}	38,436
1500	127	.800	5.67×10^{-6}	20,030	1200	187.1	1.227	5.67×10^{-5}	39,840
1500	130	.818	6.00×10^{-6}	20,724	1200	187.4	1.246	6.33×10^{-5}	41,542
1500	133	.845	9.00×10^{-6}	21,659	1200	187.7	1.265	6.33×10^{-5}	43,426
1500	135	.868	1.15×10^{-5}	22,758	1200	188	1.287	7.33×10^{-5}	45,566
1500	136	.880	1.20×10^{-5}	23,569	1200	188.3	1.332	1.50×10^{-4}	49,312
1000	139	.880	0	15,903	1200	188.6	1.377	1.50×10^{-4}	54,870

REFERENCES

[1]Petch, N. J., J. Iron and Steel Institute (London), Vol. 173, 1953, p. 25; Hall, E. O., Proc. Phys. Society (London), Vol. 64B, 1951, p. 747.

[2]Forrest, P. G. and Tate, A. E. L., "The Influence of Grain Size on the Fatigue Behavior of 70/30 Brass." Journal of the Institute of Metals, Vol. 93, 1964, pp. 438-444.

[3]Thompson, A. W. and Backofen, W. A., "The Effect of Grain Size on Fatigue." Acta Metallurgica, Vol. 19, July, 1971, pp. 597-606.

[4]McEvily, Jr., A. J. and Boettner, R. C., "On Fatigue Crack Propagation in FCC Metals." Acta Metallurgica, Vol. 11, July, 1963, pp. 725-743.

[5]Hoeppner, D. W., "The Mechanisms of Fatigue. Part I - The Effect of Grain Size on Fatigue (Preliminary Results)." Lockheed--California Company. Report LR 24368, December, 1971.

[6]Plumbridge, W. J., "Review: Fatigue Crack Propagation in Metallic and Polymeric Materials." Journal of Material Science, Vol. 7, 1972, pp. 939-962.

[7]Laird, C., "The Influence of Metallurgical Structure on the Mechanisms of Fatigue Crack Propagation." Fatigue Crack Propagation, American Society for Testing and Materials STP 415, 1967, pp. 131-180.

[8]Howie, A. and Swann, P. R., "Direct Measurement of Stacking Fault Energies from Observations of Dislocation Nodes." Philosophical Magazine, 1961, pp. 1215-1226.

[9]Thornton, et al, Philosophical Magazine, Vol. 7, 1962, p. 1349.

[10]Honeycombe, R. W. K., The Plastic Deformation of Metals, Edward Arnold (Publishers) Ltd., 1968, p. 74.

[11]Honeycombe, p. 231.

[12]Grosskreutz, J. C. and Shaw, G. G., "Fine Subgrain Structure Adjacent to Fatigue Cracks." Acta Metallurgica, Vol. 20, April, 1972, pp. 523-528.

REFERENCES (cont'd)

[13]Segall, R. L., "Lattice Defects in Fatigued Metals." Electron Microscopy and Strength of Crystals, Interscience Publishers, 1963, pp. 515-534.

[14]Miller, G. A., Avery, D. H., and Backofen, W. A., "Fatigue Crack Growth in Some Copper Base Alloys." Transactions of the Metallurgical Society of AIME, Vol. 236, December, 1966, pp. 1667-1673.

[15]Ishii, H. and Weertman, J., "Fatigue Crack Propagation in Copper and Cu-Al Single Crystals." Metallurgical Transactions, Vol. 2, December, 1971, pp. 3441-3452.

[16]Plumbridge, W. J. and Ryder, D. A., "The Metallography of Fatigue." Metallurgical Reviews, Review 136.

[17]Griffiths, J. R., Mogford, I. L., and Richards, C. E., "Influence of Mean Stress on Fatigue Crack Propagation in a Ferritic Weld Metal." Metal Science Journal, Vol. 5, 1971, pp. 150-154.

[18]Electron Fractography, American Society for Testing and Materials STP 436, 1968.

[19]Inckle, A. E., Birkbeck, G., Waldron, G. W. J., "Structure Sensitive Fatigue Fracture." Journal of Material Science, Vol. 8, 1973, pp. 1058-1059.

[20]Hoeppner, D. W., "The Effect of Grain Size on Fatigue Crack Propagation in Copper." Fatigue Crack Propagation, American Society for Testing and Materials STP 415, 1967, pp. 486-504.

[21]Thompson, A. W. and Bucci, R. J., "The Dependence of Fatigue Crack Growth Rate on Grain Size." Metallurgical Transactions, Vol. 4, April, 1973, pp. 1173-1175.

[22]McClintock, F. A. and Irwin, G. R., "Plasticity Effects of Fracture Mechanics." Fracture Toughness Testing and Its Applications, American Society for Testing and Materials STP 381, 1965, pp. 84-113.

[23]Rice, J. R., "Mechanics of Crack Tip Deformation and Extension by Fatigue." Fatigue Crack Propagation, American Society for Testing and Materials STP 415, 1967, pp. 247-311.

[24]Richards, C. E. and Lindley, T. C., "The Influence of Stress Intensity and Microstructure on Fatigue Crack Propagation in Ferritic Materials." Engineering Fracture Mechanics, Vol. 4, 1972, pp. 951-978.

REFERENCES (cont'd)

[25]McEvily, A. J. and Johnston, T. L., "The Role of Cross Slip in Brittle Fracture and Fatigue." Proceedings of the First International Conference on Fracture, Vol. 2, 1965, pp. 515-546.

[26]Dillamore, I. L. and Smallman, R. E., "The Stacking Fault Energy of FCC Metals." Philosophical Magazine, 1965, pp. 191-193.

[27]Mackay, T. L. and Tiner, N. A., "Stress Corrosion Susceptibility of Titanium Alloys in Aqueous Environment." Metals Engineering Quarterly, November, 1969, pp. 59-60.

[28]Mauney, D. A., Starke, Jr., E. A., and Hochman, R. F., "Hydrogen Embrittlement and Stress Corrosion Cracking in Ti-Al Binary Alloys." Corrosion-NACE, Vol. 29, No. 6, June, 1973, pp. 241-244.

[29]Abrams, H., "Practical Applications of Quantitative Metallography." Stereology and Quantitative Metallography, American Society for Testing and Materials STP 504, 1972, pp. 138-182.

[30]Brown, Jr., W. F. and Srawley, J. E., Plane Strain Crack Toughness Testing of High Strength Metallic Materials, American Society for Testing and Materials STP 410, 1966, p. 12.

[31]Thompson, A., "Calculation of True Volume Grain Diameter." Metallography, Vol. 5, 1962, p. 366.

[32]Lukas, P. and Klesnil, M., "Dislocation Structures in Fatigued Cu-Zn Single Crystals." Phys. Stat. Sol., Vol. 37, 1970, p. 833.

[33]Mitchell, A. B. and Teer, D. G., "The Analysis of Dislocation Structures in Fatigued Aluminum Single Crystals Exhibiting Striations."

[34]Segall, R. L., Partridge, P. G., and Hirsch, P. B., "The Dislocation Distribution in Face Centered Cubic Metals After Fatigue." Philosophical Magazine, Vol. 6, 1961, p. 1493.

[35]Grosskreutz, J. C., and Waldow, P., "Substructure and Fatigue Fracture in Aluminum." Acta Metallurgica, Vol. 11, 1963, p. 717.

[36]Karashina, S., et al, "Studies on Substructures Around a Fatigue Crack in FCC Metals and Alloys." Trans. J.I.M., p. 205.

[37]Thomas, G., "Transmission Electron Microscopy of Metals." John Wiley and Sons, Inc., New York, 1962, pp. 195-200.

REFERENCES (cont'd)

[38]Paris, P. C., "The Fracture Mechanics Approach to Fatigue." Proceedings, Tenth Sagamore Army Materials Research Conference, Syracuse: Syracuse University Press, 1964.

[39]Birkbeck G., Inckle, A. E., and Waldron, G. W. J., "Aspects of Stage II Fatigue Crack Propagation in Low Carbon Steel." Journal of Material Science, Vol. 6, 1971, pp. 319-323.

[40]Robinson, J. L. and Beevers, C. L., 2nd Internation Conference on Titanium. Cambridge, Massachusetts, 1972.

[41]Williams, J. C., et al, "The Influence of Microstructure on the Fracture Topography of Titanium Alloys." Electron Microfractography, American Society for Testing and Materials STP 453, 1968, p. 226.

[42]Griffith, A. A., "The Phenomena of Rupture and Flow in Solids." Philosophical Transactions of the Royal Society, Vol. 221A, 1920, p. 163.